MOLECULAR PATHOGENESIS OF DENTINOGENESIS IMPERFECTA ASSOCIATED

WITH DENTIN SIALOPHOSPHOPROTEIN MUTATIONS

A Dissertation

by

TIAN LIANG

Submitted to the Office of Graduate and Professional Studies of
Texas A&M University
in partial fulfillment of the requirements for the degree of

DOCTOR OF PHILOSOPHY

Chair of Committee,	Yongbo Lu
Committee Members,	Chunlin Qin
	Kathy Svoboda
	M. Douglas Benson
	Thomas Diekwisch
Head of Department,	Larry Bellinger

August 2018

Major Subject: Oral Biology

ABSTRACT

Dentin sialophosphoprotein (DSPP) is abundantly expressed by odontoblasts, and transiently expressed by ameloblasts. The mutations in *DSPP* gene can cause dentinogenesis imperfecta (DGI) type II (DGI-II) and III (DGI-III), as well as dentin dysplasia (DD) type II (DD-II). To date, 42 *DSPP* mutations in humans have been identified. However, the molecular pathogenesis has not been determined.

We used CRISPR/Cas9 technology to generate a *Dspp*-KI (knock-in) mouse model, carrying P19L mutation equivalent to the c.50C>T, p.P17L mutation in humans. Compared with wild-type control, the $Dspp^{P19L/+}$ and $Dspp^{P19L/P19L}$ (mutant) mice displayed enlarged dental pulp and thinner pulp chamber roof dentin at an early stage, representing DGI-III in humans. With age, the mutant mice showed partial pulp obliteration and thickened pulp chamber floor dentin, resembling DGI-II in humans. The mutant mice also exhibited lower dentin density, defective enamel quality, and compromised dentinoenamel junction. The pathological morphology of odontoblasts and ameloblasts, and the impaired odontoblast processes were observed. Hence, the *Dspp*-KI mice recapitulated the dentin and enamel phenotypes in human DGI patients.

In addition, we discovered reduced DSPP mRNA and accumulated DSPP protein in the odontoblasts and ameloblasts of the mutant mice. The intracellularly accumulated DSPP retained in the endoplasmic reticulum (ER), and activated unfolded protein response (UPR). A UPR branch, inositol-requiring enzyme-1 (IRE1) pathway, was highly activated in the pulp cells of the mutant mice. The activation of IRE1 specifically inhibited the synthesis of DSPP protein during the accumulation of DSPP. Thus, UPR, especially IRE1, may play a major role in DGI associated with *DSPP* mutations.

In summary, we generated a *Dspp*-KI mouse model recapitulating human DGI, and showed that UPR elicited by the *DSPP* mutation played a major role in DGI. Further elucidation of the molecular pathogenesis may offer insights for potential treatment plans for DGI.

DEDICATION

To all the mice sacrificed for this study, for my desire to understand the diseases, and hopefully for improving the quality of human life.

ACKNOWLEDGEMENTS

It's an overwhelming moment for me to think of whom I should acknowledge for the completion of my PhD study. I can never claim this study as an independent work, because I keep receiving help and love, directly or indirectly, from many. It is not true that the nobility of human would occur naturally; I even tend to say the opposite. But I'm extremely lucky.

My mentor, Dr. Bob Lu, is always available for me. He teaches me to design and perform experiments, helps me with troubleshooting, and finds alternative approaches to support a hypothesis. He also holds countless conversations with me, from science to career development. I can still remember at the end of 2016, I was so upset and frustrated when I tried to obtain data from immunofluorescence. He realized my situation, booked the confocal microscope himself, and asked me if I had interest to see how he would do the experiment. The next day, he sat in the dark room with the microscope, instructing me how to get the optimal picture patiently. Actually, he had orally taught me how to perform this experiment several times. But still, he sat there, peacefully talking about the principles and tricks, and forgot about lunch. One with some experience in science will know that research is the exploration in darkness. You may get into a topic that few people have explored before. In such darkness, there are chances that you can see nothing. You have to be the light. I was not strong enough to be the light, then Dr. Lu was there lighting up for me. I kept learning lessons from him on how to deal with the bottlenecks, how to hold the emotions, and how to keep rationality working in research.

My co-mentor, Dr. Chunlin Qin, has been playing around with DSPP for many years. His expertise on this protein helps me substantially. He will always open his door for me for whatever trivial questions. He will spend tremendous amounts of time correcting my writing,

editing my presentations, and listening to my rehearsal. Besides, he also cares about me in person. He is always trying to make sure that I keep a balance between work and life. He backs me up and offers me valuable help and suggestions, when I told him I would like to take research as my career. He makes me feel that I'm one of his family members.

Our program director, Dr. Kathy Svoboda, offers me tremendous help on research and career development. Her broad eyesight always helps me interpret my results in novel ways. She also demonstrates great efforts teaching me how to write. I'm lucky enough to be her teaching assistant for the General Histology for a semester. There I learned how to offer information in an effective way, and how to help students with difficulties.

Dr. M. Douglas Benson, is always excited about my findings, and asking more critical questions to push me ahead. His humor has brought me lots of pleasure during research.

Dr. Thomas Diekwisch, is always ready for a conversation in the hallway to inspire me. His understanding of enamel, Schubert, and even Heldegger, making this degree something really about philosophy.

I cannot thank Dr. Suzhen Wang and Dr. Hua Zhang enough, for helping and instructing me in every detail during experiments. Every piece of advice from them makes my research much easier. They treat me as family member, sharing my pleasures. Wuliji and Lili take me as their close friends. Tian Meng, Xiaohua, Chao, and Priyam taught me many techniques.

Dr. Opperman, our department head, is taking great care of graduate students, including me. I also learn a lot from her during the General Histology course. Dr. Bellinger, the professor monitoring research in the whole college, provides me many opportunities to talk about my research in the school. Dr. Feng not only generously opens his lab to the whole department, but also offers many constructive suggestions to my research. Dr. Groppe and Dr. Xiaofang Wang

helped me substantially with my preliminary exams. Dr. Tao generously offer me to use his cryosectioning microtome and microscopes. Dr. Liu opens his Nanodrop for us to work with nucleic acid.

The department is a lovely and friendly place to stay, which is made possible by Nancy, Marge, Jeanne, Darla, Kim, Richard, Jill, and Willie. Their kindness makes all the cumbersome work much easier.

My research also received help from the following individuals in the College of Dentistry: Ying, Mary, Jun, Ke, Mirali, Bei, Abby, Yan, Chaoyuan, Sufang, Jingyi, Yiqing, Yi, Priscilla, Gerald, and Connie, among many others. I also received help from Fang Li from Peking University, for the discussion of human patients with dentinogenesis imperfecta, and Hong Xie from University of Pennsylvania, for the methods of RNA extraction.

I would also like to thank all the graduate students in the program for their company.

Also, thanks for Dr. Jan Hu and Dr. James Simmer, for offering me the opportunity to further study dentinogenesis imperfecta.

For almost 30 years, my parents and my families are supporting me from every aspect. They keep working hard, inspiring me, and correcting me. Their bravery and righteousness set a good example for me. Their generosity and love make it possible for me to pursue my dream.

Mrs. Xun Yang, my high school teacher, inspired me to love literatures, philosophy, and science. Mrs. Haixia Huang, my piano teacher, taught me not only the beauty of classical music, but also the beauty of life.

Qiujian Ruan (Papa), my most intimate friend for years, keeps broadening my eyesight, inspiring me to think and to read. Xian Dai, another of my intimate friends, accompanies me during my PhD study.

The power of my words is limited. I keep having more people to thank and to appreciate. Franz Schubert wrote a piano sonata in A, D. 664. This piece of music can tell how much I treasure the experience of these years.

CONTRIBUTORS AND FUNDING SOURCES

NOMENCLATURE

DGI	Dentinogenesis imperfecta
DGI-I	Dentinogenesis imperfecta Shields type I
DGI-II	Dentinogenesis imperfecta Shields type II
DGI-III	Dentinogenesis imperfecta Shields type III
DD	Dentin dysplasia
DD-I	Dentin dysplasia Shields type I
DD-II	Dentin dysplasia Shields type II
OI	Osteoogenesis imperfecta
AI	Amelogenesis imperfecta
PDL	Periodontal ligaments
DEJ	Dentinoenamel junction
HERS	Hertwig's epithelial root sheath
DSPP	Dentin sialophosphoprotein
DSP	Dentin sialoprotein
DPP	Dentin phosphoprotein
DGP	Dentin glycoprotein
SIBLING	Small integrin-binding ligand, N-linked glycoprotein
BSP	Bone sialoprotein
OPN	Osteopontin
OC	Osteocalcin
MEPE	Matrix extracellular phosphoglycoprotein

DMP1	Dentin matrix protein 1
TGF-β	Transforming growth factor beta
TGFBR2	TGF-β receptor 2
BMP	Bone morphogenetic protein
BMP2	Bone morphogenetic protein 2
OSX	Osterix
NF-Y	Nuclear transcription factor Y
CBF	CCAAT-binding factor
NF-κB	Nuclear factor kappa-light-chain-enhancer of activated B cells
GATA	GATA binding protein
AP-1	Activator protein 1
GT-1	Trihelix transcription factor GT-1
AP-3	Activator protein 3
DF2	DSPP factor 2
R-Smad	Receptor-regulated Smad
DLX	Dll homeobox
MSX	Msh homeobox
COUP-TFII	Chicken ovalbumin upstream promoter transcription factor 2
RUNX2	Dentinogenesis imperfecta
TWIST1	Twist-related protein 1
YY1	Yin Yang 1 transcriptional repressor protein
KLF	Krüppel-like factor
WNT	Wingless-related integration site

TRPS1	Tricho-Rhino-Phalangeal Syndrome type I protein
NFIC	Nuclear factor I-C
C-6-S	Chondroitine-6-sulfate
C-4-S	Chondroitine-4-sulfate
RGD	Arginine-Glycine-Aspartic acid
IPV	Isoleucine-Proline-Valine
Ala	Alanine
Val	Valine
Thr	Threonine
Ile	Isoleucine
MAPK	Mitogen-activated protein kinase (MAP kinase)
FAK	Focal adhesion kinase
ERK	Extracellular signal-regulated kinase
ELK-1	ETS domain-containing protein ELK-1
AKT	Synonym of PKB, protein kinase B
mTOR	Mammalian target of rapamycin
KI	Knock-in
KO	Knock-out
Dpp-cKO	*Dpp* conditional knock-out
DNA	Deoxyribonucleic acid
RNA	Ribonucleic acid
nt	Nucleotide
N-terminus	Amino-terminus

C-terminus	Carbon-terminus
bp	Base pair
pI	Isoelectric point
PTM	Post-translational modification
NCP	Non-collagenous protein
CRISPR	Clustered regularly interspaced short palindromic repeats
Cas9	CRISPR-associated protein 9
crRNA	CRISPR RNA
tracrRNA	trans-activating crRNA
sgRNA	single guide RNA
DSB	Double-stranded break
PAM	Protospacer adjacent motif
ssODN	Single-stranded oligodeoxynucleotide
HDR	Homology-directed repair
gDNA	Genomic DNA
BLAST	Basic local alignment search tool
EMBL-EBI	European Molecular Biology Laboratory-European Bioinformatics Institute
ISH	*In situ* hybridization
RT-PCR	Reverse-transcription PCR
qPCR	quantitative PCR, or real-time PCR
RFLP	Restriction fragment length polymorphism
DEPC	Diethyl pyrocarbonate

DIG	Digoxigenin
NBT/BCIP	Nitro blue tetrazolium/5-bromo-4-chloro-3-indolyl-phosphate
IRES	Internal ribosome entry site
cRNA	Coding RNA
BrdU	Bromodeoxyuridine/5-bromo-2'-deoxyuridine
IHC	Immunohistochemistry
PBS	Phosphate-buffered saline
PBST	Phosphate-buffered saline with 0.01% Tween-20
EDTA	Ethylenediaminetetraacetic acid
BSA	Bovine serum albumin
NGS	Normal goat serum
DAB	3,3'-diaminobenzidine
HA	Hemagglutinin
DMEM	Dulbecco's Modified Eagle's Medium
FBS	Fetal bovine serum
CO_2	Carbon dioxide
SDS-PAGE	Sodium dodecyl sulfate-polyacrylamide gel electrophoresis
HRP	Horseradish peroxidase
DAPI	4',6-diamidino-2-phenylindole
MDPC-23	Mouse dental papilla cell-23
T4-4	An immortalized primary rat tooth germ cell clone
17IIA11	An odontoblast-like cell clone
293EBNA	Human embryonic kidney 293 Epstein-Barr Virus nuclear antigen

μCT	Micro-computed tomography
3D	Three-dimensional
SEM	Scanning electron microscopy
MMA	Methyl methacrylate
H&E	Hematoxylin and Eosin
ER	Endoplasmic reticulum
UPR	Unfolded protein response
ERAD	ER-associated degradation
ATF6	Activating transcription factor 6
PERK	Double-stranded RNA-activated protein kinase (PER)-like ER kinase
IRE1	Inositol-requiring enzyme 1
RNase	Ribonuclease
BiP	Binding immunoglobulin protein
HSP	Heat shock protein
GRP94	Glucose-regulated protein 94 kDa
XBP1	X-box binding protein 1
XBP1u	Unspliced XBP1
XBP1s	Spliced XBP1
eIF2α	Eukaryotic transcription initiation factor 2
ATF4	Activating transcription factor 4
CHOP	C/EBP homologous protein
GRDD34	Growth arrest and DNA damage-inducible protein 34
RIDD	Regulated IRE1-dependent decay

JNK	c-Jun N-terminal kinase
AGO	Argonaute protein
BCL-2	B-cell lymphoma 2
BH3	Bcl-2 homology domain 3
PUMA	p53 upregulated modulator of apoptosis
BIM	Synonym of BCL2L11, Bcl-2-like protein 11
BCL-x_L	B-cell lymphoma-extra large

TABLE OF CONTENTS

Page

LIST OF FIGURES

Page

LIST OF TABLES

CHAPTER I

INTRODUCTION

The tooth is the hardest organ in humans. It consists of four components: the three hard tissues, enamel, dentin, and cementum, and the soft tissue dental pulp. The three hard tissues are deposited by professional secretory cells: ameloblasts for enamel, odontoblasts for dentin, and cementoblasts for cementum. The deposition of these hard tissues requires the networking of inorganic materials and proteins.

Dentin sialophosphoprotein (DSPP) is a protein expressed abundantly in odontoblasts. It carries repetitive DS or DSS motifs, where D stands for aspartic acid, S stands for serines. Most of the serines in these motifs are phosphorylated. Therefore, DSPP is very acidic.

Mutations in *DSPP* gene cause non-syndromic dentinogenesis imperfecta (DGI) or dentin dysplasia (DD), the most prevalent dentin genetic disorder in humans. The features of non-syndromic DGI or DD are: tooth discoloration, severe enamel attrition, and enlarged or obliterated dental pulp (Kim and Simmer, 2007; Shields, 1983; Shields et al., 1973). Several molecular mechanisms have been proposed but remained to be proven for non-syndromic DGI or DD. The elucidation of these molecular mechanisms could lead to potential treatment options for these diseases.

This dissertation consists of three parts. First, we will review the current studies on DSPP and DGI. Second, a *Dspp* knock-in (KI) mouse model will be established to represent DGI in humans. The phenotypes of this mouse model will also be further characterized. Third, we will explore the molecular pathogenesis of DGI using this animal model, together with *in vitro* approaches.

1

I.1 Dentin Sialophosphoprotein (DSPP)

DSPP is abundantly expressed by odontoblasts. It is a member of the SIBLING (small integrin-binding ligand, N-linked glycoprotein) protein family, which also includes bone sialoprotein (BSP), osteopontin (OPN), matrix extracellular phosphoglycoprotein (MEPE), and dentin matrix protein 1 (DMP1) (Fisher et al., 2001). These five genes cluster in human chromosome 4q21. These genes may result from duplication and divergent evolution of a single gene (Fisher et al., 2001). The SIBLING protein family members share many similarities. All of their genes have a dominant last exon with most of the coding information (Fisher et al., 2001). All of the proteins are phosphorylated and glycosylated secretory proteins and are rich in glutamic acid and/or aspartic acid. These features together make them acidic. The SIBLING proteins are mainly detected in the mineralized tissues, including bones and teeth. Some of them, such as OPN, are predominantly expressed in bones, while DSPP is almost exclusively expressed by odontoblasts (Butler et al., 2003; Qin et al., 2004). Nevertheless, their distributions suggest that all these members play important roles in mineralization.

I.1.1 *DSPP* Gene and Its Regulation

The cleavage products of DSPP, namely DSP (dentin sialoprotein) (Butler et al., 1981) and DPP (dentin phosphoprotein) (Veis and Perry, 1967), were discovered before the *DSPP* gene on human chromosome 4q21.3 (MacDougall et al., 1997a; MacDougall et al., 1997b). *DSPP* gene consists of 5 exons and 4 introns. The DSP coding region extends from exon 2 to the 5' region of exon 5 (Fig. 1). While the DPP coding region is located only in exon 5 (Fig. 1) (Feng et al., 1998).

Two potential enhancers exist between -1243 to -792 nt, and between -791 to -242 nt in the mouse *Dspp* gene promoter (Feng et al., 1998). An activator/promoter element has been found between -97 to -72 nt, whereas a suppressor element has been identified between -121 to -104 nt (Chen et al., 2008b; Chen et al., 2004; Feng et al., 1998). The former promoter region extending from -97 to -72 nt contains transcription factor binding sites, including NF-κB, GATA, AP-1, NF-Y, GT-1, and AP-3 (Chen et al., 2008b). The latter suppressor element is a major regulator for the temporal and spatial expression of DSPP. It is bound by DSPP factor 2 (DF2, molecular weight ~72kDa) specifically between -110 to -104 nt (Chen et al., 2004).

Among many signaling pathways that regulate the expression of DSPP, TGF-β (transforming growth factor β) signaling is one of the most crucial. Within the TGF-β superfamily, BMP2 (bone morphogenetic protein 2) has been studied extensively in dentinogenesis. BMP2 regulates the expression of DSPP via both canonical BMP pathway (through Smad proteins) and non-canonical BMP pathway (Ryoo et al., 2006). Activation of the R-Smads (Smad 1/5/8, receptor-regulated Smads) can stimulate DSPP expression in MDPC-23 cells (Cho et al., 2010). Two homeodomain protein (DLX/MSX) response elements, at -433 nt and -415 nt, show a strong relation with DSPP expression (Cho et al., 2010). DLX5 dramatically increases DSPP expression; however, this interaction can be antagonized by MSX2 (Cho et al., 2010). In addition to the antagonistic effect on DLX5, MSX2 can physically interact with COUP-TFII, an orphan nuclear receptor, to suppress its induction of DSPP expression via a -333/-328 response element (Hur et al., 2015). In odontoblasts, BMP2 also induces DSPP expression via transcription factors DLX3 and OSX (osterix). These two transcription factors form a protein complex, binding to their corresponding response elements in -318 to +54 nt of the *Dspp* gene promoter, to regulate the expression of DSPP (Yang et al., 2017).

3

As an osteoblast-specific transcription factor of the BMP2 canonical signaling pathway, RUNX2 regulates DSPP expression as well. Three RUNX2 regulation sites, -2415 to -2410 nt, -2409 to -2404 nt, and -1796 to -1791 nt, have been identified in the mouse *Dspp* gene promoter (Chen et al., 2005). RUNX2 is expressed at a high level at the early stage of odontoblast differentiation, but is dramatically decreased later. RUNX2 can upregulate DSPP expression in preodontoblasts; however, it downregulates DSPP expression in odontoblasts (Chen et al., 2005). TWIST1, a transcription factor with a basic helix-loop-helix domain, suppresses DSPP expression potentially by its antagonistic effects on RUNX2 (Galler et al., 2007). Another transcription factor, YY1, also plays an inhibitory role in DSPP expression by binding to -622 nt of the *Dspp* gene promoter (Cho et al., 2010).

BMP2 can regulate DSPP expression through the non-canonical BMP pathway as well. One transcription factor induced by BMP2 and regulating DSPP expression is NF-Y (nuclear transcription factor Y), also called CBF (CCAAT-binding factor). Upon its nuclear accumulation, NF-Y binds to an inverted CCAAT box in the previous activator/promoter region of the *Dspp* gene promoter, between -97 to -72 nt, to increase the expression of DSPP (Chen et al., 2008b; Chen et al., 2004).

In addition to BMP2 signaling pathways, some other pathways within the TGF-β superfamily are also involved in the regulation of DSPP expression. In the MDPC-23 mouse odontoblast cell line, TGF-β1 induces Smad3 translocating into the nucleus. The latter cooperates with Smad4 to inhibit the expression of DSPP (He et al., 2004). In contrast, in an isolated embryonic mouse mandible model, TGF-β1 induces the expression of DSPP, together with DMP1, during odontoblastic differentiation (Chen et al., 2016). Different Krüppel-like factors regulated by TGF-β1 may account for the difference, which will be discussed later.

4

Interestingly, DSP and DPP can help preserve TGF-β1 activity (Yamakoshi et al., 2014). In a molar explant model, exogenous TGF-β2 can induce ectopic expression of DSPP (Oka et al., 2007). Results from a TGFBR2 (TGF-β receptor 2) conditional knock-out mouse model also indicated that TGF-β is indispensable for DSPP expression and odontoblast differentiation (Oka et al., 2007).

Another signaling pathway involved in the regulation of DSPP expression is the WNT pathway. One odontoblast differentiation inducer, WNT10a, is an upstream regulator of DSPP (Liu et al., 2013; Yamashiro et al., 2007). β-catenin, the central component of WNT signaling, can also induce DSPP expression potentially via its activation of RUNX2 (Han et al., 2014).

Apart from the GATA binding sites in the aforementioned promoter region between -97 to -72 nt, many other GATA transcription factor binding elements have been identified in the *Dspp* gene promoter (Napierala et al., 2012). One of the GATA-type transcription factor, TRPS1 (Tricho-Rhino-Phalangeal Syndrome), directly binds to the *Dspp* promoter to repress its expression (Napierala et al., 2012). TRPS1 may repress DSPP expression indirectly via supporting RUNX2 expression as well (Kuzynski et al., 2014). Supportively, TRPS1-overexpressing mice demonstrate a dental phenotype similar to *Dspp*-KO (knock out) mice, which display DGI-III phenotypic characteristics (Mobley et al., 2015; Napierala et al., 2012). However, the phenotypes of the TRPS1-overexpressing mice can be partially DSPP-independent (Mobley et al., 2015; Napierala et al., 2012).

DMP1 is a close peer of DSPP. Surprisingly, it can bind to the promoter region of *Dspp* promoter region from -417 to -353 nt, and activates its transcription (Narayanan et al., 2006). The 57kDa C-terminal fragment of DMP1 can enter the nucleus and interact with the *Dspp*

promoter (Gibson et al., 2013d; Siyam et al., 2012). DSPP is also responsible for the dental defects in *Dmp1*-KO mice (Gibson et al., 2013d).

There is also evidence that Krüppel-like factor (KLF) family proteins, a set of transcription factors containing a zinc-finger DNA-binding domain in their C-terminus, actively regulate the expression of DSPP (Chen et al., 2016). KLF10 promotes DSPP expression by its binding domains located between -5.6kb to -2.6kb in the *Dspp* promoter in a dose-dependent manner (Chen et al., 2016). NFIC (nuclear factor I-C) and KLF4 (Krüppel-like factor 4) were also proposed to regulate DSPP via an NFIC-KLF4-DMP1-DSPP cascade (Feng et al., 2017; Lee et al., 2014). Although the inhibition of NFIC or KLF4 led to the downregulation of both DMP1 and DSPP in this study, the regulation of DSPP by NFIC/KLF4 was not proven to be DMP1-dependent. In addition, cross-talk between TGF-β1 and NFIC has been investigated in the odontoblastic differentiation. The gradual increase of NFIC is accompanied by the decrease of TGF-β1, together promoting the expression of DSPP (Lee et al., 2011a; Lee et al., 2014). In contrast, in the isolated embryonic mouse mandible model mentioned previously, TGF-β1 induces the expressions of KLF10 and KLF5, together with the expressions of DSPP and DMP1 (Chen et al., 2016).

It is not surprising that as a relatively terminal target and a strong executor during dentinogenesis, DSPP is closely regulated by many pathways. Also, the regulation of DSPP expression involves cross-talk among these pathways. However, cells do not just closely monitor and regulate DSPP during its transcription, but during all the following molecular events as well.

I.1.2 DSPP Proteins and Functions

As DPP is about ten times abundant in the dentin matrix compared with DSP, people did not realize that they are the proteolytic products of a single precursor protein, until the discovery of their common transcript and gene.

However, DSPP can be cleaved into more than two fragments. In porcine DSPP only, a third fragment, DGP (dentin glycoprotein) has been identified between the N-terminal DSP and the C-terminal DPP (Yamakoshi et al., 2005). In addition, DSP can be cleaved into smaller fragments (Tsuchiya et al., 2011; Yamakoshi et al., 2006); DPP also presents variations in length (Tsuchiya et al., 2011; Yamakoshi et al., 2008). Full-length DSPP has also been extracted from pulp/odontoblast complex, as well as dentin extracellular matrix, adding to the existing derivatives of a single precursor protein (Sun et al., 2010).

Even though the cleavage products of DSPP have been identified by multiple approaches, the mechanism of DSPP cleavage has not been elucidated yet. Many groups have investigated the astacin protease family on DSPP cleavage via different approaches. Among all the astacin proteases, the bone morphogenetic protein 1(BMP1)/tolloid-like protein family members, especially BMP1, have been proposed as the key proteases for initial DSPP proteolysis (Sun et al., 2010; Tsuchiya et al., 2011; von Marschall and Fisher, 2010; Zhu et al., 2012a; Zhu et al., 2012b). For mouse DSPP, a predominant cleavage site for BMP1 is between Gly^{451}-Asp^{452}, releasing the N-terminal DSP or DSP/DGP, and the C-terminal DPP (Zhu et al., 2012a; Zhu et al., 2012b). Failure of DSPP activation by BMP1-induced proteolysis will lead to a DGI-III-like phenotype, similar to *Dspp*-KO mice (Zhang et al., 2017; Zhu et al., 2012a). The *Dspp*-KO mice display enlarged pulp chamber, thinner dentin walls, widened predentin zone throughout their life, which is quite similar to the young DGI-III patients (Sreenath et al., 2003a).

7

After the initial cleavage of porcine DSPP, MMP-20 is likely to mediate cleavage between DSP and DGP, as well as cleavages in the N-terminal part of DSP, releasing fragments of 25-38 kDa (Yamakoshi et al., 2006). MMP-2, however, will process cleavage near the C-terminal of DSP (Yamakoshi et al., 2006). Another astacin protease, MEP1B, is likely to give rise to a 36-amino-acid-shorter version of DPP, and can degrade DPP when the high concentration of DPP is depleting the free calcium (Tsuchiya et al., 2011). Besides, MMP-9 is critical for DSP processing and dentinogenesis, indicated by the results from *Mmp-9*-KO mice (Yuan et al., 2017).

After synthesis, DSPP undergoes extensive post-translational modifications (PTM). DSP dimers have been identified in pigs and mice (Sun et al., 2010; Yamakoshi et al., 2008). Taking porcine DSP for example, disulfide bridge is located at Cys^{190} (Yamakoshi et al., 2011). In the N-terminal part of the disulfide bridge, there are many N-glycosylation, with one sialic acid, typically the N-acetylneuraminic acid, per N-glycosylation site on average (Yamakoshi et al., 2011). However, these N-glycosylation sites are not well conserved among species. In the C-terminal part of the disulfide bridge, there are two glycosaminoglycan (GAG) attachment sites, Ser^{238} and Ser^{250}, and two O-glycosylation sites, possibly Thr^{200}, Thr^{216}, or Thr^{316} (Yamakoshi et al., 2011). The GAG chain attachment sites and O-glycosylation sites are well conserved. The components of disaccharide group are chondroitine-6-sulfate (C-6-S) and chondroitine-4-sulfate (C-4-S), with a ratio of 7:3 (Yamakoshi et al., 2011). Similarly, the proteoglycan forms of DSP (DSP-PG), also called high molecular weight DSP (HMW-DSP) previously, have been identified in rats. The GAG attachment sites in rat DSP are Ser^{241} and Ser^{243}, with the disaccharide groups in its GAG chains being C-4-S exclusively (Qin et al., 2003a; Zhu et al., 2010). These various forms of DSP, including its core protein, its proteoglycan form, and its smaller fragments, if all

8

taken into account, may partially explain why DSP extracted from dentin matrix is only about 1/10 of DPP (Yamakoshi et al., 2008; Yamakoshi et al., 2011).

The major modifications in DSP are glycosylations, whereas most features of DPP are related to its acidity. DPP is the most acidic protein identified so far, with the isoelectric point of 1.1 (Jonsson et al., 1978). The major contributor to its low pI is the repetitive DS and DSS motifs. The carboxylic acid group in the aspartic acid residue is acidic. Also, the serine residues are highly phosphorylated. In porcine DPP with less than 600 amino acid residues, more than half of them are serines, half of which are phosphorylated (Yamakoshi et al., 2008). On the one hand, the negatively charged DPP can facilitate conformational changes in the positively charged type I collagen at its relatively unstable fibril overlapping zone to promote collagen aggregation (Dahl et al., 1998; He et al., 2005b). On the other hand, the phosphorylation on serine residues leads to a higher affinity to calcium (He et al., 2005b; Villarreal-Ramirez et al., 2017). With the presence of calcium, DPP is converted to ordered β-sheet-like structure to stimulate the formation and growth of hydroxyapatite (He et al., 2005b; Villarreal-Ramirez et al., 2017; Villarreal-Ramirez et al., 2014). In addition to phosphorylation, two N-glycosylation sites have been determined in porcine DSPP: Asn[525] and Asn[937] (Yamakoshi et al., 2008). Due to the highly repetitive sequence, the DPP portion of the gene displays polymorphism by carrying in-frame insertions and deletions. These allelic variations may lead to the dynamics in its length and the molecular weight between or even within individuals (Yamakoshi et al., 2008; Yang et al., 2016).

DSPP is predominantly expressed in odontoblasts. With immunohistochemistry (IHC), DSPP can be identified in mouse incisors as early as postnatal day 1 (Hao et al., 2009), and in the rat first molar as early as postnatal day 1 (Baba et al., 2004). However, reverse-transcription PCR

9

(RT-PCR), which sensitively detects minor amount of mRNA, identified DSPP transcript in mouse cap stage molars as early as embryonic 14 days old (D'Souza et al., 1997). The expression of DSPP is maintained throughout dentinogenesis. The localizations of DSP and DPP proteins are different. DSP stains strongly in the cytoplasm of odontoblast cell bodies, odontoblast processes, mineralization front, and dentinal tubules (Baba et al., 2004; Hao et al., 2009); however, DPP mainly locates in the mineralization front (Hao et al., 2009). At a later stage, DPP is also observed in the nucleus of odontoblasts (Hao et al., 2009). Similarly, DSP is also present in the nucleus of two mouse odontoblastic cell lines (Chen et al., 2008a). A closer look at DSP fragments also shows that the N-terminal fragment tends to locate in the non-mineralized predentin and odontoblasts, while the C-terminal fragment preferentially stays in the mineralized portion, including the dentinal tubules and peritubular dentin (Yuan et al., 2012).

The function of DSP in dentinogenesis is largely unknown. *In vitro* study showed that DSP has a limited effect on hydroxyapatite formation and growth (Boskey et al., 2000). Phenotypes from a *Dpp* conditional knock-out (*Dpp*-cKO) mouse model suggest that DSP may be associated with the initiation of dentin mineralization, that is, conversion of predentin into dentin (Suzuki et al., 2009). Overexpressing DSP in *Dspp*-KO mice leads to a worsened condition compared with *Dspp*-KO mice, namely thinner, more poorly mineralized, less organized dentin, suggesting that DSP may play an inhibitory role for dentin mineralization (Gibson et al., 2013b). The distinct localizations of DSP fragments also imply that the N-terminal DSP may inhibit mineralization, whereas C-terminal DSP may participate in the maintenance of mineralized tissue microenvironment (Yuan et al., 2012). The function of DPP in dentinogenesis has been partially clarified. At a low concentration (0.01-1µg/mL), DPP facilitates hydroxyapatite formation *in vitro*; in contrast, at a high concentration (100µg/mL),

10

DPP inhibits mineralization (Boskey et al., 1990). Based on its structure, DPP is unlikely to initiate fibril formation (He et al., 2005b). Instead, DPP is indispensable for mineral maturation, indicated by the *Dpp*-cKO mouse model (Suzuki et al., 2009). Evidently, the post-translational modifications are critical for the functions of DSP and DPP. Since the discovery of full-length DSPP in dentin matrix, people believe that it may play certain distinct roles from DSP and DPP in dentinogenesis (Sun et al., 2010).

The expression of DSPP in ameloblasts can be detected in mouse incisor as early as embryonic day 16.5, and in mouse molar embryonic day 18.5 (D'Souza et al., 1997; Verdelis et al., 2016). Its expression is confined to presecretory and early secretory ameloblasts (D'Souza et al., 1997; Wang et al., 2011). Recently, DSPP was claimed to be detected in secretory ameloblasts in mouse incisor and molar (Verdelis et al., 2016). However, its function in amelogenesis is largely unknown. In two human families with DGI caused by mutations in *DSPP*, vertical bands of hypoplastic enamel can be observed (Wang et al., 2011). However, the authors thought that this was caused by transient ER stress in the ameloblasts, but DSPP was not indispensable for amelogenesis (Wang et al., 2011). In *Dspp*-KO mice, enamel secretion and maturation are accelerated; however, no phenotypic difference in the mature enamel is demonstrated (Verdelis et al., 2016). Instead, a compromised dentinoenamel junction (DEJ), and widened odontoblast processes with fewer branches have been observed (Verdelis et al., 2016). Expression of DSP and DPP in secretory ameloblasts driven by the amelogenin promoter suggest that such ectopic expression of DSP does not harm amelogenesis generally, but the ectopic expression of DPP largely impairs enamel and DEJ formation (Paine et al., 2005; White et al., 2007). To date, there is no evidence supporting the idea that DSPP would be responsible for the

enamel lesion observed in DGI. The defective enamel is considered as an indirect consequence of the defective underlying dentin, or the disrupted DEJ.

DSPP has also been detected in the periodontium (Baba et al., 2004; Prasad et al., 2010). DSP signals are observed in both cementoblasts and cementum matrix (Baba et al., 2004; Prasad et al., 2010). The loss of DSPP expression in the cementum of the *Dspp*-KO mice exhibit a significant loss of cementum (Gibson et al., 2013c). Similarly, *Dspp*-KO mice display disrupted alveolar bone structure, including increasing porosity, and less-organized lacuna-canalicular system (Gibson et al., 2013c). These conditions in cementum and alveolar bone are worsened by overexpressing DSP (Gibson et al., 2014). These results suggest that DSP inhibits cementogenesis and osteogenesis in the periodontium. The defective cementum and alveolar bone further lead to detachment of the periodontal ligaments (PDL) (Gibson et al., 2014; Gibson et al., 2013c). In addition, C-terminal DSP was detected in the PDL cells in mouse periodontium (Ozer et al., 2013). *In vitro* approaches using recombinant C-terminal DSP also demonstrate that this fragment may facilitate the attachment, proliferation, and differentiation of PDL stem cells (Ozer et al., 2013).

Apart from alveolar bone, DSPP is also expressed by osteoblast-like cell lines and osteoblasts in long bones and calvaria. The expression of DSPP in bone is about 1/400 of that in dentin (Qin et al., 2003b; Qin et al., 2002). *Dspp*-KO mice also show modestly but significantly accelerated mineralization at early stages in the femurs, which is reversed later (Verdelis et al., 2008). These structural and material deficits suggest that DSPP regulates the mineralization and remodeling of bones (Verdelis et al., 2008).

In addition to its expression in mineralized tissues, DSPP expression has been detected in many other tissues and organs, including cartilage, salivary glands, kidney, brain, liver, hair

12

follicles, and breast and lung cancer (Fisher et al., 2004; Prasad et al., 2011; Tang et al., 2011). Its roles in these non-mineralized tissues are largely unknown. DPP expression in embryonic stages suggests that it may be important for lung and kidney organogenesis and epithelial-mesenchymal interactions (Alvares et al., 2006).

As indicated in their names, the SIBLING family proteins share a common feature: each of them has an RGD (Arginine-Glycine-Aspartic acid) binding motif to target the integrin. DSPP has an RGD domain in the N-terminal part of DPP. Therefore, it is not surprising that DPP binds to integrin $\alpha_v\beta_3$ in human mesenchymal stem cells to activate MAPK signaling pathway for the further activation of osteoblastic transcription factors, such as RUNX2 and OSX (Jadlowiec et al., 2004). DPP treatment also leads to the phosphorylation of Smad1 and the activation of Smad6, DLX5, and RUNX2, independent of BMP2, the canonical ligand for the activation of Smad proteins (Jadlowiec et al., 2006). In addition to its effects on osteogenic markers, DPP also facilitates the expression of odontogenic markers. In undifferentiated mesenchymal stem cells and pulp cells, DPP binds to integrin $\alpha_v\beta_1$ via its RDG motif, activating the focal adhesion kinase (FAK) and anchorage-dependent ERK signaling (Eapen et al., 2012). The nuclear translocation of the transcription factor phosphorylated ELK-1 will, in turn, activate DMP1 and DSP (Eapen et al., 2012). In T4-4, a preodontoblastic cell line, DPP upregulates the expression of integrin $\alpha_4\beta_1$ to activate FAK and the AKT-mTOR-NF-κB pathway (Eapen and George, 2015). DPP can also facilitate the survival, proliferation, and terminal differentiation of T4-4 cells (Eapen and George, 2015). Therefore, a positive feedback loop may exist for DSPP expression. Apart from the RGD motif, there is another possible pathway for DSPP to upregulate its own expression. DSPP binds to integrin β_6 via amino acid residues 183-219 (mouse) in its DSP portion, then phosphorylates p38, ERK1/2, Smad1/5/8 (Wan et al., 2016). Phosphorylated Smad 1/5/8 enters

13

the nucleus and binds to -211 to -183 nt in the *Dspp* promoter to activate the transcription of DSPP (Wan et al., 2016).

Several reports pointed out that the C-terminal of DMP1 translocates into the nucleus and regulates the expression of other genes, including DSPP (Gibson et al., 2013d; Narayanan et al., 2006; Siyam et al., 2012). Interestingly, a plausible IRES (internal ribosome entry site) element was also discovered near the boundary between DSP coding region and DPP coding region, which might lead to an isoform of DPP that enters the nucleus (Zhang et al., 2014). However, many questions remain regarding this phenomenon.

Collectively, DSPP is heavily modified post-translationally. These PTMs, such as proteolysis, glycosylation, and phosphorylation, are essential for its multiple functions. Apart from its canonical function, namely, facilitating hydroxyapatite nucleation in dentinogenesis, DSPP also plays many other roles in many other organs, including but not limited to enamel, cementum, and bone. These roles are largely undetermined. Also, it may function as a ligand to activate several signaling pathways for gene regulation; it might even enter the nucleus and regulate gene expression as well. Given its very distinct features from the DNA level to protein level, more effort should be devoted to elucidating its intense regulations, from transcriptional to post-translational levels, and its diverse functions, from dentinogenesis to potential roles throughout the body.

I.2 Dentinogenesis Imperfecta (DGI) and Dentin Dysplasia (DD)

In the 1950s and 1960s, a multidisciplinary team investigated a racially isolated group in Brandywine, Maryland, USA (Hursey et al., 1956; Witkop et al., 1966). The isolate had mixed ancestors of Caucasian, African, and American Indian. They were not accepted by the Caucasian

14

communities, and they did not consider themselves as Africans, either. Such social segregation resulted in an in-marriage pattern within 15 families for over 100 years. The long-term inbreeding mating pattern further made the Brandywine isolate reservoirs of genetic diseases. Among albinism, congenital heart disease, polycystic kidneys, and congenital deafness, the Brandywine isolate specifically demonstrated a high incidence of dentinogenesis imperfecta (DGI), especially in several family lines (Hursey et al., 1956; Witkop et al., 1966).

In the Brandywine isolate, DGI demonstrated an autosomal dominant inheritance. Members with DGI showed severe enamel attrition and dentin discoloration. The pulp chambers and root canals of some teeth in some young affected individuals were enlarged with very thin walls of dentin outlining the teeth, and were referred to as "shell teeth". In contrast, other dental pulps of the same young affected individuals and the dental pulps of the elder affected individuals were obliterated. Some patients requested full dentures to re-establish their occlusion (Hursey et al., 1956).

Before the thorough investigation in Brandywine, DGI had been reported as spontaneous cases in many other areas. The earliest record dates back to 1882 (Barrett, 1883). Taking advantage of a topical fluoride program, Witkop conducted a survey of 64,000 children and suspected families from 42 counties of the State of Michigan. Afterward, he claimed the prevalence of DGI to be 1:6000 to 1:8000 (0.013% to 0.017%) in the general population, which made it the most common genetic disorder in dentin (Witkop, 1957). Recent epidemiological studies reported even higher prevalence of DGI, 0.09% in India (Gupta et al., 2011) and 0.057% in France (Cassia et al., 2017).

I.2.1 Classification

A variety of names have been used to describe the disorders, including "crownless teeth", "hypoplasia of enamel", "hypoplasia of dentin", "Capdepont's teeth", etc. The most popular names of them are "dentinogenesis imperfecta" and "(hereditary) opalescent dentin" (Finn, 1938; Witkop, 1971). For historical reasons, Witkop proposed using "dentinogenesis imperfecta" for brown opalescent teeth found in patients with the systemic disorder osteogenesis imperfecta (OI), whereas isolated abnormalities of dentin formation were referred to as "hereditary opalescent dentin" (Table 1) (Witkop, 1971). A third group was added to this classification as "Brandywine isolate hereditary opalescent dentin", because the above-mentioned "shell teeth" feature was rarely observed for the affected individuals outside the Brandywine isolate (Table 1) (Witkop, 1971).

In 1973, Shields et al. proposed a classification widely accepted in clinical practice today (Table 1) (Shields, 1983; Shields et al., 1973). There were two entities in his classification, dentin dysplasia (DD) and dentinogenesis imperfecta (DGI). Two types of DD were proposed: the radicular type I (DD-I, OMIM#125400) and the coronal type II (DD-II, OMIM#125420). Three types of DGI recognized the three types of diseases proposed by Witkop: the bone-associated type I (DGI-I, OMIM#166200, #166220, #259420), the non-systemic type II (DGI-II, OMIM#125490), the Brandywine isolate type III (DGI-III, OMIM#125500).

I.2.1.1 DD-I (Radicular Dentin Dysplasia)

The discovery of DD-I is quite different from the others. It was first identified as "rootless teeth" in 1920 by Ballschmiede (Kalk et al., 1998). The general morphology and color of teeth in primary and secondary dentitions are within normal range. Radiographically, the

dominant feature, short roots, can be observed, typically with sharp, conical, apical constriction.

The dental pulps of both dentitions are usually absent (Shields et al., 1973). Carroll et al. further

proposed four subtypes for DD-I depending on the extent that the root was developed, primarily

for clinical treatment options (Carroll and Duncan, 1994). Kalk et al. claimed the incidence of

DD-I to be 1:100,000 (Kalk et al., 1998). When Shields proposed the classification, DD-I was

thought to be an autosomal dominant trait (Shields et al., 1973). The inheritance has been widely

supported (Kalk et al., 1998; O. Carroll and Duncan, 1994). In a Turkish family and a Pakistani

family, however, a new "subtype" with extreme microdontia and misshapen teeth was proposed.

The homozygosity of this "subtype" was identified with the mutations in the candidate gene,

SMOC2 (Alfawaz et al., 2013; Bloch-Zupan et al., 2011). This "subtype" should be considered

as another entity.

I.2.1.2 DD-II (Coronal Dentin Dysplasia)

The primary teeth of DD-II patients appear opalescent, with severe occlusal attrition and

obliterated pulps. Compared with DD-I, the root shape of primary teeth is normal. These features

are very typical for both dentitions of DGI-II patients. The permanent teeth of DD-II suffer much

less than the primary ones. The color of permanent teeth is usually normal. The attrition is much

less. However, its radiographic characteristics are unique: the dental pulps of single-root teeth

are of thistle-tube-like shape (a relatively normal-sized pulp chamber with a hairline-like root

canal), usually with pulp stones in its chamber. It is inherited in an autosomal dominant pattern

(Shields et al., 1973; Witkop, 1971). Mutations of DD-II can be identified in dentin

sialophosphoprotein (*DSPP*) gene, the same as DGI-II and DGI-III (Kim and Simmer, 2007).

I.2.1.3 DGI-I (Dental Manifestations in Osteogenesis Imperfecta)

This type of DGI is used to describe the dental manifestations of osteogenesis imperfecta (OI). It is very similar to DGI-II: it has amber translucency, enamel fractures, and narrow pulps. However, these manifestations are more variable in DGI-I, and the primary and permanent dentitions may not be equally affected (Shields et al., 1973). The genetic mutations may be found in COL1A1 or COL1A2 genes, the two genes coding two sorts of α chains in type I collagen (Kim and Simmer, 2007). Apart from OI, there are some other systemic diseases with a dental phenotype similar to DGI-II: Ehlers-Danlos syndrome, Goldblatt syndrome (OMIM184260), Schimke immuno-osseous dysplasia (OMIM#242900), etc.

I.2.1.4 DGI-II (Hereditary Opalescent Dentin)

Amber brown tooth discoloration, sometimes blueish grey, is observed in both dentitions. Severe enamel attrition on the occlusal surface is very common, sometimes even with enamel fractures or enamel dislodged from the underlying dentin. Radiographically, bulbous crowns may be seen. The dental pulps are narrower than normal, sometimes even obliterated (Kim and Simmer, 2007; Shields et al., 1973; Witkop, 1971). The same as DD-II, DGI-II is transmitted in an autosomal dominant manner. The mutations causing DGI-II can also be mapped to the *DSPP* gene (Kim and Simmer, 2007).

I.2.1.5 DGI-III (Brandywine Isolate Hereditary Opalescent Dentin)

The feature that distinguishes DGI-III from DGI-II is the "shell teeth" feature. In some very young patients, their teeth display an extremely thin dentin layer of the tooth around an enlarged dental pulp radiographically. The thin layer of dentin sometimes leads to multiple pulp exposures. This feature is not routinely observed in other young patients, so it was once thought

to be unique to the Brandywine isolate (Shields et al., 1973). Also, patients with "shell teeth" later may develop pulp obliteration with age (Witkop et al., 1966). However, more and more cases with this feature have been reported (Clergeau-Guerithault and Jasmin, 1985; Heimler et al., 1985; Kim et al., 2005; Lee et al., 2009; Lee et al., 2013; Li et al., 2017; Rushton, 1954; Song et al., 2006; Suzuki et al., 1977).

Several researchers have pointed out the disadvantages of this category. Witkop pointed out that it was hard to specify adult patients with DGI-III from those with DGI-II (Witkop, 1988). Other researchers also doubted whether DGI-III was just a variant of DGI-II (Clergeau-Guerithault and Jasmin, 1985; Heimler et al., 1985). Obviously, DGI-III has an autosomal dominant inheritance. The mutations, either from the Brandywine isolate or from cases irrelevant to the Brandywine isolate, can be detected in *DSPP* gene (Hart and Hart, 2007; Kim et al., 2005; Lee et al., 2009; Lee et al., 2013; Li et al., 2017; Song et al., 2006).

Since the genetic causes detected in DD-II, DGI-II, and DGI-III are all from mutations in *DSPP* gene, de La Dure-Molla proposed a new classification system for isolated/non-syndromic dentinogenesis imperfecta, with DD-II being the mild form, DGI-II being the moderate form, and DGI-III being the severe form (Table 1) (de La Dure-Molla et al., 2015).

As the Shields classification is the most acknowledged today, we will use this system in our following text.

I.2.2 DGI Pathological Mechanisms

To date, a total of 42 *DSPP* mutations have been identified (Table 2). These mutations are classified into two categories, *DSPP* 5' mutations and *DSPP* 3' mutations (Wang et al., 2011). *DSPP* 5' mutations include the mutations that locate within the signal peptide coding

region, DSP coding region, and introns. *DSPP* 3' mutations exclusively locate in DPP coding region (exon 5). Eighteen of these mutations belong to *DSPP* 5' mutations so far, whereas the rest 24 are *DSPP* 3' mutations.

DSPP 5' mutations can be further grouped into the followings. Mutations #1-2 altered amino acid residues in the signal peptide coding region. Mutations #3-5 and #11-12 substituted the amino acid residues in the IPV (isoleucine-proline-valine) motif, the first three amino acid residues after signal peptide cleavage site. Mutations #6-10 and #14-17 disrupted the splicing acceptor site (3' splice site) of intron 2 or at the splicing donor site (5' splice site) of intron 3. Two mutations (#13 and #18) did not belong to any of the above. The majority of these mutations cause DGI-II or DGI-III, with the only #1 and #9 resulting in DD-II. Several proposals have been made to explain the mechanisms. The mutations within the signal peptide coding region may affect the removal of the signal peptide (Malmgren et al., 2004; Rajpar et al., 2002). An *in vitro* mammalian cell model suggested that many of the mutations around both ends of exon 3 caused partial or complete skipping of exon 3, with associated nonsense-mediated mRNA decay (Lee et al., 2011c). The skipping of exon 3 led to an in-frame deletion of the protein, with an IPD motif (D for aspartic acid) replacing the IPV motif. These mutations include but are not limited to #6-11 and #13-15, accounting for at least half of the *DSPP* 5' mutations. Later, Dr. Fisher's group proved that IPV motif is essential for the trafficking of the DSPP protein via *in vitro* approaches (von Marschall et al., 2012). By comparing the sequences of several secretory proteins, they proposed that the properties of the first three amino acid residues in a subset of proteins are very critical for protein trafficking: the first residue can be a hydrophobic residue, the second one has to be proline, and the third residue should be a polar but not charged residue (Nam et al., 2014). The Proline in the IPV motif of DSPP is highly conserved among species

20

(Table 3). Other studies have also shown that the proline as the second amino acid residue after signal peptide cleavage site is critical for transporting proteins (Tsukumo et al., 2009). The failure of DSPP trafficking to the Golgi apparatus then extracellular matrix will result in its accumulation in the endoplasmic reticulum (ER). These accumulated DSPP that are highly negatively charged can deplete cations in the ER, especially calcium, which further forms precipitate. The precipitate will trap both the mutant and normal DSPP protein, by either the large negatively charged DPP domain, or the covalent disulfide bridge in the DSP region. Such changes may disrupt ER homeostasis, and cause cell pathology through dominant negative effect (von Marschall et al., 2012; Wang et al., 2011; Yang et al., 2016). The proposed mechanism also helps explain the autosomal dominant pattern of DGI in humans.

As a consequence of the highly repetitive DPP coding region, DNA replication slippage may be responsible for the 3' *DSPP* mutations. The replication slippage may lead to in-frame insertions or deletions, -2 frameshift mutations, or -1 frameshift mutations. The in-frame mutations cause an insertion or deletion (indels) of several amino acid residues without interrupting the reading frame. To date, a total of 32 indels arranged in 36 different patterns have been characterized. None of these indels is likely to cause DGI (McKnight et al., 2008b; Song et al., 2008; Yang et al., 2016). -2 frameshift mutations in the DPP region will introduce a premature stop codon in no more than 13 amino acid residues after the mutation site (Wang et al., 2011). Compared with -2 frameshift mutations, -1 frameshift mutations will not cause nonsense mutation. Instead, the translation will move on until a termination signal appears downstream to the natural DSPP stop codon. The normal DPP mainly consists of aspartic acids and serines. Alternatively, -1 frameshift mutation will give rise to a long chain of hydrophobic amino acid residues. For example, if we delete the first nucleotide of the DPP coding region, a

mutant DPP consisting of 35% Ala (alanine), 23% Val (valine), 20% Thr (threonine), and 12% Ile (isoleucine) will be generated (Wang et al., 2011). All the disease-causing 3' *DSPP* mutations identified so far are -1 frameshift mutations. It is not sure whether these -1 frameshift mutations will affect the trafficking of the mutant DSPP, or even normal DSPP. However, as the hydrophilic acidic domain is vital for the function of DSPP, we may assume that the -1 frameshift mutant DSPP protein is non-functional or even malfunctional. Interestingly, it is likely that the mutations located in the 5' portion of the DPP coding region tend to cause the milder form DD-II (#19-26, #34), whereas the 3' portion mutations potentially lead to the more severe DGI-II or DGI-III. A plausible explanation is that the 5' mutations in DPP coding region are less likely to create a DSPP protein with the highly negatively charged acidic domain, which can entrap the normal DSPP protein (von Marschall et al., 2012). However, this explanation will be feasible only if the mutant hydrophobic DSPP protein is retained in the ER, possibly via the protein quality control system.

The mechanisms of *DSPP* mutations causing the non-systemic DGI are still largely unclarified. Thus, it inspires this research project, aiming at elucidating the underlying molecular pathogenesis of non-systemic DGI.

CHAPTER II

ESTABLISHMENT OF A DENTIN SIALOPHOSPHOPROTEIN (DSPP) KNOCK-IN (KI)

MOUSE MODEL MIMICKING HUMAN DENTINOGENESIS IMPERFECTA (DGI)

II.1 Introduction

A tooth is composed of four major tissues: enamel, dentin, cementum, and pulp. To date, most human DGI cases point out that dentin and enamel are involved in the DGI associated with *DSPP* mutations.

Dentin is a bulk of hard tissue residing between enamel and dental pulp in the crown, or between cementum and the dental pulp in the root of a tooth. It consists of approximately 70% inorganic materials (excluding water), 20% organic materials, and 10% water by weight (Nanci, 2017). The majority of the inorganic material is hydroxyapatite. The organic phase is made up of 90% collagen, mainly type I collagen, and 10% non-collagenous proteins (NCPs), including DPP, DSP, and DMP1. The cells responsible for dentin formation are odontoblasts. Odontoblast cell bodies reside immediately on the pulpal side of the dentin, while odontoblast processes are embedded in dentin. The majority of dentin is circumpulpal dentin. Between circumpulpal dentin and enamel lies a thin layer of first formed dentin, the mantle dentin. The circumpulpal dentin contains numerous dentinal tubules, through which odontoblast processes go. According to the association with the dentinal tubules, circumpulpal dentin is further classified into two portions, the peritubular (intratubular) dentin within the dentin tubules, and the intercellular dentin outside the dentinal tubules. A layer of non-mineralized dentin, namely predentin, resides between circumpulpal dentin and odontoblasts.

Dentinogenesis, or the formation of dentin, is widely considered to be a two-step process. First, the collagen fibers and NCPs are laid down; second, the inorganic hydroxyapatite is deposited onto the collagen scaffold with the guidance of NCPs. DSP and DPP are the major NCPs in dentin. Interestingly, the two cleavage products of DSPP locate differently in dentin, with DSP in the odontoblast process, mineralization front, and dentinal tubules, and DPP mainly in the mineralization front (Hao et al., 2009). The functions of DSP and DPP remain largely unknown. The overexpression of DSP suggests that it may play an inhibitory role for dentin mineralization (Gibson et al., 2013b). The *Dpp*-cKO mouse model, as mentioned previously, indicates that DPP may be involved in the maturation of mineralized dentin (Suzuki et al., 2009).

Enamel is the hardest tissue in the human body. Mature enamel consists of 96% mineral and 4% organic components (Nanci, 2017). The mineral component is hydroxyapatite, the same as dentin. In contrast, the majority of the organic component is amelogenin, instead of collagen. The majority of enamel is structured as enamel rod and interrod, except the initial and final layers. Amelogenesis, or enamel formation, is executed by ameloblasts. Amelogenesis, as well as the life cycle of ameloblast, is divided into three major stages: presecretory, secretory, and maturation stages (Hu et al., 2007). During the presecretory stage, ameloblasts degrade the basement membrane between ameloblasts and the newly formed predentin. Once the basement membrane disappears, secretory ameloblasts develop a specialized structure, the Tomes' process. Secretory ameloblasts secret both enamel matrix proteins and hydroxyapatite, with the former guiding the appositional growth, or the growth in thickness, of the latter. Impaired secretory ameloblasts result in insufficient appositional growth of enamel, or hypoplastic enamel (Hu et al., 2007; Simmer et al., 2010). After the enamel achieves its final thickness, the Tomes' process disappears, and a new basement membrane is formed. During the maturation stage, ameloblasts

transit between ruffled- and smooth-border ameloblasts, secreting proteases to degrade the enamel matrix proteins, and promoting mineral deposition on the sides of previously formed enamel crystals. Failure of organic matrix removal leads to a hypomaturation form of amelogenesis imperfecta (AI), while enamel with deficient mineral deposition is termed hypocalcified enamel (Hu et al., 2007). DSPP is detected in presecretory ameloblasts and early secretory ameloblasts (D'Souza et al., 1997; Hao et al., 2009). However, its function in amelogenesis is unclear.

How *DSPP* mutations lead to DGI has been studied for a long time. Many studies on the functions of DSP and DPP have been carried out *in vitro*. These studies have brought part of DSPP functions to light; however, they are unable to answer how mutations in the *DSPP* gene result in DGI in humans.

The first successful attempt to generate a mutant *Dspp* mouse model, the *Dspp* knock out (*Dspp*-KO, *Dspp* null, or *Dspp*$^{-/-}$) mouse, was reported in 2003 (Sreenath et al., 2003a; Sreenath et al., 2003b). The inheritance pattern of the model is autosomal recessive, which means that only *Dspp*$^{-/-}$ mice display defective phenotypes. The tooth defects of *Dspp*$^{-/-}$ mice include enlarged pulp surrounded by thin dentin walls, widened predentin, pulp exposure, dentin hypomineralization, and compromised dentin-enamel junction (DEJ) (Sreenath et al., 2003a; Verdelis et al., 2016). These phenotypes represent human DGI-III. The enlarged pulp surrounded by thin dentin, referred to as "shell teeth", is consistent throughout the lifespan of *Dspp*$^{-/-}$ mice (Sreenath et al., 2003a). However, the "shell teeth" feature is, for the most part, only observed in very young human patients (Clergeau-Guerithault and Jasmin, 1985; Heimler et al., 1985; Witkop et al., 1966). In addition, the inheritance pattern of non-syndromic DGI in humans is autosomal dominant, instead of autosomal recessive. Therefore, even though this mouse model

has helped substantially to elucidate some functions of DSPP, the underlying mechanisms of human non-syndromic DGI have not been revealed.

Some other mutant *Dspp* mouse models were generated. For example, the 3.6kb-*Col1a1*-promoter-driven normal or D452A *Dspp* mouse models were generated to study the cleavage of DSPP (Zhu et al., 2012b). A 3.6kb-*Col1a1*-promoter-driven *Dsp* mouse model was used to study the function of DSP in dentin and periodontium (Gibson et al., 2013a; Gibson et al., 2014; Gibson et al., 2013b; Gibson et al., 2013c). A 3.6kb-Col1a1-promoter-driven *Dpp* mouse model was generated to investigate the impact of DPP overexpression in dentin and bone (Zhang et al., 2016; Zhang et al., 2018). *Dspp*-promoter-driven *Dsp* mouse model was crossbred with the *Dspp*-KO mouse model to distinguish the functions of DSP and DPP (Suzuki et al., 2009). Amelogenin-promoter-driven *Dsp* and *Dpp* mouse models were used to study the functions of DSP and DSP in amelogenesis (Paine et al., 2005; White et al., 2007). However, none of these mice models mimics the genetic changes in human DGI patients. Therefore, a *Dspp* mouse model carrying a mutation equivalent to human patients is in demand to reveal the molecular pathogenesis of DGI.

A novel powerful gene-editing tool, namely, clustered regularly interspaced short palindromic repeats (CRISPR)/CRISPR-associated protein 9 (Cas9) system, has been developed in the recent years. In this system, CRISPR RNA (crRNA) and trans-activating crRNA (tracrRNA), often engineered into a single guide RNA (sgRNA), are critical for the introduction of endonuclease Cas9 to generate a targeted double-stranded break (DSB) in DNA. A protospacer adjacent motif (PAM) sequence neighboring the targeted DSB is necessary for the binding of Cas9. In the presence of a single-stranded oligodeoxynucleotide (ssODN), which contains the modified nucleotides flanked by sequences homologous to the sequences flanking

DSB, cells can carry out homology-directed repair (HDR) to repair the previously generated DSB and to precisely introduce desired modifications into the targeted gene (Doudna and Charpentier, 2014). The CRISPR/Cas9 system has been used extensively for the generation of animal models recently. Thus, it is a desirable tool for the generation of a *Dspp* knock-in (KI) mouse model.

As discussed previously, *DSPP* mutations in humans are categorized into 5' *DSPP* mutations and 3' *DSPP* mutations. For 5' *DSPP* mutations, many kindreds carries mutations altering the IPV motif, the first three amino acid residues following signal peptide cleavage site (von Marschall et al., 2012). The IPV motif, especially the proline residue, has been claimed to be critical for the trafficking of DSPP (Tsukumo et al., 2009; von Marschall et al., 2012) (Table 2). Interestingly, a c.50C>T, p.P17L mutation caused DGI-II in a 46-year-old Chinese woman, and DGI-III in a 2.5-year-old Korean girl (Lee et al., 2013; Li et al., 2012a). Herein, we selected this mutation for the generation of mouse model, and propose that this *Dspp*-KI mouse model represents human DGI.

II.2 Materials and Methods

II.2.1 Generation of *Dspp*$^{P19L/+}$ KI Mouse Model by CRISPR/Cas9 System

The guide sequence of the sgRNA consisted of 20 nucleotides (nt) located on the antisense strand and directly opposite to the codon 19 of the mouse *Dspp* gene, which was the equivalent of human codon 17, and a typical PAM sequence (AGG) was immediately adjacent to its 3' end (Fig. 2A).

The 199 nt ssODN repair template contained the centrally located intended pathogenic mutation (CCG>CTG) as well as a silent mutation (GCC>GCG) flanked by two arms of

homologous genomic sequence (Fig. 2A). The pathogenic mutation resulted in the substitution of the proline residue at position 19 of mouse DSPP by a leucine residue (P19L), in accordance with the c.50C>T, p.P17L DSPP mutation in humans. The silent mutation did not change the amino acid sequence of mouse DSPP; instead, it prevented the further targeting of sgRNA/Cas9 to the modified sequence.

A mixture of Cas9 mRNA (100 ng/μL), sgRNA (25 ng/μL) and ssODN repair template (100 ng/μL) was microinjected into the cytoplasm of C57BL6/J mouse embryos. The survived embryos were subsequently implanted into pseudopregnant CD1 female mice. All mice generated were analyzed for potential $Dspp^{P19L/+}$ or $Dspp^{P19L/P19L}$ KI founders by polymerase chain reaction (PCR) and DNA sequencing, as described later. The potential founders (F0) were then bred with wild-type C57BL6/J mice to obtain F1 mice and to confirm the germline transmission of the desired mutations. The animal protocols for this study were approved by the Animal Welfare Committee of Texas A&M University, College of Dentistry (Dallas, TX).

A combination of PCR, enzymatic digestion, and DNA sequencing was performed to screen for the $Dspp^{P19L/+}$ mice. Genomic DNA was extracted from mouse tail biopsies. The genomic region around the intended mutation site was amplified by PCR using GoTaq Green Master Mix (Promega) with the following primers, sp276.cel.F (5'-GAGCATGCTGAGGCCCCCACATACC-3') and sp276.cel.R (5'-TGTGTTTGCCTTCATCGAGACCCCA-3'). The PCR program was set as 95 °C for 5 min, followed by 35 cycles of (95 °C for 30 sec, 59 °C for 30 sec, and 72 °C for 45 sec), and 72 °C for 7 min. The PCR products were digested using the HpaII restriction endonuclease, recognizing the CCGG sequence at the targeted site, for the restriction fragment length polymorphism (RFLP) analysis. The PCR products amplified from wild-type mice were completely cleaved by

HpaII into two fragments of 249 bp and 183 bp, whereas the PCR products from any potential founders were either partially digested (heterozygous) or completely undigested (homozygous). The PCR products amplified from the potential founders were further cloned into TOPO vector (Life Technologies Corporation, Grand Island, NY, USA) for DNA sequencing analysis to confirm the presence of correct point mutations and the absence of other undesired modifications in the adjacent loci.

II.2.2 Stereo Microscopy, Plain X-Ray Radiography and Micro-Computed Tomography (μCT)

The mandibles were dissected from 3-, 8-, and 24-week-old $Dspp^{+/+}$, $Dspp^{P19L/+}$, $Dspp^{P19L/P19L}$ mice, fixed in 4% paraformaldehyde overnight, and then stored in 70% ethanol until analysis. The mandibular molars were photographed using a high-precision stereo Olympus SZX16 microscope (Olympus Corporation, Tokyo, Japan). The mandibles were analyzed with a high-resolution Faxitron MX-20 Specimen Radiography system (Faxitron X-ray Corp., Buffalo Grove, IL) at 6s/26kV.

A high-resolution scan in 3.5μm slice increment using a μ-CT35 imaging system (Scanco Medical, Basserdorf, Switzerland) was performed on the left mandibular first molars, at 70 kV, 145 A, and 300 integration time, as previously described (Meng et al., 2015; Zhang et al., 2016). The three-dimensional (3D) structure was reconstructed for dentin and cementum together, and enamel separately. Thresholds were chosen age-specifically based on the visual comparisons, that could tell the targeted tissue apart from its surrounding tissues. For the measurements of dentin thickness, section crossing both the most proximal and distal pulp horns, and with the largest apex openings of both proximal and distal root canals was selected. The lowest point at

the upper border of the roof dentin central concave, and the highest point at the lower border of the floor dentin convex were selected as reference points. Roof dentin thickness and floor dentin thickness were defined as the thickness of dentin on the line determined by the two reference points. The morphometric parameters, including the volume and density, were evaluated using the built-in software for the μCT system.

II.2.3 Backscattered and Resin-Casted Scanning Electron Microscopy (SEM)

The 3- and 24-week-old mandible samples for plain X-ray and μCT were further used for SEM analysis, as described previously (Zhang et al., 2015). The samples were dehydrated in gradient ethanol (from 70% to 100%) and xylene before embedded in methyl methacrylate (MMA). The buccal-lingual sections crossing the middle of the proximal root of the mandibular first molar were chosen. The cut surface was polished and dehydrated, followed by gold coating. Scanning was performed in BES mode in a JEOL JSM-6010 LA SEM (JEOL, Japan).

After the removal of the coating particles and being re-polished, the surface was etched with 10% phosphoric acid for 7 seconds for 3-week-old samples and 14 seconds for 24-week-old samples, and soaked in 5% sodium hypochlorite for 20 minutes twice. Samples were gold-coated and scanned in SEI mode in the same SEM.

II.2.4 Histological Analysis

The mandibular jaws from postnatal 0-day-old, 1-, 3-, and 8-week-old $Dspp^{+/+}$, $Dspp^{P19L/+}$ and $Dspp^{P19L/P19L}$ mice were harvested and fixed in 4% paraformaldehyde in diethyl pyrocarbonate(DEPC)-treated 0.1M phosphate-buffered saline (PBS) for 24 hours, followed by decalcification in 15% ethylenediaminetetraacetic acid (EDTA) (pH 7.4) at 4 °C for 3 days to 2 weeks, age-specifically. The decalcified jaws were then dehydrated in gradient ethanol and

xylene, embedded in paraffin, and cut into 5-µm serial proximal-distal sections for Hematoxylin and Eosin (H&E) staining. Pictures were taken using Olympus BX51 microscope.

Roof predentin thickness was defined as the predentin thickness at the lowest part of the roof dentin central concave on the comparable central section. Floor predentin thickness was defined as the predentin thickness at the highest part of the floor dentin convex on the same section.

II.3 Results

II.3.1 Generation of *Dspp*$^{P19L/+}$ KI Mouse Model by CRISPR/Cas9 System

The portion of sgRNA sequence used to generate targeted DSB, and ssODN used as a template for DNA repair are shown in Fig. 2A. After the microinjection of Cas9 mRNA, sgRNA and ssODN into the cytoplasm of C57BL6/J mouse embryos, and subsequent implantation into pseudopregnant CD1 mice, a total of 9 pups were generated. All 9 pups were first genotyped using a combination of PCR and restriction fragment length polymorphism (RFLP) using the HpaII restriction enzyme (Fig. 2B). The PCR products amplified from mice #3-5, #8, and #9, were cleaved by HpaII into two smaller fragments in the same manner as the wild-type control mouse. The PCR products from mouse #1 and #2 contained abnormally large bands. Only the PCR products from mouse #6 and 7 were partially or completely undigested by HpaII with bands of expected sizes. The DNA sequencing results further confirmed that only mouse #7 carried the desired mutations, including both the disease-causing mutation and the silent mutation (Fig. 2C). This founder mouse was then bred with wild-type C57BL6/J mice to establish the mouse line. DNA sequencing results from the offspring confirmed the germline transmission of the desired mutations (Fig. 2D).

31

II.3.2 A Dentin Phenotype Resembling both DGI-III and DGI-II in Mutant Mice

With the mouse line established, we first examined the overall dentin phenotype of the mutant mice, including $Dspp^{P19L/+}$ and $Dspp^{P19L/P19L}$ mice, compared with the wild-type or $Dspp^{+/+}$ mice. At 3 weeks old, a relatively young age, both the plain X-ray and μCT images of the molars of mutant mice showed enlarged pulp chambers, accompanied by a significantly reduced thickness of pulp chamber roof dentin, and a slightly increased thickness of pulp chamber floor dentin (Fig. 3 A-C and 5A row 1). Quantitative μCT results confirmed the statistical significance of the enlargement of pulp chamber, the decrease in roof dentin thickness, and the increase in floor dentin thickness in mutant mice (Table 4). Although dentin and cementum were hard to be distinguished by μCT, little cementum was deposited at 3 weeks old. Thus, the volume of dentin and cementum together largely represented that of dentin. Quantitative μCT data also showed that significantly reduced dentin was formed in mutant mice (Table 4). The phenotype in the younger mutant mice mimicked DGI-III in humans.

At 8 weeks old, the dental pulp volumes were indistinguishable among the three groups of mice, both visually and quantitatively (Fig. 3 D-F, Fig. 5A row 2, and Table 4). Meanwhile, the significantly reduced thickness of roof dentin and the significantly increased thickness of floor dentin sustained in the mutant mice (Fig. 3 D-F, Fig. 5A row 2, and Table 4).

The reduction in roof dentin thickness and the increase in floor dentin thickness were more evident in 24-week-old mutant mice (Fig. 3 G-I, Fig. 5A row 3, and Table 4). The dental pulps of the mutant mice were almost completely obliterated (Fig. 3 G-I, Fig. 5A row 3, and Table 4). The dentin phenotype of the older mutant mice was similar to that of the human DGI-II.

A substantial amount of roof dentin had been laid down by the end of the first week (Fig. 7 D'-F'). In comparison, the root dentin processes did not contact to close the pulp chamber floor dentin until 2 weeks (Shimazu et al., 2009). As the formation of roof dentin preceded the formation of the floor dentin, the enlarged dental pulp in young mutant mice can be mainly attributed to the reduced roof dentinogenesis. In all the three groups, the roof dentin thickness in 24-week-old mutant mice was less than two fold of the 3-week-old mice. In contrast, the floor dentin thickness grew about 4 times more from 3 weeks to 24 weeks (Table 4). Therefore, the enhanced floor dentin deposition contributed greatly to the dental pulp obliteration in mutant mice.

Collectively, the younger mutant mice displayed a DGI-III phenotype, with enlarged pulp chamber, reduced roof dentin thickness, and increased floor dentin thickness. The older mutant mice developed a DGI-II phenotype, where the dental pulp was almost obliterated. These results resembled the equivalent *DSPP* mutation in human patients: the 2.5-year-old girl and the 46-year-old woman were diagnosed as DGI-III and DGI-II, respectively.

II.3.3 Impaired Dentin Mineralization and Ultrastructure in Mutant Mice

Next, we wondered if the dentin mineralization and ultrastructure were altered in the mutant mice. From the H&E staining of the new-born and 1-week-old samples, the predentin thickness was similar in all the mice (Fig. 7 A-F, and J). However, at 3 weeks old, although the predentin thickness of the chamber floor dentin was not different among the three groups, the predentin thickness of the chamber roof dentin was significantly reduced in the mutant mice (Fig. 7 G-I, and K-L). The predentin thickness was even significantly different between the

33

molars of $Dspp^{P19L/+}$ and $Dspp^{P19L/P19L}$ mice (Fig. 7K). These results implied that the mutant mice possibly had suppression of mineralization inhibition in the predentin.

Because μCT was not able to distinguish dentin from cementum, we performed the density comparison for dentin and cementum together. We were able to see slightly lower dentin and cementum density in the mutant mice throughout the observation period, mostly with statistical difference (Table 4). Even though the mineralization inhibition in the dentin was repressed, the mineralization was defective.

Although we were not able to tell the slight difference in mineral density from backscattered SEM (Fig. 6 A"-C"), the phosphoric acid-etched intertubular dentin surface seemed to contain some lower mineralized areas in the 3-week-old $Dspp^{P19L/P19L}$ mice (Fig. 6F" and F'''), compared with that of 3-week-old $Dspp^{+/+}$ and $Dspp^{P19L/+}$ mice (Fig. 6 D"-E" and D'''-E''').

We further focused on the dentinal tubules and odontoblast processes. From the backscattered SEM at 24 weeks old, fewer dentinal tubules with reduced diameters were observed (Fig. 6H"-I"). From acid-etched samples at 3 weeks old, the odontoblastic processes in $Dspp^{P19L/P19L}$ mice had fewer branches in the mantle dentin (Fig. 6F'''). Moreover, compared with those of $Dspp^{+/+}$ and $Dspp^{P19L/+}$ mice, the odontoblast processes in $Dspp^{P19L/P19L}$ mice retracted from the mantle dentin (Fig. 6F'''). At 24-week-old, the branches of odontoblast processes were still evident near to DEJ in $Dspp^{+/+}$ mice (Fig. 6J"). In strong contrast, hollow dentinal tubules were predominant in dentin near DEJ and pulp, in both $Dspp^{P19L/+}$ and $Dspp^{P19L/P19L}$ mice (Fig. 6K"-L"). In addition, the radicular dentin of $Dspp^{P19L/P19L}$ mice seemed to possess fewer odontoblast processes, compared with $Dspp^{+/+}$ and $Dspp^{P19L/+}$ mice (Fig. 6F'''' and L'''').

In summary, as early as 3 weeks, the mineralization inhibition was suppressed in both $Dspp^{P19L/+}$ and $Dspp^{P19L/P19L}$ mice, while the mineralization was defective in both mutant mice throughout our observation periods. Meanwhile, fewer dentinal tubules and impaired odontoblast processes were evident in both $Dspp^{P19L/+}$ and $Dspp^{P19L/P19L}$ mice.

II.3.4 Compromised Enamel Quality and Dentinoenamel Junction (DEJ) in Mutant Mice

Since DSPP is expressed in presecretory ameloblasts and early secretory ameloblasts transiently, most researchers think that DSPP is not critical for amelogenesis (Wang et al., 2011). We did observe an enamel phenotype very similar to that of human DGI patients in the $Dspp$-KI mouse model. Images of the mandibles dissected from 24-week-old $Dspp^{+/+}$ and $Dspp^{P19L/+}$ mice showed that $Dspp^{P19L/+}$ mice had a rough enamel surface, blunted cusps, and second molar discoloration, which suggested necrotic pulpitis (Fig. 4B and D). The blunt cusps were also clear in 24-week-old $Dspp^{P19L/+}$ and $Dspp^{P19L/P19L}$ mice, indicated by plain X-ray images (Fig. 3 H-I). The significantly reduced enamel volume further confirmed the severe attrition on the enamel throughout the observation periods (Table 4).

Interestingly, although the gross enamel phenotypes of $Dspp^{P19L/+}$ and $Dspp^{P19L/P19L}$ mice were similar, their enamel structures were quite different. Compared with $Dspp^{+/+}$ mice, $Dspp^{P19L/+}$ mice displayed apparent enamel rod structure with shorter range at 3 weeks old (Fig. 6B'). At 24 weeks old, the enamel rod structure was less visible from backscattered SEM (Fig. 6H'). From phosphoric acid-etched enamel, the rods were shorter and thinner (Fig. 6K'). By comparing the 3-week-old and 24-week-old mouse enamel, the enamel of $Dspp^{P19L/+}$ mice was less durable. The $Dspp^{P19L/+}$ mice displayed the scalloped DEJ (Fig. 6E' and K'), similar to

Dspp$^{+/+}$ mice (Fig. 6D' and J'). At 24 weeks, a very obvious gap was observed between enamel and dentin in *Dspp*$^{P19L/+}$ mice (Fig. 6K').

Strikingly, we barely saw any enamel rod structure in *Dspp*$^{P19L/P19L}$ mice (Fig. 6C', F', I', and L'). The DEJ was very smooth, with a smear-like structure filling the gap between enamel and dentin at 3 weeks (Fig. 6F'). At 24 weeks old, the gap was even larger; besides, a wavy internal surface of enamel was observed (Fig. 6L').

Notably, in all mice, we saw increasing enamel density with age, where the enamel densities of 24-week-old mice were statistically higher than those of the 3-week-old (Table 4). Although the enamel mineral can only be deposited from saliva after ameloblasts are gone, it is apparent that the enamel mineralization benefits significantly from saliva after tooth eruption.

In summary, the results of stereo-microscopy images, plain X-ray, µCT, and SEM indicated that the enamel quality and DEJ were compromised in *Dspp*$^{P19L/+}$ and *Dspp*$^{P19L/P19L}$ mice after tooth eruption. However, how the defective enamel and DEJ were developed remained to be answered.

II.3.5 Pathological Morphology of Odontoblasts and Ameloblasts in Mutant Mice

As both dentinogenesis and amelogenesis were impeded in the mutant mice, we traced back to observe their functional cells, odontoblasts and ameloblasts, respectively. In *Dspp*$^{+/+}$ mice, odontoblasts were aligned as a single layer with a highly columnar morphology (Fig. 7D' and G'). In contrast, the height of odontoblasts was diminished in 1-week-old *Dspp*$^{P19L/+}$ and *Dspp*$^{P19L/P19L}$ mice (Fig. 7 E'-F'). In 3-week-old *Dspp*$^{P19L/+}$ and *Dspp*$^{P19L/P19L}$ mice, much less polarized irregular odontoblasts constituted the odontoblast layer (Fig. 7 H'-I'). No obvious difference was observed in the floor odontoblasts (Fig. 7 H''-I'').

36

Healthy ameloblasts at early secretory and secretory stages were highly polarized and columnar, with their Tomes' processes attaching to the forming outer enamel (Fig. 7D"). However, in 1-week-old $Dspp^{P19L/+}$ and $Dspp^{P19L/P19L}$ mice, the height of ameloblasts, from presecretory stage to secretory stage, was reduced (Fig. 7 E"-F"). The cellular content seemed to condense, instead of evenly distributed throughout the cell (Fig. 7 E"-F"). Besides, the Tomes' processes easily detached from the forming enamel, upon histological processing (Fig. 7 E"-F").

Since the pathological morphology of odontoblasts and ameloblasts was observed in the mutant mice, in the next chapter, we will further investigate the pathological conditions in both odontoblasts and ameloblasts at a molecular level, to elucidate the underlying mechanisms of DGI.

II.4 Discussion

A mouse model for studying the mechanisms of a particular disease should be carefully selected. Most studies on gene functions rely on KO animal models, in which the expression of a specific gene is nullified. However, this does not represent the natural changes in human patients. Fortunately, more and more gene editing tools become available today. One of them is the CRISPR/Cas9 system. Here, we reported the first DGI mouse model generated by CRISPR/Cas9 system, which carries a $Dspp$ mutation equivalent to that observed in the human patients.

Although CRISPR/Cas9 may induce off-target mutations at the genomic loci with sequences similar to the target site, it was unlikely that the observed dental phenotype of the $Dspp^{P19L/+}$ mice was caused by or partially attributed to any non-specific off-target mutations. As we BLASTed the 23 nt gRNA sequence as shown in Fig. 2A using Ensembl by EMBL-EBI

(Zerbino et al., 2018), the only gene locus in mouse apart from *Dspp* that was targeted by the 3'

16 nt sequence located in mouse chromosome 17, not within any protein-coding gene,

pseudogene, or RNA gene. If we BLASTed the 199 nt ssODN sequence, it only targeted to the

Dspp gene in mouse. In addition, we analyzed the dental phenotype of F3 and the generations

after F3. If there was any off-target mutation in founder #7, it should be diluted by breeding with

wild-type mice. Moreover, we found that the dental phenotype was consistent throughout all

generations examined and was well segregated by the intended mutations in the *Dspp* gene. Most

importantly, the $Dspp^{P19L/+}$ mice recapitulated the tooth phenotype of human patients carrying

DSPP c.50C>T, p.P17L mutation (Lee et al., 2013; Li et al., 2012a). Therefore, we concluded

that the single amino acid substituted in DSPP accounted for the dental phenotype of the

$Dspp^{P19L/+}$ mice.

Currently, the clinical diagnosis of DGI and DD is heavily impacted by the Shields

classification of DD and DGI (Shields et al., 1973). An effort in the clinical diagnosis is to

segregate DGI-II from DGI-III, as they both severely affect deciduous and permanent dentitions.

The major difference between DGI-II and DGI-III is that the teeth of the former are represented

by pulp obliteration, but the teeth of the latter are featured as "shell teeth". Interestingly, in the

Dspp-KI mouse model we generated, we observed enlarged pulp chamber, recapitulating DGI-

III, at a younger age; with age, these mice developed smaller pulp chamber, or partial pulp

chamber obliteration, resembling DGI-II. Notably, the roof dentin thickness of the pulp chamber

was reduced at all ages examined in the mutant mice, whereas the floor dentin thickness of the

pulp chamber was always increased in the mutant mice. The former may account for the enlarged

pulp chamber at the early stage, while the latter may explain the partial pulp obliteration at the

later stage. However, there is no human report documenting the changes in the roof or floor dentin thickness of the pulp chamber so far.

Changes in dentin mineralization and ultrastructure were reported in human DGI cases. Lower mineralized "hyaline areas" were described in the dentin of human patients (Malmgren et al., 2004). Fewer dentin tubules with reduced diameter from mantle dentin to circumpulpal dentin were also reported (Clergeau-Guerithault and Jasmin, 1985; Jasmin and Clergeau-Guerithault, 1984; Levin et al., 1983; Song et al., 2006; Suzuki et al., 1977). We confirmed these findings in our mouse model. Evidently, we also observed retracted odontoblast processes in the mutant mice.

Although DSPP is only expressed in presecretory and early secretory ameloblasts transiently, enamel phenotype in erupted teeth of DGI patients has been reported for decades. Enamel was reported to be thinner, or even lost in some cases (Clergeau-Guerithault and Jasmin, 1985; Suzuki et al., 1977), but relatively normal in others (Jasmin and Clergeau-Guerithault, 1984; Malmgren et al., 1988). Enamel rod structure was missing (Song et al., 2006; Suzuki et al., 1977); instead, a laminar-type pattern was observed (Song et al., 2006). Vertical bands in hypoplastic enamel were reported in young patients (Wang et al., 2011). Relatively smooth DEJ without the typical scalloped shape was consistently reported (Clergeau-Guerithault and Jasmin, 1985; Jasmin and Clergeau-Guerithault, 1984; Song et al., 2006; Suzuki et al., 1977). In *Dspp*-KO mice, a compromised DEJ was reported; however, no major differences in mature enamel was demonstrated (Verdelis et al., 2016). Here, we confirmed reduced enamel volume after tooth eruption. However, the missing enamel rod structure and DEJ lacking scalloped contour were only observed in $Dspp^{P19L/P19L}$ mice. Moreover, characterization of unerupted enamel is in

demand to distinguish whether the enamel defects observed in erupted tooth are developmental or secondary defects.

The visual and quantitative results of dentin explained the findings in human DGI cases. Regarding the c.50C>T, p.P17L *DSPP* mutation in humans, the 2.5-year-old Korean girl was diagnosed as DGI-III, but the 46-year-old Chinese woman was recognized as DGI-II (mutation #5 in Table 2) (Lee et al., 2013; Li et al., 2012a). Recently, a Caucasian family was also reported with the same mutation, with the adult affected members diagnosed as DGI-II (unpublished data from Drs. Simmer and Hu Lab). Within the pool of isolated DGI cases, DGI-II and DGI-III can be identified in the same families. Long-term follow-up in affected Brandywine children (*DSPP* mutation identified as c.49C>T, p.P17S; mutation #4, family #6 in Table 2) (Hart and Hart, 2007) also showed that the enlarged dental pulps of "shell teeth" were gradually obliterated (Witkop et al., 1966). In a Korean family carrying a c.53T>A, p.V18D *DSPP* mutation (mutation #12, family #22 in Table 2), the 2.5-year-old boy was determined as DGI-III, whereas the elder family members were diagnosed as DGI-II (Lee et al., 2009). A similar phenomenon was observed in a Chinese family carrying a c.133C>T, p.V18_Q45del *DSPP* mutation as well (mutation #13, family #26 in Table 2) (Song et al., 2006). Also, for the same mutations causing DGI-II and DGI-III in different families (mutation #4, #5, and #11-13 in Table 2), DGI-III was always identified in young patients. In contrast, DGI-II was observed in some young patients and all the adult patients. Herein, our $Dspp^{P19L/+}$ KI mouse model, with DGI-III phenotype developed into DGI-II phenotype with age, potentially resembled the 5' *DSPP* mutations.

The changes observed in our mouse model may not represent all human DGI cases. Many isolated DGI caused by 3' *DSPP* mutations should be carefully examined in separate models. Many of them are diagnosed as DD-II, in which the enamel displays normal appearance in

40

permanent dentition. Since mice only have one dentition, a potential challenge is how a mouse model can show the differences between primary and secondary dentitions in humans. Moreover, even though the rest of isolated DGI cases caused by 3' *DSPP* mutations were diagnosed as DGI-II, the underlying mechanisms may be distinct. In addition, 5' *DSPP* mutations #1 and #6 resulted in DD-II, which cannot be explained by this model. Another interesting exception is the only "shell teeth" case documented in adult human patient reported in 1954, where a 21-year-old male in England with non-syndromic "shell teeth" displayed enlarge pulp cavities in many teeth (Rushton, 1954). In that time genomic sequencing technique was far from available, we are not able to tell whether this phenotype is the result of *DSP*P mutation. However, its phenotype was quite similar to that of *Dspp*-KO mice with persisting enlarged dental pulp.

In conclusion, we used CRISPR/Cas9 system to generate a *Dspp*-KI mouse model, representing human DGI patients, particularly for the majority of those caused by 5' *DSPP* mutations. The successful establishment of the DGI mouse model allows us to examine the molecular pathogenesis further in the next chapter.

CHAPTER III

UNFOLDED PROTEIN RESPONSE (UPR) ELICITED BY DENTIN

SIALOPHOSPHOPROTEIN (DSPP) MUTATION PLAYS A MAJOR ROLE IN

DENTINOGENESIS IMPERFECTA (DGI).

III.1 Introduction

Endoplasmic reticulum (ER) is a critical organelle for secretory proteins. After their

synthesis at ribosomes, secretory proteins translocate into the ER, which is responsible for their

proofreading, folding, assembly, and part of modifications. Professional secretory cells,

including β cells in the pancreatic islets, hepatocytes, osteocytes, odontoblasts, and ameloblasts,

may have to cope with a condition called ER stress, when a large burden of unfolded proteins

accumulate in the ER (Bernales et al., 2006). These cells rely on a collection of signaling

pathways, together termed unfolded protein response (UPR), for sensing and resolving the stress.

Three ER stress sensors, ATF6 (activating transcription factor 6), PERK [double-stranded RNA-

activated protein kinase (PER)-like ER kinase], and IRE1 (inositol-requiring enzyme 1), play

principal roles in UPR (Walter and Ron, 2011). All three pathways can induce the expression of

genes to increase protein folding capacity. Besides, PERK and IRE1 pathways can decrease

protein load in the ER. PERK and IRE1 pathways are also involved in cell fate decision if ER

stress persists (Walter and Ron, 2011).

ATF6 is first synthesized as an ER transmembrane protein. Upon ER stress, it is

delivered to Golgi complex, and cleaved by site-1 and site-2 protease (Shen et al., 2002; Ye et

42

al., 2000). Then, the N-terminal cytosolic ATF6 acts as a transcription factor to activate the expression of genes, such as BiP, GRP94, and XBP1 (Yoshida et al., 2001; Yoshida et al., 2000).

Upon the accumulation of unfolded proteins, PERK on the ER membrane can be activated by oligomerization and autophosphorylation (Korennykh and Walter, 2012). It can phosphorylate eIF2α to shut down global translation initiation to reduce protein load for the ER (Harding et al., 1999; Scheuner et al., 2001). However, some mRNAs, such as the mRNA for the transcription factor ATF4, can be preferentially translated (Scheuner et al., 2001). Targets of ATF4 include CHOP and GADD34. CHOP is involved in apoptosis, whereas GADD34 can protect cells when prolonged protein translation inhibition by eIF2α phosphorylation occurs (Marciniak et al., 2004; Novoa et al., 2001).

While ATF6 and PERK are present only in metazoan cells, IRE1 is conserved in eukaryotes. When cells encounter ER stress, IRE1 oligomerizes and autophosphorylates to activate its ribonuclease (RNase) domain (Cox and Walter, 1996; Credle et al., 2005; Gardner and Walter, 2011; Pincus et al., 2010). The activated RNase domain functions in two mechanisms. Upon minor activation of IRE1, the RNase domain unconventionally splices XBP1 mRNA at a dual stem-loop structure to generate a transcription factor XBP1s, which further upregulates the expression of proteins involved in protein folding, ER expansion, and ER-associated degradation (ERAD) (Aragon et al., 2009; Calfon et al., 2002; Cox and Walter, 1996). If the stress is elevated, regulated IRE1-dependent decay (RIDD) is activated to degrade other mRNAs selectively, the majority of which contain stem-loop structure (Han et al., 2009; Hollien et al., 2009; Hollien and Weissman, 2006; Moore and Hollien, 2015). Thus, RIDD decreases the protein load for the ER. Moreover, IRE1 can also induce apoptosis through the JNK pathway (Urano et al., 2000).

Obviously, UPR is essential for odontoblasts and ameloblasts. For example, mutations in amelogenin and enamelin can cause amelogenesis imperfecta (AI) via UPR (Barron et al., 2010; Brookes et al., 2014; Brookes et al., 2017). Besides, *DSPP* mutations can also cause its accumulation within the ER (von Marschall et al., 2012). However, how UPR is involved in DGI is largely unknown. Here, we propose that UPR plays a major role in DGI, which is caused by *DSPP* mutations.

III.2 Materials and Methods

III.2.1 Proliferation and Apoptosis Assays

Bromodeoxyuridine (BrdU) staining was performed to evaluate the proliferative level, as described previously (Zhang et al., 2016). The 1- and 3-week-old mice were injected with BrdU (100μg/g, Sigma) twice, 24 hours and 1.5 hours before harvest. The BrdU-labelled cells were detected using a BrdU staining kit (Invitrogen), according to the manufacturer's instruction.

Apoptosis analysis was performed for the postnatal 0-day-old, 1- and 3-week-old mice using the TACS TdT *In Situ* Apoptosis Detection Kit (Trevigen), according to the manufacturer's instruction.

III.2.2 *In Situ* Hybridization (ISH)

ISH was performed to detect the mRNA as previously described (Meng et al., 2015; Zhang et al., 2015). Digoxigenin(DIG)-labelled (Roche) mouse antisense cRNA probes for a 1.1kb DSPP fragment, a 0.8kb DMP1 fragment, and a 0.5kb type I collagen fragment were generated. After antigen retrieval by protease K (10μg/mL for 5 min, Ambion), sections were hybridized with 1μg/mL probes at 65 °C for 16 hours. Following stringent washes and RNase A treatment (5μg/mL for 45 min at 37 °C, Ambion), sections were blocked, immunostained with an

44

anti-digoxigenin antibody conjugated to alkaline phosphatase (1:2000, Roche), and developed

with an NBT/BCIP (nitro blue tetrazolium/5-bromo-4-chloro-3-indolyl-phosphate) substrate

system (Roche). Counterstain with nuclear fast red (Sigma) was performed.

III.2.3 Immunohistochemistry (IHC)

IHC was carried out to detect the protein amount and localization as previously described

(Meng et al., 2015; Zhang et al., 2016). The following antibodies were used: rabbit polyclonal

anti-DSPP (1:1000, from Dr. Qin), rabbit polyclonal anti-DMP1 (1:800, #857 from Dr. Qin),

rabbit monoclonal anti-GRP78 BiP (1:200, Abcam), rabbit polyclonal anti-IRE1α (pSer724)

(1:200, Novus), rabbit polyclonal anti-XBP1 (1:400, Novus), rabbit polyclonal anti-p-Smad1/5/8

(pSer463/Ser465) (1:50, Santa Cruz), and biotinylated goat anti-rabbit IgG(H+L) (1:200, Vector)

antibodies. After antigen retrieval by sodium citrate and endogenous peroxidase quenching,

sections were blocked by 3% bovine serum albumin (BSA) and 10% normal goat serum (NGS)

in 0.1M PBST (0.1M PBS with 0.01% Tween-20), and incubated with primary then secondary

antibodies diluted in 2% NGS. The signals were visualized with the DAB (3,3'-

diaminobenzidine) kit (Vector Laboratories). Counterstain was performed by methyl green

(Sigma).

III.2.4 Mouse Molar RNA Extraction, Reverse Transcription, and Quantitative PCR

The 3-week-old $Dspp^{+/+}$ and $Dspp^{P19L/+}$ mice, four mice in each group, were subjected to

molar RNA extraction. Both the maxillary and mandibular first and second molars were

extracted from each mice and were freshly frozen by liquid nitrogen. A total of 8 molars per

mice were crushed into powder and transferred to an RNase-free EP tube. RNA extraction was

performed using the RNeasy Mini Kit (QIAGEN), according to the manufacturer's instruction.

After RNA extraction, 500ng RNA from per mice was applied for gDNA elimination and reverse transcription using the QuantiTect Reverse Transcription Kit (QIAGEN), according to the manufacturer's instruction. cDNA samples were 1:8 diluted before quantitative PCR (qPCR).

Quantitative PCR for RNA extracted from mouse molars was performed using the GoTaq qPCR Master Mix (Promega), according to the manufacturer's instruction. The qPCR program was set as 95 °C for 3 min, followed by 40 cycles of (95 °C for 30 sec, 60 °C for 60 sec, and plate read), and 72 °C for 7 min. Table 5 showed the primers used in this study. A BioRad CFX96 machine with its built-in software was used for quantitation.

III.2.5 DNA Constructs

Two DSPP DNA constructs were generated in the pcDNA3 backbone. A hemagglutinin (HA) tag was inserted into the N-terminal portion of DPP region of mouse normal DSPP or P19L-DSPP cDNA sequences before inserted into the multiple cloning site of pcDNA3 (Fig. 12A). A DMP1 DNA construct was generated in the pcDNA3 backbone, with an HA tag inserted into the N-terminal of the 57kDa fragment as well (Liang et al., 2016). Normal human IRE1α sequence and three IRE1α variants, K599A-IRE1α with an impaired ATP-binding pocket in the kinase domain, and N906A- or K907A-IRE1α with defective RNase domain, were also inserted into the pcDNA3 plasmid. (Han et al., 2009) All constructs were generated by PCR or by site-directed mutagenesis using the QuickChange mutagenesis kit (Stratagene). The modifications on the constructs were confirmed by DNA sequencing. Empty vector pcDNA3 was used as a control.

III.2.6 Cell Culture and DNA Transfection

17IIA11 mouse odontoblast-like cells and 293EBNA (human embryonic kidney 293

Epstein-Barr Virus Nuclear Antigen) cells were cultured in Dulbecco's Modified Eagle's Medium (DMEM) with the addition of 10% fetal bovine serum (FBS) in a humidified incubator with 5% CO_2 at 37 °C. DNA plasmid was transfected into cells using the X-tremeGENE 9 reagent (Roche), according to the manufacturer's instruction.

III.2.7 mRNA Stability Analysis

For mRNA stability analysis, cell culture media were changed to serum-free DMEM with 1µg/mL Actinomycin D (Sigma), an RNA synthesis inhibitor. Total RNA was harvested using the TRIzol Reagent (Ambion) with Chloroform (Sigma), according to the manufacturer's instruction, at 0, 2, 4, 8 hours after RNA synthesis inhibition.

RNase-free DNase I (Ambion) was used to eliminate gDNA and transfected DNA constructs, according to the manufacturer's instruction. DNase I was inactivated by 1:1 phenol-chloroform (Fisher Scientific) extraction. Reverse transcription was performed using the QuantiTect Reverse Transcription Kit (QIAGEN). Samples were 1:4 diluted before qPCR. qPCR was performed in the same way as described above.

III.2.8 Western-blotting Analysis

For western-blotting analysis, cell culture media were changed to serum-free DMEM during transfection. Total cell lysate and conditioned media were harvested 48 hours after transfection for western-blotting analysis.

The western-blotting analysis was performed as previously described (Liang et al., 2016). Total cell lysate or conditioned media were electrophoresed on self-casted 8% or commercial available 4-15% gradient (BioRad) SDS-PAGE (sodium dodecyl sulfate-polyacrylamide gel electrophoresis) gels, and transferred to a PVDF membrane (EMD

Millipore). The membranes were then blocked in 5% milk (Labscientific), and immunoblotted with antibody incubation. Antibodies used for western-blotting were: mouse monoclonal anti-HA.11 antibody (1:1000, Covance), mouse monoclonal anti-IRE1α antibody (1:1000; Santa Cruz Biotechnology), horseradish peroxidase (HRP)-conjugated rabbit polyclonal anti-IRE1α (pSer724) antibody (1:5000; Novus), peroxidase-conjugated mouse monoclonal anti-β-actin antibody (1:50000; Sigma), HRP-conjugated goat anti-rabbit IgG antibody (1:2000; Santa Cruz Biotechnology), and HRP-conjugated goat anti-mouse IgG antibody (1:1500; Santa Cruz Biotechnology). The immunoblotted membraned were detected with ECL^{TM} Chemiluminescent detection reagents (Pierce Biotechnology, Inc.), and imaged by a CL-XPosure film (Pierce Biotechnology, Inc.).

III.2.9 Immunofluorescent Staining

Immunofluorescent staining was conducted as described previously (Liang et al., 2016). Transfected cells were plated into 4-well chamber slides (LAB-TEK) 24 hours after transfection, and were cultured in the chamber for another 24 hours before the immunofluorescent staining. After fixation and blocking, the transfected cells were incubated with mouse anti-HA.11 monoclonal antibody (1:1000; Covance), which targeted HA-tagged DSPP, together with Golgi complex-recognizing rabbit anti-GM130 polyclonal antibody (1:1000, Abcam), or endoplasmic reticulum (ER)-recognizing rabbit anti-calreticulin polyclonal antibody (1:1000, Santa Cruz Biotechnology). Fluorescent secondary antibodies were used: Alexa Fluor 555 conjugated goat anti-mouse IgG(H+L) (1:1000; Invitrogen) and Alexa Fluor 488 conjugated goat anti-rabbit IgG(H+L) (1:1000; Invitrogen). Counterstain was performed with DAPI. A Leica DM6000 CFS confocal microscope was used to image the immunofluorescent-stained cells.

III.3 Results

III.3.1 Reduced DSPP mRNA in Odontoblasts and Ameloblasts of Mutant Mice

To explore the molecular mechanisms in which P19L-DSPP caused DGI phenotype in mutant mice, we started with detecting DSPP in developing teeth, at both mRNA and protein levels.

Using an antisense cRNA DSPP probe, we performed ISH on 1-week-old and 3-week-old mouse molars. In $Dspp^{+/+}$ mice, DSPP mRNA was strongly detected in the roof-forming odontoblasts in the pulp chamber at 1 and 3 weeks old, and in the floor-forming odontoblasts in the pulp chamber at 3 weeks old (Fig. 8A', G', and G"). However, the DSPP mRNA signal in the roof- and floor-forming odontoblasts was much weaker in $Dspp^{P19L/+}$ mice, at both 1 and 3 weeks old (Fig. 8B', H', and H"). The signal was even weaker in $Dspp^{P19L/P19L}$ mice (Fig. 8C', I', and I"). Similarly, in 1-week-old $Dspp^{+/+}$ mice, DSPP mRNA was detectable in the presecretory and early secretory ameloblasts, near the Hertwig's epithelial root sheath (HERS) (Fig. 8A"). In contrast, the signal was much weaker in the presecretory and early secretory ameloblasts of $Dspp^{P19L/+}$ mice, and barely detectable in $Dspp^{P19L/P19L}$ mice (Fig. 8B" and C"). To further quantify the results, total RNA was extracted from 3-week-old mouse molars. As in Fig. 8M, the DSPP mRNA in molars of $Dspp^{P19L/+}$ mice was about 1/8 of that of the $Dspp^{+/+}$ mice, indicating that the DSPP mRNA in mutant mice was dramatically reduced.

We further wondered if P19L-DSPP mRNA was unstable after transcription, so we overexpressed normal DSPP, P19L-DSPP, or their combination in 293EBNA cells. After RNA synthesis inhibition by Actinomycin D, all of them degraded very similarly: within about 2 hours, they were degraded to about 30% of their original levels (Fig. 12B).

Herein, the DSPP mRNA was dramatically reduced both in odontoblasts and ameloblasts in *Dspp*$^{P19L/+}$ and *Dspp*$^{P19L/P19L}$ mice, compared with *Dspp*$^{+/+}$ mice. However, *in vitro* results showed that the stability of normal DSPP and P19L-DSPP mRNA was similar, indicating some specific mechanisms were regulating the degradation of DSPP mRNA.

III.3.2 Intracellular Retention of DSPP in Odontoblasts and Ameloblasts of Mutant Mice

We further used a polyclonal antibody against DSP to perform IHC. In 1-week-old mice, the signal was strongly detected in both odontoblasts and dentin matrix (Fig. 8 D-F). For signal within odontoblasts in *Dspp*$^{+/+}$ mice, it was orderly arranged in the area distal to the nucleus (Fig. 8D"); in contrast, the signal in *Dspp*$^{P19L/+}$ and *Dspp*$^{P19L/P19L}$ mice was throughout the odontoblasts (Fig. 8 E" and F"). The signal in the dentin matrix in all three groups of mice was similar in intensity, and was mainly within the dentinal tubules (Fig. 8 D'-F'). Similarly, there was only weak DSP signal detected in ameloblasts of *Dspp*$^{+/+}$ mice (Fig. 8D"), but very profound DSP signal was detected in presecretory ameloblasts and early secretory ameloblasts of *Dspp*$^{P19L/+}$ and *Dspp*$^{P19L/P19L}$ mice (Fig. 8 E" and F").

In 3-week-old mouse molars, DSP was strongly detected within the odontoblasts (Fig. 8 J-L, J'-L', and J"-L"). A significant amount of DSP was detected in the dentinal tubules of roof dentin matrix (Fig. 8J'); however, the signal in the dentin matrix of *Dspp*$^{P19L/+}$ and *Dspp*$^{P19L/P19L}$ mice was much weaker, compared with that of *Dspp*$^{+/+}$ mice (Fig. 8 K' and L'). Considering that the amount of DSPP mRNA was much less in *Dspp*$^{P19L/+}$ and *Dspp*$^{P19L/P19L}$ mice, it suggested that the proportion of intracellularly accumulated DSP was dramatically elevated in the mutant mice. Interestingly, a notable amount of DSP was detected in the pulp cells apart from

odontoblasts in $Dspp^{+/+}$ mice (Fig. 8J); however, these signals were mostly missing in $Dspp^{P19L/+}$ and $Dspp^{P19L/P19L}$ mice (Fig. 8 K and L).

We further employed *in vitro* approaches to confirm our findings. By transiently transfecting 293EBNA cells with normal DSPP, we were able to see that most DSPP signal was detected in the conditioned medium, whereas very little amount of the signal was seen in the cell lysate (Fig. 12C, lane 2 and 5). The results were reversed, if 293EBNA cells were transfected with P19L-DSPP: most of the DSPP signal was detected in the cell lysate, with very little amount secreted to the conditioned medium (Fig. 12C, lane 3 and 6). Careful examination of the DSPP molecular weight, we saw the intracellular retained P19L-DSPP had only one strong sharp band (Fig. 12C, lane 3). In contrast to the intracellular P19L-DSPP (Fig. 12C, lane 3), the normal DSPP in the cell lysate (Fig. 12C, lane 2), the secreted normal DSPP (Fig. 12C, lane 5), and the secreted P19L-DSPP (Fig. 12C, lane 6) had a sharp band with the molecular weight slightly higher than the accumulated P19L-DSPP, and a smear with even higher molecular weights. These results implied that the intracellularly located P19L-DSPP lacked certain PTMs.

We further used confocal microscopy to determine the subcellular location of P19L-DSPP in 17IIA11 cells. We observed that normal DSPP was colocalized with Gm130, a cis-Golgi resident protein (Fig. 12D, upper row). In contrast, P19L-DSPP was co-localized with Calreticulin, an ER resident protein (Fig. 12D, lower row). The ER retention of P19L-DSPP is in accordance with missing certain PTMs previously proposed, because some PTMs occur in Golgi complex.

In summary, our results suggested that P19L-DSPP was accumulated within the ER in the odontoblasts of the $Dspp^{P19L/+}$ and $Dspp^{P19L/P19L}$ mutant mice.

III.3.3 Increased Amount of DMP1 in Dentin Matrix of Mutant Mice

Due to the similarities between DSPP and DMP1, we further explored DMP1 localization

in $Dspp^{P19L/+}$ and $Dspp^{P19L/P19L}$ mice. At mRNA level, DMP1 expression in odontoblasts was

relatively low in $Dspp^{+/+}$ mice at 3 weeks old (Fig. 9A). However, it was dramatically increased

in $Dspp^{P19L/+}$ and $Dspp^{P19L/P19L}$ mice, both in the roof- and floor-forming odontoblasts (Fig. 9 B-

C). Results from qPCR confirmed that DMP1 expression was increased about 5 times in the

molars of $Dspp^{P19L/+}$ mice, compared with that of $Dspp^{+/+}$ mice (Fig. 9M). Using an antibody

against the C-terminal of DMP1, DMP1 signal was detected in 3-week-old teeth restricted to

predentin in $Dspp^{+/+}$ mice (Fig. 9D'). However, DMP1 was strongly positive throughout the

dentin matrix in $Dspp^{P19L/+}$ and $Dspp^{P19L/P19L}$ mice, mainly in the dentinal tubules (Fig. 9 E'-F').

Very little DMP1 was detected in odontoblasts, implying that no intracellular retention of DMP1

was present (Fig. 9 D'-F').

Since odontoblasts synthesize a great amount of type I collagen, and common regulatory

elements were shared by $Dspp$ and type I collagen promoters (Chen 2008), we also examined the

expression of type I collagen mRNA at 3 weeks. Type I collagen expression was very similar in

molars of all three groups of mice (Fig. 9 G-I). Results from qPCR also confirmed that the

expression of type I collagen (Fig. 9N), as well as HSP47 (heat shock protein 47), the chaperone

assisting the folding of collagen, was approximately the same in molars between $Dspp^{+/+}$ and

$Dspp^{P19L/+}$ mice (Fig. 11L).

Apart from DMP1 and type I collagen, we also examined the expression of some other

dentin matrix proteins by qPCR. However, we did not recognize any differences in the

expression of bone sialoprotein (BSP), osteocalcin (OC), or osteopontin (OPN) between

$Dspp^{P19L/+}$ and $Dspp^{+/+}$ mice (Fig. 9 O-Q).

As mentioned previously, a predominant signaling pathway regulating DSPP expression is the BMP2 signaling pathway. Herein, we examined the level of the canonical BMP2 pathway effectors, phosphorylated Smad1/5/8 at 3 weeks by IHC. Fig. 9 J-L, and J'-L' showed that the activation level of this pathway was similar in all three groups of mice.

We also wondered if proliferation and apoptosis levels were altered in the teeth of mutant mice. Using BrdU assay, we were able to see that most of the proliferating cells located near the HERS and the future chamber floor dentin at 1 week old (Fig. 10 A-C, and A'-C'), and the proliferation signal was about the same among the three groups of mice. At 3 weeks, proliferation signal was randomly distributed in the pulp, and was similar in the three groups of mice (Fig. 10 D-F, and D'-F'). We also used TdT to detect apoptotic signal in the teeth. However, we barely found any apoptotic signal in all the mouse molars (Fig. 10 G-O).

In summary, DMP1 expression was substantially increased in the odontoblasts, and secreted to the dentinal tubules in $Dspp^{P19L/+}$ and $Dspp^{P19L/P19L}$ mice. Its localization in the dentinal tubules, where less DSP was detected in $Dspp^{P19L/+}$ and $Dspp^{P19L/P19L}$ mice, implied that it might compensate for the function of DSP in this region. However, the type I collagen expression, phosphorylated Smad1/5/8 level, proliferation and apoptosis levels were similar among the three groups of mice.

III.3.4 Unfolded Protein Response Regulated the Expression of DSPP

As the mutant protein accumulated in the ER, we further asked whether it induced ER stress and unfolded protein response (UPR). We first examined some chaperones. BiP, an important chaperone assisting protein folding, was downregulated in both roof- and floor-forming odontoblasts of $Dspp^{P19L/+}$ and $Dspp^{P19L/P19L}$ mice at 3 weeks (Fig. 11 A-C, and A'-C').

qPCR results showed that BiP mRNA was downregulated in the $Dspp^{P19L/+}$ mice to about 70% of the $Dspp^{+/+}$ mice (Fig. 11J). Another essential chaperone, HSP90B, was also reduced in the $Dspp^{P19L/+}$ mice to about 60% of the $Dspp^{+/+}$ mice (Fig. 11K). The downregulation of chaperone proteins at 3 weeks may be a chronic response to the accumulated mutant DSPP. However, its downregulation was in accordance with the reduced nascent protein load entering the ER, as a consequence of the decreased DSPP mRNA in odontoblasts of $Dspp^{P19L/+}$ and $Dspp^{P19L/P19L}$ mice.

For the three UPR pathways, we first examined the ATF6 pathway, as it is the acute responder upon ER stress in mammalian cells. At 3 weeks, no difference was demonstrated from ATF6 mRNA level between $Dspp^{P19L/+}$ and $Dspp^{+/+}$ mice (Fig. 11M).

Next, we examined the PERK pathway by qPCR. Although we were not able to identify differences in PERK, ATF4, or GADD34 at mRNA level between $Dspp^{P19L/+}$ and $Dspp^{+/+}$ mice at 3 weeks (Fig. 11 N, O, and Q), CHOP mRNA was upregulated in $Dspp^{P19L/+}$ mice to about 3 times the amount of $Dspp^{+/+}$ mice (Fig. 11P). Therefore, the PERK pathway was activated in odontoblasts of mutant mice.

The IRE1 pathway is the most conserved ER stress pathway in eukaryotes. It can deal with ER stress by unconventional splicing of XBP1 mRNA, or regulated IRE1-dependent decay (RIDD). Using qPCR, we did not detect changes at mRNA level of IRE1α (Fig. 11R). When using an antibody detecting IRE1α phosphorylation at Serine 724, we were only able to visualize weak signal in $Dspp^{+/+}$ mice at 3 weeks old (Fig. 11D and D'). Strikingly, the signals for phosphorylated (activated) IRE1α was very strong in the pulp cells of $Dspp^{P19L/+}$ and $Dspp^{P19L/P19L}$ mice, especially in those cells near the pulp chamber floor dentin and within the root canals (Fig. 11 E, F, E', and F').

Since IRE1 pathway was activated, we further examined unconventional splicing of XBP1 mRNA and RIDD, respectively. The expression of total XBP1 mRNA can be upregulated by transcription factor ATF6. The qPCR result showed no difference in total XBP1 mRNA between $Dspp^{+/+}$ and $Dspp^{P19L/+}$ mice (Fig. 11S). However, when an anti-XBP1 polyclonal antibody was used to detect both unspliced and spliced XBP1 proteins in the pulp, XBP1 proteins was more intense in the odontoblasts of $Dspp^{P19L/+}$ and $Dspp^{P19L/P19L}$ mice (Fig. 11 H, I, H', and I'). Since the XBP1s (spliced XBP1) protein is more stable for detection, the upregulation in XBP1 proteins indicated by IHC was probably XPB1s protein, due to the enhanced unconventional splicing of XBP1 mRNA.

We further intended to explore the interaction between IRE1α and DSPP by *in vitro* approaches. Since the RNase domain of IRE1α was activated by its autophosphorylation, several variants of IRE1α with mutations in the kinase domain and RNase domain were used: K599A-IRE1α had an altered ATP-binding pocket in its kinase domain, while N906A- or K907A-IRE1α had an impaired RNase domain (Han et al., 2009). Normal DSPP and different IRE1α variants were co-transfected into 293EBNA cells. A minor amount of endogenous IRE1α was detected in the cell lysate of 293EBNA cells (Fig. 13A, row 3, lane 1 and 2), but the detected endogenous IRE1α was barely phosphorylated (Fig. 13A, row 2, lane 1 and 2). As expected, the overexpression of exogenous normal IRE1α, N906A-IRE1α or K907A-IRE1α, but not the K599A-IRE1α, led to the phosphorylation of IRE1 (Fig. 13A, row 2, lane 3-6). In the absence of IRE1α, a significant amount of DSPP was detected in the conditioned medium (Fig. 13A, row 1, lane 2); in contrast, in the presence of normal IRE1α, DSPP signal was largely diminished (Fig. 13A, row 1, lane 3). However, both the kinase catalytic mutant K599A-IRE1α and RNase catalytic mutant N906A- and K907A-IRE1α resulted in more DSPP detected in the conditioned

55

medium (Fig. 13A, row 1, lane 4-6), compared with DSPP transfection alone (Fig. 13A, row 1, lane 2). It implied that the endogenous IRE1α also participated in the regulation of DSPP protein synthesis; upon the overexpression of non-functional IRE1α mutants, the function of endogenous IRE1α on DSPP was inactivated in a dominant negative manner. In comparison, we co-transfected DMP1, the close relative of DSPP, with or without normal IRE1α into 293EBNA cells. Similarly, overexpression of normal IRE1α led to its autophosphorylation (Fig. 13B, row 2-3, lane 3). However, the amounts of DMP1 in the absence and presence of IRE1α were very similar (Fig. 13B, row 1, lane 2-3), which indicated IRE1α played little role in DMP1 regulation.

In summary, UPR actively participated in the regulation of DSPP. In 3-week-old $Dspp^{P19L/+}$ and $Dspp^{P19L/P19L}$ mice, chaperone proteins, such as BiP and HSP90B, were downregulated possibly as a consequence of chronic stress. PERK pathway was activated but did not lead to apoptosis. IRE1 pathway actively participated in the regulation of DSPP protein synthesis. The pulp cells of $Dspp^{P19L/+}$ and $Dspp^{P19L/P19L}$ mice displayed strong phosphorylated IRE1α activity at 3 weeks. XBP1 proteins were upregulated in the odontoblasts of $Dspp^{P19L/+}$ and $Dspp^{P19L/P19L}$ mice. Using *in vitro* methods, we further determined that IRE1α specifically inhibited DSPP protein synthesis. However, how IRE1α recognized DSPP needs to be clarified in the future.

III.4 Discussion

In the last chapter, we confirmed that the dental phenotype of the *Dspp*-KI mouse model resembling that of human DGI patients, especially for those caused by 5' *DSPP* mutations. In this chapter, we hoped to elucidate how the defective dental phenotype was developed at a molecular level.

Using ISH and qPCR analyses, we proved that DSPP mRNA was dramatically reduced in the roof- and floor-forming odontoblasts, as well as in the presecretory and early secretory ameloblasts, in $Dspp^{P19L/+}$ and $Dspp^{P19L/P19L}$ mice. Possible reasons for the reduced DSPP mRNA include less DSPP mRNA transcribed from $Dspp$ gene, instability of P19L-DSPP mRNA, and regulated DSPP mRNA degradation. Since one of the major signaling pathways regulating DSPP expression is the canonical BMP2 signaling pathway, we tested the phosphorylation of Smad1/5/8 by IHC. As no change in pSmad1/5/8 was demonstrated, the changes in $Dspp$ promoter activity, if any, should not be attributed to the canonical BMP2 pathway. If we would like to address the $Dspp$ promoter activity in the future, we may use *in vitro* approaches. Next, we wondered if the stability of normal and mutant DSPP mRNA were the same. A transcriptome-wide identification of microRNA binding sites by AGO (argonaute protein) in 293 cells offered 20 microRNAs targeting the 3' UTR of DSPP mRNA (Hafner et al., 2010). The microRNA binding to 3'UTR may destabilize the targeted mRNA (Bartel, 2009). So we compared the stability of normal DSPP and P19L-DSPP *in vitro*, using an RNA synthesis inhibitor, Actinomycin D. We did not detect any difference in the stability between the two molecular variants of DSPP. Then, insights from the interaction between DSPP and IRE1α offered us some clues, which will be discussed later.

In vitro studies pointed out that several 5' *DSPP* mutations resulted in the skipping of exon 3 (Lee et al., 2011c). *In silico* assays suggested that this particular mutation, c.50C>T, p.P17L in *DSPP*, did not alter mRNA splicing (Li et al., 2012a). We intended to test this result *in vivo*. Therefore, we designed two sets of primers to amplify DSPP mRNA extracted from molars, with one set amplifying DSPP mRNA from exon 2 to exon 4, and the other set amplifying DSPP mRNA from exon 3 to exon 4. We showed that the amounts of mRNA amplified by these two

sets of primers were similar (data not shown). So defective mRNA splicing should not be a potential mechanism underlying this particular mutation.

In vitro evidence from several groups indicated that the IPV motif in DSPP was essential for DSPP secretion (Lee et al., 2013; von Marschall et al., 2012). Using the *in vivo Dspp*-KI mouse model, we confirmed the intracellular accumulation of DSPP in odontoblasts, as well as in presecretory and early secretory ameloblasts, in $Dspp^{P19L/+}$ and $Dspp^{P19L/P19L}$ mice. The secretion of DSPP in $Dspp^{P19L/+}$ and $Dspp^{P19L/P19L}$ mice was not completely blocked, as a significant amount of DSP signal was observed in the dentin matrix, especially in the dentinal tubules. We further employed an *in vitro* model to determine the secretion and subcellular localization of P19L-DSPP. Our results showed that the normal DSPP was rapidly transported to Golgi complex and secreted outside the cells. In contrast, P19L-DSPP had difficulty leaving the ER, though a very small amount was detected in the conditioned medium of cultured mammalian cells. Besides, the ER-retained P19L-DSPP was less modified. It was proposed that a cargo receptor on the ER membrane was critical for the trafficking of DSPP via the IPV motif (Nam et al., 2014; von Marschall et al., 2012). We tried to detect such a cargo receptor by co-immunoprecipitation, protein crosslinking, and mass spectrometry. There were hints that P19L-DSPP might interact with some proteins that normal DSPP did not (data not shown); however, the critical evidence was still missing.

DSPP was claimed to be expressed exclusively by odontoblast, but not by other pulp cells. However, using various antibodies in IHC and DSP probe in ISH, Baba et al. detected DSPP mRNA and protein in the rat molar pulp cells (Baba et al., 2004). Indirect comparison of microarray data also revealed that the human third molars had DSPP mRNA expression in the pulp, about 3% of the DSPP mRNA in the odontoblasts (Paakkonen et al., 2008). When we

58

performed IHC using a DSP polyclonal antibody, we consistently observed moderate DSP signal in the pulp of 3-week-old $Dspp^{+/+}$ mice, but barely in $Dspp^{P19L/+}$ and $Dspp^{P19L/P19L}$ mice. In addition, a single layer of polarized odontoblasts was observed immediately at the pulpal side of dentin in 3-week-old $Dspp^{+/+}$ mice, but less polarized and less organized odontoblasts occupied the corresponding area in $Dspp^{P19L/+}$ and $Dspp^{P19L/P19L}$ mice. Interestingly, the odontoblasts in the molars of $Dspp$-KO mice lacked a typical polarized morphology (data not shown). The results from a previous study implied that DSPP might be important for odontoblast lineage differentiation (Guo et al., 2014). It might help explain the relationship between the missing DSP signal and the loss of typical odontoblast morphology in the mutant mice.

Both DSPP and DMP1 are the SIBLING family proteins; in addition, DSPP was proposed to be the duplication of DMP1 during evolution (Fisher, 2011). In $Dspp$-KO mice, the level of DMP1 expression by odontoblasts was similar to the wild-type control (data not shown). Although the DSPP mRNA level in $Dspp^{P19L/+}$ mice was reduced to 1/8 of $Dspp^{+/+}$ mice at 3 weeks, the DMP1 mRNA level elevated to about 5 times the normal control. The DMP1 protein signal, detected by an antibody recognizing 57kDa DMP1, located to the predentin area in 3-week-old $Dspp^{+/+}$ mice; however, strong DMP1 staining was observed in the dentinal tubules in $Dspp^{P19L/+}$ and $Dspp^{P19L/P19L}$ mice. It was noted that IHC using DSP polyclonal antibody displayed strong signal in dentinal tubules of $Dspp^{+/+}$ mice, whereas the signal in the dentinal tubules of $Dspp^{P19L/+}$ and $Dspp^{P19L/P19L}$ mice was largely reduced. It implied that the upregulation of DMP1 compensated for the loss of DSP in the dentinal tubules. *In vitro* studies suggest that DMP1 facilitates linear assembly and lateral growth of collagen fibers during dentinogenesis, as well as stabilizes newly deposited hydroxyapatite on the collagen surface (He et al., 2003; He et al., 2005a; He and George, 2004). *In vivo* data also show that the 57kDa fragment is the

functional fragment of DMP1 (Lu et al., 2009). The presence of DMP1 in the dentinal tubules partially revealed the function of DMP1 exerting in the dentin matrix of $Dspp^{P19L/+}$ and $Dspp^{P19L/P19L}$ mice. It is also interesting that only DMP1, but not other dentin matrix proteins examined, displayed an elevated level of expression. How DMP1 expression was upregulated upon the reduction of DSPP mRNA, and what was the exact function of DMP1 in the dentin tubules, should be further studied.

As aforementioned, an opinion shared among several groups studying $DSPP$ mutations is that the mutations in and around the IPV motif affect DSPP protein trafficking. The accumulation of DSPP further elicits ER stress. However, minimal evidence has shown the activation of ER stress due to $DSPP$ mutations. Here for the first time, we determined that the ER stress sensors were activated in $Dspp^{P19L/+}$ and $Dspp^{P19L/P19L}$ mice.

Several molecules in UPR pathways are involved in making cell fate decision. On the one hand, CHOP is a pro-apoptotic transcription factor. However, upon CHOP mRNA upregulation, we were not able to detect any increased apoptosis activities from new-born to 3-week-old $Dspp^{P19L/+}$ and $Dspp^{P19L/P19L}$ mice. CHOP can activate pro-apoptotic BH3-only proteins PUMA and BIM, and downregulate the anti-apoptotic BCL-2 (Puthalakath et al., 2007; Rodriguez et al., 2011). However, the CHOP-dependent apoptosis induced by ER stress can be countered by BCL-x_L protein (Gaudette et al., 2014). The BCL-2 family proteins act as a rheostat so that CHOP may not necessarily induce apoptosis. How apoptosis was avoided in P19L-DSPP-induced CHOP upregulation should be detailed by more experiments in the future. On the other hand, GADD34, a downstream target of CHOP, may be activated to avoid prolonged protein translation inhibition by eIF2α phosphorylation (Marciniak et al., 2004; Novoa et al., 2001). Evidently, protein synthesis was not generally suppressed in odontoblasts of $Dspp^{P19L/+}$ and

Dspp^{P19L/P19L} mice, since we still observed a significant amount of DSPP and even upregulated DMP1 in odontoblasts of *Dspp^{P19L/+}* and *Dspp^{P19L/P19L}* mice. Also, we did not observe changes in GADD34 expression. These results implied the chronic adaptation to the persisted stress in odontoblasts of *Dspp^{P19L/+}* and *Dspp^{P19L/P19L}* mice. How professional secretory cells like odontoblasts maintain a balance to control protein load in the ER without inhibition of global translation is another interesting topic to explore.

Strikingly, we demonstrated that IRE1α was dramatically activated in the pulp cells of *Dspp^{P19L/+}* and *Dspp^{P19L/P19L}* mice. IRE1α regulates ER stress via unconventional XBP1 splicing and regulated IRE1-dependent decay (RIDD). It was proposed that the former was activated at a minor stress level, whereas the latter was employed upon acute or prolonged stress (Moore and Hollien, 2015). We detected elevated XBP1 protein expression in odontoblasts of *Dspp^{P19L/+}* and *Dspp^{P19L/P19L}* mice, which was probably due to the enhanced unconventional splicing of XBP1 mRNA. A stem-loop secondary mRNA structure is required for the recognition of both XBP1 mRNA and RIDD targets by the RNase domain of IRE1α (Moore and Hollien, 2015). When we predicted DSPP mRNA structure via the online software RNAfold provided by the University of Vienna, we noted that DSPP mRNA was highly structured, especially in its 3' highly repetitive region (data not shown). Since we did observe the accumulation of DSPP when P19L-DSPP was present, a reasonable explanation is that the accumulation of DSPP protein in the ER activated RIDD, which further degraded DSPP mRNA by recognizing its highly structured region. Our results did support that the overexpression of IRE1α largely reduced the amount of DSPP protein. Since the functional domain of IRE1α is the RNase domain, the reduction of DSPP protein was probably due to the degradation of DSPP mRNA. However, we still need direct evidence to prove that it is the DSPP mRNA that IRE1α recognizes specifically. Further, the

exact regions on DSPP mRNA that IRE1α recognizes, and the nuclease machinery that IRE1α employed for mRNA decay should be elaborated in future studies.

Last but not the least, clarifying the exact mechanisms of DGI will possibly offer us treatment options for this genetic disorder in the near future. In an X chromosome-linked amelogenesis imperfecta (AI) mouse model caused by Y64H-Amelogenin mutation, the administration of 4-phenylbutyrate, a chemical chaperone, rescued the enamel phenotype in affected females (Brookes et al., 2014). With the elaboration of molecular pathological changes in the *Dspp*-KI mouse model, the chances are that we may further target some molecules to alleviate the symptoms.

In summary, in $Dspp^{P19L/+}$ and $Dspp^{P19L/P19L}$ mice, DSPP mRNA was significantly reduced, while DSPP protein showed increased intracellular retention. IRE1α may play a major role in its regulation. At the same time, DMP1 expression was upregulated, possibly to compensate for the reduced function of DSPP in dentinogenesis. However, more efforts are warranted to elaborate the molecular mechanisms of DGI. The successful elucidation of the mechanisms may offer insights for potential treatment plans for this most common hereditary dentin disorder.

CHAPTER IV

CONCLUSION

The most prevalent dentin genetic disorder, non-syndromic dentinogenesis imperfecta (DGI), was first reported more than 100 years ago. It is featured by tooth discoloration, severe enamel attrition, and obliterated or enlarged dental pulp. Unlike many other dental diseases, DGI can be exclusively due to the mutations in dentin sialophosphoprotein (*DSPP*) gene. DSPP is abundantly expressed by odontoblasts, and transiently expressed by ameloblasts. After the translation of full-length DSPP, DSPP is cleaved into the N-terminal dentin sialoprotein (DSP), and the C-terminal dentin phosphoprotein (DPP). DPP is the most acidic protein.

To date, there have been 42 *DSPP* mutations reported. These mutations have been divided into two categories: the missense substitution in the 5' *DSPP* region, and the -1 frameshift mutation in the 3' *DSPP* region. The majority of the identified 5' *DSPP* mutations are related to the IPV (isoleucine-proline-valine) motif, the first three amino acid residues after the removal of the signal peptide. While the 3' *DSPP* mutations will change the hydrophilic acidic protein into a hydrophobic protein. Various potential pathological mechanisms have been proposed, but evidence was lacking.

Here, we chose a specific mutation, the c.50C>T, p.P17L *DSPP* mutation for the generation of a mouse model to exemplify human DGI. This mutation altered the proline residue in the IPV motif. In addition, it caused DGI-II in a 46-year-old Chinese woman, and DGI-III in a 2.5-year-old Korean girl (Lee et al., 2013; Li et al., 2012a). We used CRISPR/Cas9 system to generate a *Dspp*-KI mouse model carrying a P19L-DSPP mutation, equivalent to the P17L-DSPP mutation identified in human patients.

63

The dental phenotype of the mouse model resembled both the dentin and enamel changes of human DGI patients. We did see the typical features of DGI, including tooth discoloration, severe enamel attrition, and "shell teeth" becoming pulp obliteration, in the mutant mice. We for the first time provided evidence from an animal model that DGI-III was an early phase of DGI-II, at least for the majority of DGI caused by 5' *DSPP* mutations. Moreover, the mutant mice exhibited impaired dentin mineralization, altered or even missing enamel structure, and compromised DEJ. The pathological morphology of odontoblasts and ameloblasts led us to study the molecular events related to the DSPP mutation inside these cells.

The molecular mechanisms were examined from various aspects. We observed a reduced amount of DSPP mRNA, but a strong intracellular retention of DSPP protein in the odontoblasts and ameloblasts of the mutant mice. The secretion of mutant DSPP protein was defective; moreover, the mutant DSPP protein accumulated in the endoplasmic reticulum (ER).

The accumulation of DSPP protein in the ER did cause ER stress, and further activated unfolded protein response (UPR). IRE1 pathway, the most conservative pathway of UPR, was activated in the pulp cells of the mutant mice. The activation of IRE1 pathway was further demonstrated by changes in unconventional splicing of XBP1 mRNA, and regulated IRE1-dependent decay (RIDD). Our data suggested that unconventional splicing of XBP1 was upregulated in the odontoblasts of the mutant mice. We also confirmed that IRE1α specifically inhibited the production of DSPP protein. Since DSPP mRNA displayed complex secondary structure in its repetitive region, DSPP mRNA is probably a RIDD target of IRE1α. Therefore, IRE1α specifically inhibited DSPP protein production, probably via the degradation of DSPP mRNA, that is, via RIDD.

UPR did not activate apoptosis in odontoblasts of the mutant mice. Instead, these odontoblasts adapted to the chronic stress condition caused by the accumulation of DSPP protein. On the one hand, DSPP mRNA was downregulated, so the amount of intracellular retained DSPP protein was reduced. Odontoblasts actively secreted the mutant DSPP to the dentin matrix to facilitate dentinogenesis, as well as to reduce the burden of odontoblasts. On the other hand, odontoblasts synthesized and secreted more DMP1 protein to the dentin matrix, probably to compensate for the reduction of DSPP protein.

There are some questions remaining to be answered. First, we need to study the details by which IRE1α regulates DSPP. Our current data implied that IRE1α inhibited DSPP protein production via the degradation of DSPP mRNA. However, we have not provided the direct evidence that DSPP mRNA is degraded via RIDD. We have not determined the exact region of DSPP mRNA that IRE1α recognizes, either. By answering how DSPP mRNA is recognized and degraded, we will not only establish DSPP mRNA as a novel RIDD target, but also offer insights for the diseases related to ER stress.

Second, the dynamic of ER stress in odontoblasts and ameloblasts remains to be addressed. We primarily examined ER stress in odontoblasts at 3 weeks old. It turned out that odontoblasts had already adapted to the chronic stress at this stage. How odontoblasts dealt with the acute ER stress at earlier stages should be elucidated. We may choose an earlier time point, for example, postnatal day 4 or 7, and odontoblasts at a specific region, for example, odontoblasts near the HERS, to examine the stress condition. Although IRE1 pathway was strongly activated in the pulp cells, the other two UPR pathways, PERK and ATF6 pathways, may be more actively involved in the early stress condition. In addition, ameloblasts and odontoblasts may deal with ER stress caused by DSPP mutation by divergent mechanisms.

Although we can use the same approaches to determine the dynamic of ER stress caused by DSPP mutation in ameloblasts, different results should be expected.

Third, enamel phenotype in the mutant mice should be further examined before tooth eruption. In this study, we primarily characterized enamel phenotype after tooth eruption. Although we saw the pathological morphology of ameloblasts, we did not provide evidence that enamel was already defective before eruption, which, if proven, indicates that the enamel defects in the mutant mice are developmental. Therefore, enamel phenotype of molars at an early stage, for example, postnatal day 14, should be demonstrated. Taking advantages of the consecutively erupting mouse incisors, we may also characterize the development of enamel in incisors. We may also use the mouse incisors to determine the regulation of DSPP, and the dynamic of ER stress in both odontoblasts and ameloblasts.

Fourth, DGI caused by 3' *DSPP* mutations should be studied. The majority of 5' *DSPP* mutations are related to the IPV motif, which affects the secretion of DSPP protein. However, 3' *DSPP* mutations identified so far are all -1 frameshift mutations, resulting in hydrophobic mutant DSPP proteins. Therefore, the mechanisms can be distinct for these two categories of *DSPP* mutations.

Fifth, after elucidating the mechanisms, we can seek for potential non-invasive treatment options for DGI. Previous studies found that 4-PBA, a chemical chaperone, rescued the X-linked amelogenesis imperfecta caused by ER stress in female mice. Since enamel is the outer layer of tooth, and enamel was severely affected in our *Dspp*-KI mouse model, we may focus on alleviating the ER stress in ameloblasts using chemical chaperones.

Although more efforts are warranted, a complete understanding of the molecular pathogenesis of DGI will allow us to design treatment options for DGI in the near future. In

addition, the understanding of the mechanism of DGI will shed light on diseases related to ER

stress.

REFERENCES

Alfawaz, S., Fong, F., Plagnol, V., Wong, F.S., Fearne, J., and Kelsell, D.P. (2013). Recessive oligodontia linked to a homozygous loss-of-function mutation in the SMOC2 gene. Archives of oral biology *58*, 462-466.

Alvares, K., Kanwar, Y.S., and Veis, A. (2006). Expression and potential role of dentin phosphophoryn (DPP) in mouse embryonic tissues involved in epithelial-mesenchymal interactions and branching morphogenesis. Developmental dynamics : an official publication of the American Association of Anatomists *235*, 2980-2990.

Aragon, T., van Anken, E., Pincus, D., Serafimova, I.M., Korennykh, A.V., Rubio, C.A., and Walter, P. (2009). Messenger RNA targeting to endoplasmic reticulum stress signalling sites. Nature *457*, 736-740.

Baba, O., Qin, C., Brunn, J.C., Jones, J.E., Wygant, J.N., McIntyre, B.W., and Butler, W.T. (2004). Detection of dentin sialoprotein in rat periodontium. European journal of oral sciences *112*, 163-170.

Bai, H., Agula, H., Wu, Q., Zhou, W., Sun, Y., Qi, Y., Latu, S., Chen, Y., Mutu, J., and Qiu, C. (2010). A novel DSPP mutation causes dentinogenesis imperfecta type II in a large Mongolian family. BMC medical genetics *11*, 23.

Barrett, W.C. (1883). The Description of a Case Having Roots of a Full Denture but No Crowns. The Missouri dental journal *15*, 117-124.

Barron, M.J., Brookes, S.J., Kirkham, J., Shore, R.C., Hunt, C., Mironov, A., Kingswell, N.J., Maycock, J., Shuttleworth, C.A., and Dixon, M.J. (2010). A mutation in the mouse Amelx tri-tyrosyl domain results in impaired secretion of amelogenin and phenocopies human X-linked amelogenesis imperfecta. Human molecular genetics *19*, 1230-1247.

68

Bartel, D.P. (2009). MicroRNAs: target recognition and regulatory functions. Cell *136*, 215-233.

Bernales, S., Papa, F.R., and Walter, P. (2006). Intracellular signaling by the unfolded protein response. Annual review of cell and developmental biology *22*, 487-508.

Bloch-Zupan, A., Huckert, M., Stoetzel, C., Meyer, J., Geoffroy, V., Razafindrakoto, R.W., Ralison, S.N., Randrianaivo, J.C., Ralison, G., Andriamasinoro, R.O.*, et al.* (2016). Detection of a Novel DSPP Mutation by NGS in a Population Isolate in Madagascar. Frontiers in physiology *7*, 70.

Bloch-Zupan, A., Jamet, X., Etard, C., Laugel, V., Muller, J., Geoffroy, V., Strauss, J.P., Pelletier, V., Marion, V., Poch, O.*, et al.* (2011). Homozygosity mapping and candidate prioritization identify mutations, missed by whole-exome sequencing, in SMOC2, causing major dental developmental defects. American journal of human genetics *89*, 773-781.

Boskey, A., Spevak, L., Tan, M., Doty, S.B., and Butler, W.T. (2000). Dentin sialoprotein (DSP) has limited effects on in vitro apatite formation and growth. Calcified tissue international *67*, 472-478.

Boskey, A.L., Maresca, M., Doty, S., Sabsay, B., and Veis, A. (1990). Concentration-dependent effects of dentin phosphophoryn in the regulation of in vitro hydroxyapatite formation and growth. Bone and mineral *11*, 55-65.

Brookes, S.J., Barron, M.J., Boot-Handford, R., Kirkham, J., and Dixon, M.J. (2014). Endoplasmic reticulum stress in amelogenesis imperfecta and phenotypic rescue using 4-phenylbutyrate. Human molecular genetics *23*, 2468-2480.

Brookes, S.J., Barron, M.J., Smith, C.E.L., Poulter, J.A., Mighell, A.J., Inglehearn, C.F., Brown, C.J., Rodd, H., Kirkham, J., and Dixon, M.J. (2017). Amelogenesis imperfecta caused by

N-terminal enamelin point mutations in mice and men is driven by endoplasmic reticulum stress. Human molecular genetics *26*, 1863-1876.

Butler, W.T., Bhown, M., Dimuzio, M.T., and Linde, A. (1981). Nonocollagenous proteins of dentin. Isolation and partial characterization of rat dentin proteins and proteoglycans using a three-step preparative method. Collagen and related research *1*, 187-199.

Butler, W.T., Brunn, J.C., and Qin, C. (2003). Dentin extracellular matrix (ECM) proteins: comparison to bone ECM and contribution to dynamics of dentinogenesis. Connective tissue research *44 Suppl 1*, 171-178.

Calfon, M., Zeng, H., Urano, F., Till, J.H., Hubbard, S.R., Harding, H.P., Clark, S.G., and Ron, D. (2002). IRE1 couples endoplasmic reticulum load to secretory capacity by processing the XBP-1 mRNA. Nature *415*, 92-96.

Cassia, A., Aoun, G., El-Outa, A., Pasquet, G., and Cavezian, R. (2017). Prevalence of Dentinogenesis Imperfecta in a French Population. Journal of International Society of Preventive & Community Dentistry *7*, 116-119.

Chen, S., Chen, L., Jahangiri, A., Chen, B., Wu, Y., Chuang, H.H., Qin, C., and MacDougall, M. (2008a). Expression and processing of small integrin-binding ligand N-linked glycoproteins in mouse odontoblastic cells. Archives of oral biology *53*, 879-889.

Chen, S., Chen, S., Rani, S., Wu, Y., Unterbrink, A., Gu, T.T., Gluhak-Heinrich, J., Chuang, H.H., and Macdougall, M. (2005). Differential regulation of dentin sialophosphoprotein expression by Runx2 during odontoblast cytodifferentiation. Scientific reports *280*, 29717-29727.

Chen, S., Gluhak-Heinrich, J., Martinez, M., Li, T., Wu, Y., Chuang, H.H., Chen, L., Dong, J., Gay, I., and MacDougall, M. (2008b). Bone morphogenetic protein 2 mediates dentin

sialophosphoprotein expression and odontoblast differentiation via NF-Y signaling. The Journal of biological chemistry *283*, 19359-19370.

Chen, S., Unterbrink, A., Kadapakkam, S., Dong, J., Gu, T.T., Dickson, J., Chuang, H.H., and MacDougall, M. (2004). Regulation of the Cell Type-specific dentin sialophosphoprotein gene expression in mouse odontoblasts by a novel transcription repressor and an activator CCAAT-binding factor. The Journal of biological chemistry *279*, 42182-42191.

Chen, Z., Li, W., Wang, H., Wan, C., Luo, D., Deng, S., Chen, H., and Chen, S. (2016). Klf10 regulates odontoblast differentiation and mineralization via promoting expression of dentin matrix protein 1 and dentin sialophosphoprotein genes. Cell and tissue research *363*, 385-398.

Cho, Y.D., Yoon, W.J., Woo, K.M., Baek, J.H., Park, J.C., and Ryoo, H.M. (2010). The canonical BMP signaling pathway plays a crucial part in stimulation of dentin sialophosphoprotein expression by BMP-2. The Journal of biological chemistry *285*, 36369-36376.

Clergeau-Guerithault, S., and Jasmin, J.R. (1985). Dentinogenesis imperfecta type III with enamel and cementum defects. Oral surgery, oral medicine, and oral pathology *59*, 505-510.

Cox, J.S., and Walter, P. (1996). A novel mechanism for regulating activity of a transcription factor that controls the unfolded protein response. Cell *87*, 391-404.

Credle, J.J., Finer-Moore, J.S., Papa, F.R., Stroud, R.M., and Walter, P. (2005). On the mechanism of sensing unfolded protein in the endoplasmic reticulum. Proceedings of the National Academy of Sciences of the United States of America *102*, 18773-18784.

D'Souza, R.N., Cavender, A., Sunavala, G., Alvarez, J., Ohshima, T., Kulkarni, A.B., and MacDougall, M. (1997). Gene expression patterns of murine dentin matrix protein 1 (Dmp1) and

dentin sialophosphoprotein (DSPP) suggest distinct developmental functions in vivo. Journal of bone and mineral research : the official journal of the American Society for Bone and Mineral Research *12*, 2040-2049.

Dahl, T., Sabsay, B., and Veis, A. (1998). Type I collagen-phosphophoryn interactions: specificity of the monomer-monomer binding. Journal of structural biology *123*, 162-168.

de La Dure-Molla, M., Philippe Fournier, B., and Berdal, A. (2015). Isolated dentinogenesis imperfecta and dentin dysplasia: revision of the classification. European journal of human genetics : EJHG *23*, 445-451.

Doudna, J.A., and Charpentier, E. (2014). Genome editing. The new frontier of genome engineering with CRISPR-Cas9. Science (New York, NY) *346*, 1258096.

Eapen, A., and George, A. (2015). Dentin phosphophoryn in the matrix activates AKT and mTOR signaling pathway to promote preodontoblast survival and differentiation. Frontiers in physiology *6*, 221.

Eapen, A., Ramachandran, A., and George, A. (2012). Dentin phosphoprotein (DPP) activates integrin-mediated anchorage-dependent signals in undifferentiated mesenchymal cells. The Journal of biological chemistry *287*, 5211-5224.

Feng, J., Jing, J., Li, J., Zhao, H., Punj, V., Zhang, T., Xu, J., and Chai, Y. (2017). BMP signaling orchestrates a transcriptional network to control the fate of mesenchymal stem cells in mice. *144*, 2560-2569.

Feng, J.Q., Luan, X., Wallace, J., Jing, D., Ohshima, T., Kulkarni, A.B., D'Souza, R.N., Kozak, C.A., and MacDougall, M. (1998). Genomic organization, chromosomal mapping, and promoter analysis of the mouse dentin sialophosphoprotein (Dspp) gene, which codes for both

dentin sialoprotein and dentin phosphoprotein. The Journal of biological chemistry *273*, 9457-9464.

Finn, S.B. (1938). Hereditary opalescent dentin. I. An analysis of the literature on hereditary anomalies of tooth color. Jour ADA & D Cos *25*, 1240-1249.

Fisher, L.W. (2011). DMP1 and DSPP: evidence for duplication and convergent evolution of two SIBLING proteins. Cells, tissues, organs *194*, 113-118.

Fisher, L.W., Jain, A., Tayback, M., and Fedarko, N.S. (2004). Small integrin binding ligand N-linked glycoprotein gene family expression in different cancers. Clinical cancer research : an official journal of the American Association for Cancer Research *10*, 8501-8511.

Fisher, L.W., Torchia, D.A., Fohr, B., Young, M.F., and Fedarko, N.S. (2001). Flexible structures of SIBLING proteins, bone sialoprotein, and osteopontin. Biochemical and biophysical research communications *280*, 460-465.

Galler, K.M., Yasue, A., Cavender, A.C., Bialek, P., Karsenty, G., and D'Souza, R.N. (2007). A novel role for Twist-1 in pulp homeostasis. Journal of dental research *86*, 951-955.

Gardner, B.M., and Walter, P. (2011). Unfolded proteins are Ire1-activating ligands that directly induce the unfolded protein response. Science (New York, NY) *333*, 1891-1894.

Gaudette, B.T., Iwakoshi, N.N., and Boise, L.H. (2014). Bcl-xL protein protects from C/EBP homologous protein (CHOP)-dependent apoptosis during plasma cell differentiation. The Journal of biological chemistry *289*, 23629-23640.

Gibson, M.P., Jani, P., Liu, Y., Wang, X., Lu, Y., Feng, J.Q., and Qin, C. (2013a). Failure to process dentin sialophosphoprotein into fragments leads to periodontal defects in mice. European journal of oral sciences *121*, 545-550.

Gibson, M.P., Jani, P., Wang, X., Lu, Y., and Qin, C. (2014). Overexpressing the NH2-terminal fragment of dentin sialophosphoprotein (DSPP) aggravates the periodontal defects in Dspp knockout mice. Journal of oral biosciences *56*, 143-148.

Gibson, M.P., Liu, Q., Zhu, Q., Lu, Y., Jani, P., Wang, X., Liu, Y., Paine, M.L., Snead, M.L., Feng, J.Q*., et al.* (2013b). Role of the NH2 -terminal fragment of dentin sialophosphoprotein in dentinogenesis. European journal of oral sciences *121*, 76-85.

Gibson, M.P., Zhu, Q., Liu, Q., D'Souza, R.N., Feng, J.Q., and Qin, C. (2013c). Loss of dentin sialophosphoprotein leads to periodontal diseases in mice. Journal of periodontal research *48*, 221-227.

Gibson, M.P., Zhu, Q., Wang, S., Liu, Q., Liu, Y., Wang, X., Yuan, B., Ruest, L.B., Feng, J.Q., D'Souza, R.N*., et al.* (2013d). The rescue of dentin matrix protein 1 (DMP1)-deficient tooth defects by the transgenic expression of dentin sialophosphoprotein (DSPP) indicates that DSPP is a downstream effector molecule of DMP1 in dentinogenesis. The Journal of biological chemistry *288*, 7204-7214.

Guo, S., Lim, D., Dong, Z., Saunders, T.L., Ma, P.X., Marcelo, C.L., and Ritchie, H.H. (2014). Dentin sialophosphoprotein: a regulatory protein for dental pulp stem cell identity and fate. Stem cells and development *23*, 2883-2894.

Gupta, S.K., Saxena, P., Jain, S., and Jain, D. (2011). Prevalence and distribution of selected developmental dental anomalies in an Indian population. Journal of oral science *53*, 231-238.

Hafner, M., Landthaler, M., Burger, L., Khorshid, M., Hausser, J., Berninger, P., Rothballer, A., Ascano, M., Jr., Jungkamp, A.C., Munschauer, M*., et al.* (2010). Transcriptome-

wide identification of RNA-binding protein and microRNA target sites by PAR-CLIP. Cell *141*, 129-141.

Han, D., Lerner, A.G., Vande Walle, L., Upton, J.P., Xu, W., Hagen, A., Backes, B.J., Oakes, S.A., and Papa, F.R. (2009). IRE1alpha kinase activation modes control alternate endoribonuclease outputs to determine divergent cell fates. Cell *138*, 562-575.

Han, N., Zheng, Y., Li, R., Li, X., Zhou, M., Niu, Y., and Zhang, Q. (2014). beta-catenin enhances odontoblastic differentiation of dental pulp cells through activation of Runx2. PloS one *9*, e88890.

Hao, J., Ramachandran, A., and George, A. (2009). Temporal and spatial localization of the dentin matrix proteins during dentin biomineralization. The journal of histochemistry and cytochemistry : official journal of the Histochemistry Society *57*, 227-237.

Harding, H.P., Zhang, Y., and Ron, D. (1999). Protein translation and folding are coupled by an endoplasmic-reticulum-resident kinase. Nature *397*, 271-274.

Hart, P.S., and Hart, T.C. (2007). Disorders of human dentin. Cells, tissues, organs *186*, 70-77.

He, G., Dahl, T., Veis, A., and George, A. (2003). Nucleation of apatite crystals in vitro by self-assembled dentin matrix protein 1. Nature materials *2*, 552-558.

He, G., Gajjeraman, S., Schultz, D., Cookson, D., Qin, C., Butler, W.T., Hao, J., and George, A. (2005a). Spatially and temporally controlled biomineralization is facilitated by interaction between self-assembled dentin matrix protein 1 and calcium phosphate nuclei in solution. Biochemistry *44*, 16140-16148.

He, G., and George, A. (2004). Dentin matrix protein 1 immobilized on type I collagen fibrils facilitates apatite deposition in vitro. The Journal of biological chemistry *279*, 11649-11656.

He, G., Ramachandran, A., Dahl, T., George, S., Schultz, D., Cookson, D., Veis, A., and George, A. (2005b). Phosphorylation of phosphophoryn is crucial for its function as a mediator of biomineralization. The Journal of biological chemistry *280*, 33109-33114.

He, W.X., Niu, Z.Y., Zhao, S.L., Jin, W.L., Gao, J., and Smith, A.J. (2004). TGF-beta activated Smad signalling leads to a Smad3-mediated down-regulation of DSPP in an odontoblast cell line. Archives of oral biology *49*, 911-918.

Heimler, A., Sciubba, J., Lieber, E., and Kamen, S. (1985). An unusual presentation of opalescent dentin and Brandywine isolate hereditary opalescent dentin in an Ashkenazic Jewish family. Oral surgery, oral medicine, and oral pathology *59*, 608-615.

Holappa, H., Nieminen, P., Tolva, L., Lukinmaa, P.L., and Alaluusua, S. (2006). Splicing site mutations in dentin sialophosphoprotein causing dentinogenesis imperfecta type II. European journal of oral sciences *114*, 381-384.

Hollien, J., Lin, J.H., Li, H., Stevens, N., Walter, P., and Weissman, J.S. (2009). Regulated Ire1-dependent decay of messenger RNAs in mammalian cells. The Journal of cell biology *186*, 323-331.

Hollien, J., and Weissman, J.S. (2006). Decay of endoplasmic reticulum-localized mRNAs during the unfolded protein response. Science (New York, NY) *313*, 104-107.

Hu, J.C., Chun, Y.H., Al Hazzazzi, T., and Simmer, J.P. (2007). Enamel formation and amelogenesis imperfecta. Cells, tissues, organs *186*, 78-85.

Hur, S.W., Oh, S.H., Jeong, B.C., Choi, H., Kim, J.W., Lee, K.N., Hwang, Y.C., Ryu, J.H., Kim, S.H., and Koh, J.T. (2015). COUP-TFII Stimulates Dentin Sialophosphoprotein Expression and Mineralization in Odontoblasts. Journal of dental research *94*, 1135-1142.

Hursey, R.J., Jr., Witkop, C.J., Jr., Miklashek, D., and Sackett, L.M. (1956). Dentinogenesis imperfecta in a racial isolate with multiple hereditary defects. Oral surgery, oral medicine, and oral pathology *9*, 641-658.

Jadlowiec, J., Koch, H., Zhang, X., Campbell, P.G., Seyedain, M., and Sfeir, C. (2004). Phosphophoryn regulates the gene expression and differentiation of NIH3T3, MC3T3-E1, and human mesenchymal stem cells via the integrin/MAPK signaling pathway. The Journal of biological chemistry *279*, 53323-53330.

Jadlowiec, J.A., Zhang, X., Li, J., Campbell, P.G., and Sfeir, C. (2006). Extracellular matrix-mediated signaling by dentin phosphophoryn involves activation of the Smad pathway independent of bone morphogenetic protein. The Journal of biological chemistry *281*, 5341-5347.

Jasmin, J.R., and Clergeau-Guerithault, S. (1984). A scanning electron microscopic study of dentin dysplasia type II in primary dentition. Oral surgery, oral medicine, and oral pathology *58*, 57-63.

Jonsson, M., Fredriksson, S., Jontell, M., and Linde, A. (1978). Isoelectric focusing of the phosphoprotein of rat-incisor dentin in ampholine and acid pH gradients. Evidence for carrier ampholyte-protein complexes. Journal of chromatography *157*, 235-242.

Kalk, W.W., Batenburg, R.H., and Vissink, A. (1998). Dentin dysplasia type I: five cases within one family. Oral surgery, oral medicine, oral pathology, oral radiology, and endodontics *86*, 175-178.

Kida, M., Tsutsumi, T., Shindoh, M., Ikeda, H., and Ariga, T. (2009). De novo mutation in the DSPP gene associated with dentinogenesis imperfecta type II in a Japanese family. European journal of oral sciences *117*, 691-694.

Kim, J.W., Hu, J.C., Lee, J.I., Moon, S.K., Kim, Y.J., Jang, K.T., Lee, S.H., Kim, C.C., Hahn, S.H., and Simmer, J.P. (2005). Mutational hot spot in the DSPP gene causing dentinogenesis imperfecta type II. Human genetics *116*, 186-191.

Kim, J.W., Nam, S.H., Jang, K.T., Lee, S.H., Kim, C.C., Hahn, S.H., Hu, J.C., and Simmer, J.P. (2004). A novel splice acceptor mutation in the DSPP gene causing dentinogenesis imperfecta type II. Human genetics *115*, 248-254.

Kim, J.W., and Simmer, J.P. (2007). Hereditary dentin defects. Journal of dental research *86*, 392-399.

Korennykh, A., and Walter, P. (2012). Structural basis of the unfolded protein response. Annual review of cell and developmental biology *28*, 251-277.

Kuzynski, M., Goss, M., Bottini, M., Yadav, M.C., Mobley, C., Winters, T., Poliard, A., Kellermann, O., Lee, B., Millan, J.L.*, et al.* (2014). Dual role of the Trps1 transcription factor in dentin mineralization. The Journal of biological chemistry *289*, 27481-27493.

Lee, D.S., Yoon, W.J., Cho, E.S., Kim, H.J., Gronostajski, R.M., Cho, M.I., and Park, J.C. (2011a). Crosstalk between nuclear factor I-C and transforming growth factor-beta1 signaling regulates odontoblast differentiation and homeostasis. Development (Cambridge, England) *6*, e29160.

Lee, H.K., Lee, D.S., Park, S.J., Cho, K.H., Bae, H.S., and Park, J.C. (2014). Nuclear factor I-C (NFIC) regulates dentin sialophosphoprotein (DSPP) and E-cadherin via control of

Kruppel-like factor 4 (KLF4) during dentinogenesis. The Journal of biological chemistry *289*, 28225-28236.

Lee, K.E., Kang, H.Y., Lee, S.K., Yoo, S.H., Lee, J.C., Hwang, Y.H., Nam, K.H., Kim, J.S., Park, J.C., and Kim, J.W. (2011b). Novel dentin phosphoprotein frameshift mutations in dentinogenesis imperfecta type II. Clinical genetics *79*, 378-384.

Lee, K.E., Lee, S.K., Jung, S.E., Lee, Z., and Kim, J.W. (2011c). Functional splicing assay of DSPP mutations in hereditary dentin defects. Oral diseases *17*, 690-695.

Lee, S.K., Hu, J.C., Lee, K.E., Simmer, J.P., and Kim, J.W. (2008). A dentin sialophosphoprotein mutation that partially disrupts a splice acceptor site causes type II dentin dysplasia. Journal of endodontics *34*, 1470-1473.

Lee, S.K., Lee, K.E., Hwang, Y.H., Kida, M., Tsutsumi, T., Ariga, T., Park, J.C., and Kim, J.W. (2011d). Identification of the DSPP mutation in a new kindred and phenotype-genotype correlation. Oral diseases *17*, 314-319.

Lee, S.K., Lee, K.E., Jeon, D., Lee, G., Lee, H., Shin, C.U., Jung, Y.J., Lee, S.H., Hahn, S.H., and Kim, J.W. (2009). A novel mutation in the DSPP gene associated with dentinogenesis imperfecta type II. Journal of dental research *88*, 51-55.

Lee, S.K., Lee, K.E., Song, S.J., Hyun, H.K., Lee, S.H., and Kim, J.W. (2013). A DSPP mutation causing dentinogenesis imperfecta and characterization of the mutational effect. BioMed research international *2013*, 948181.

Levin, L.S., Leaf, S.H., Jelmini, R.J., Rose, J.J., and Rosenbaum, K.N. (1983). Dentinogenesis imperfecta in the Brandywine isolate (DI type III): clinical, radiologic, and scanning electron microscopic studies of the dentition. Oral surgery, oral medicine, and oral pathology *56*, 267-274.

Li, D., Du, X., Zhang, R., Shen, B., Huang, Y., Valenzuela, R.K., Wang, B., Zhao, H., Liu, Z., Li, J*., et al.* (2012a). Mutation identification of the DSPP in a Chinese family with DGI-II and an up-to-date bioinformatic analysis. Genomics *99*, 220-226.

Li, F., Liu, Y., Liu, H., Yang, J., Zhang, F., and Feng, H. (2017). Phenotype and genotype analyses in seven families with dentinogenesis imperfecta or dentin dysplasia. Oral diseases *23*, 360-366.

Li, L., Shu, Y., Lou, B., and Wu, H. (2012b). Candidate-gene exclusion in a family with inherited non-syndromic dental disorders. Gene *511*, 420-426.

Liang, T., Meng, T., Wang, S., Qin, C., and Lu, Y. (2016). The LPV Motif Is Essential for the Efficient Export of Secretory DMP1 From the Endoplasmic Reticulum. Journal of cellular physiology *231*, 1468-1475.

Liu, Y., Han, D., Wang, L., and Feng, H. (2013). Down-regulation of Wnt10a affects odontogenesis and proliferation in mesenchymal cells. Biochemical and biophysical research communications *434*, 717-721.

Liu, Y., Huang, Y., Gao, J., Li, S., Zhao, X., and Zhang, X. (2016). [Identification of a novel mutation of DSPP gene in a Chinese family affected with dentinogenesis imperfecta shields type II]. Zhonghua yi xue yi chuan xue za zhi = Zhonghua yixue yichuanxue zazhi = Chinese journal of medical genetics *33*, 34-37.

Lu, Y., Qin, C., Xie, Y., Bonewald, L.F., and Feng, J.Q. (2009). Studies of the DMP1 57-kDa functional domain both in vivo and in vitro. Cells, tissues, organs *189*, 175-185.

MacDougall, M., Simmons, D., Luan, X., Gu, T.T., and DuPont, B.R. (1997a). Assignment of dentin sialophosphoprotein (DSPP) to the critical DGI2 locus on human chromosome 4 band q21.3 by in situ hybridization. Cytogenetics and cell genetics *79*, 121-122.

MacDougall, M., Simmons, D., Luan, X., Nydegger, J., Feng, J., and Gu, T.T. (1997b). Dentin phosphoprotein and dentin sialoprotein are cleavage products expressed from a single transcript coded by a gene on human chromosome 4. Dentin phosphoprotein DNA sequence determination. The Journal of biological chemistry *272*, 835-842.

Malmgren, B., Lindskog, S., Elgadi, A., and Norgren, S. (2004). Clinical, histopathologic, and genetic investigation in two large families with dentinogenesis imperfecta type II. Human genetics *114*, 491-498.

Malmgren, B., Lundberg, M., and Lindskog, S. (1988). Dentinogenesis imperfecta in a six-generation family. A clinical, radiographic and histologic comparison of two branches through three generations. Swedish dental journal *12*, 73-84.

Marciniak, S.J., Yun, C.Y., Oyadomari, S., Novoa, I., Zhang, Y., Jungreis, R., Nagata, K., Harding, H.P., and Ron, D. (2004). CHOP induces death by promoting protein synthesis and oxidation in the stressed endoplasmic reticulum. Genes & development *18*, 3066-3077.

McKnight, D.A., Simmer, J.P., Hart, P.S., Hart, T.C., and Fisher, L.W. (2008a). Overlapping DSPP mutations cause dentin dysplasia and dentinogenesis imperfecta. Journal of dental research *87*, 1108-1111.

McKnight, D.A., Suzanne Hart, P., Hart, T.C., Hartsfield, J.K., Wilson, A., Wright, J.T., and Fisher, L.W. (2008b). A comprehensive analysis of normal variation and disease-causing mutations in the human DSPP gene. Human mutation *29*, 1392-1404.

Meng, T., Huang, Y., Wang, S., Zhang, H., Dechow, P.C., Wang, X., Qin, C., Shi, B., D'Souza, R.N., and Lu, Y. (2015). Twist1 Is Essential for Tooth Morphogenesis and Odontoblast Differentiation. The Journal of biological chemistry *290*, 29593-29602.

Mobley, C.G., Kuzynski, M., Zhang, H., Jani, P., Qin, C., and Napierala, D. (2015). Dspp-independent Effects of Transgenic Trps1 Overexpression on Dentin Formation. Journal of dental research *94*, 1128-1134.

Moore, K., and Hollien, J. (2015). Ire1-mediated decay in mammalian cells relies on mRNA sequence, structure, and translational status. Molecular biology of the cell *26*, 2873-2884.

Nam, A.S., Yin, Y., von Marschall, Z., and Fisher, L.W. (2014). Efficient trafficking of acidic proteins out of the endoplasmic reticulum involves a conserved amino terminal IleProVal (IPV)-like tripeptide motif. Connective tissue research *55 Suppl 1*, 138-141.

Nanci, A. (2017). Ten Cate's Oral Histology 9th Edition: Development, Structure, and Function. Elservier, Amesterdam.

Napierala, D., Sun, Y., Maciejewska, I., Bertin, T.K., Dawson, B., D'Souza, R., Qin, C., and Lee, B. (2012). Transcriptional repression of the Dspp gene leads to dentinogenesis imperfecta phenotype in Col1a1-Trps1 transgenic mice. Journal of bone and mineral research : the official journal of the American Society for Bone and Mineral Research *27*, 1735-1745.

Narayanan, K., Gajjeraman, S., Ramachandran, A., Hao, J., and George, A. (2006). Dentin matrix protein 1 regulates dentin sialophosphoprotein gene transcription during early odontoblast differentiation. The Journal of biological chemistry *281*, 19064-19071.

Nieminen, P., Papagiannoulis-Lascarides, L., Waltimo-Siren, J., Ollila, P., Karjalainen, S., Arte, S., Veerkamp, J., Tallon Walton, V., Chimenos Kustner, E., Siltanen, T.*, et al.* (2011). Frameshift mutations in dentin phosphoprotein and dependence of dentin disease phenotype on mutation location. Journal of bone and mineral research : the official journal of the American Society for Bone and Mineral Research *26*, 873-880.

Novoa, I., Zeng, H., Harding, H.P., and Ron, D. (2001). Feedback inhibition of the unfolded protein response by GADD34-mediated dephosphorylation of eIF2alpha. The Journal of cell biology *153*, 1011-1022.

O. Carroll, M.K., and Duncan, W.K. (1994). Dentin dysplasia type I. Radiologic and genetic perspectives in a six-generation family. Oral surgery, oral medicine, and oral pathology *78*, 375-381.

Oka, S., Oka, K., Xu, X., Sasaki, T., Bringas, P., Jr., and Chai, Y. (2007). Cell autonomous requirement for TGF-beta signaling during odontoblast differentiation and dentin matrix formation. Mechanisms of development *124*, 409-415.

Ozer, A., Yuan, G., Yang, G., Wang, F., Li, W., Yang, Y., Guo, F., Gao, Q., Shoff, L., Chen, Z*., et al.* (2013). Domain of dentine sialoprotein mediates proliferation and differentiation of human periodontal ligament stem cells. PloS one *8*, e81655.

Paakkonen, V., Vuoristo, J.T., Salo, T., and Tjaderhane, L. (2008). Comparative gene expression profile analysis between native human odontoblasts and pulp tissue. International endodontic journal *41*, 117-127.

Paine, M.L., Luo, W., Wang, H.J., Bringas, P., Jr., Ngan, A.Y., Miklus, V.G., Zhu, D.H., MacDougall, M., White, S.N., and Snead, M.L. (2005). Dentin sialoprotein and dentin phosphoprotein overexpression during amelogenesis. The Journal of biological chemistry *280*, 31991-31998.

Pincus, D., Chevalier, M.W., Aragon, T., van Anken, E., Vidal, S.E., El-Samad, H., and Walter, P. (2010). BiP binding to the ER-stress sensor Ire1 tunes the homeostatic behavior of the unfolded protein response. PLoS biology *8*, e1000415.

Prasad, M., Butler, W.T., and Qin, C. (2010). Dentin sialophosphoprotein in biomineralization. Connective tissue research *51*, 404-417.

Prasad, M., Zhu, Q., Sun, Y., Wang, X., Kulkarni, A., Boskey, A., Feng, J.Q., and Qin, C. (2011). Expression of dentin sialophosphoprotein in non-mineralized tissues. The journal of histochemistry and cytochemistry : official journal of the Histochemistry Society *59*, 1009-1021.

Puthalakath, H., O'Reilly, L.A., Gunn, P., Lee, L., Kelly, P.N., Huntington, N.D., Hughes, P.D., Michalak, E.M., McKimm-Breschkin, J., Motoyama, N.*, et al.* (2007). ER stress triggers apoptosis by activating BH3-only protein Bim. Cell *129*, 1337-1349.

Qin, C., Baba, O., and Butler, W.T. (2004). Post-translational modifications of sibling proteins and their roles in osteogenesis and dentinogenesis. Critical reviews in oral biology and medicine : an official publication of the American Association of Oral Biologists *15*, 126-136.

Qin, C., Brunn, J.C., Baba, O., Wygant, J.N., McIntyre, B.W., and Butler, W.T. (2003a). Dentin sialoprotein isoforms: detection and characterization of a high molecular weight dentin sialoprotein. European journal of oral sciences *111*, 235-242.

Qin, C., Brunn, J.C., Cadena, E., Ridall, A., and Butler, W.T. (2003b). Dentin sialoprotein in bone and dentin sialophosphoprotein gene expressed by osteoblasts. Connective tissue research *44 Suppl 1*, 179-183.

Qin, C., Brunn, J.C., Cadena, E., Ridall, A., Tsujigiwa, H., Nagatsuka, H., Nagai, N., and Butler, W.T. (2002). The expression of dentin sialophosphoprotein gene in bone. Journal of dental research *81*, 392-394.

Rajpar, M.H., Koch, M.J., Davies, R.M., Mellody, K.T., Kielty, C.M., and Dixon, M.J. (2002). Mutation of the signal peptide region of the bicistronic gene DSPP affects translocation

to the endoplasmic reticulum and results in defective dentine biomineralization. Human molecular genetics *11*, 2559-2565.

Rodriguez, D., Rojas-Rivera, D., and Hetz, C. (2011). Integrating stress signals at the endoplasmic reticulum: The BCL-2 protein family rheostat. Biochimica et biophysica acta *1813*, 564-574.

Rushton, M.A. (1954). A new form of dentinal dysplasia: shell teeth. Oral surgery, oral medicine, and oral pathology *7*, 543-549.

Ryoo, H.M., Lee, M.H., and Kim, Y.J. (2006). Critical molecular switches involved in BMP-2-induced osteogenic differentiation of mesenchymal cells. Gene *366*, 51-57.

Scheuner, D., Song, B., McEwen, E., Liu, C., Laybutt, R., Gillespie, P., Saunders, T., Bonner-Weir, S., and Kaufman, R.J. (2001). Translational control is required for the unfolded protein response and in vivo glucose homeostasis. Molecular cell *7*, 1165-1176.

Shen, J., Chen, X., Hendershot, L., and Prywes, R. (2002). ER stress regulation of ATF6 localization by dissociation of BiP/GRP78 binding and unmasking of Golgi localization signals. Developmental cell *3*, 99-111.

Shields, E.D. (1983). A new classification of heritable human enamel defects and a discussion of dentin defects. Birth defects original article series *19*, 107-127.

Shields, E.D., Bixler, D., and el-Kafrawy, A.M. (1973). A proposed classification for heritable human dentine defects with a description of a new entity. Archives of oral biology *18*, 543-553.

Shimazu, Y., Sato, K., Aoyagi, K., Nango, N., and Aoba, T. (2009). Hertwig's Epithelial Cells and Multi-root Development of Molars in Mice. Journal of oral biosciences *51*, 210-217.

Simmer, J.P., Papagerakis, P., Smith, C.E., Fisher, D.C., Rountrey, A.N., Zheng, L., and Hu, J.C. (2010). Regulation of dental enamel shape and hardness. Journal of dental research *89*, 1024-1038.

Siyam, A., Wang, S., Qin, C., Mues, G., Stevens, R., D'Souza, R.N., and Lu, Y. (2012). Nuclear localization of DMP1 proteins suggests a role in intracellular signaling. Biochemical and biophysical research communications *424*, 641-646.

Song, Y., Wang, C., Peng, B., Ye, X., Zhao, G., Fan, M., Fu, Q., and Bian, Z. (2006). Phenotypes and genotypes in 2 DGI families with different DSPP mutations. Oral surgery, oral medicine, oral pathology, oral radiology, and endodontics *102*, 360-374.

Song, Y.L., Wang, C.N., Fan, M.W., Su, B., and Bian, Z. (2008). Dentin phosphoprotein frameshift mutations in hereditary dentin disorders and their variation patterns in normal human population. Journal of medical genetics *45*, 457-464.

Sreenath, T., Thyagarajan, T., Hall, B., Longenecker, G., D'Souza, R., Hong, S., Wright, J.T., MacDougall, M., Sauk, J., and Kulkarni, A.B. (2003a). Dentin sialophosphoprotein knockout mouse teeth display widened predentin zone and develop defective dentin mineralization similar to human dentinogenesis imperfecta type III. The Journal of biological chemistry *278*, 24874-24880.

Sreenath, T.L., Cho, A., Thyagarajan, T., and Kulkarni, A.B. (2003b). Odontoblast-specific expression of cre recombinase successfully deletes gene segments flanked by loxP sites in mouse teeth. Genesis (New York, NY : 2000) *35*, 94-99.

Sun, Y., Lu, Y., Chen, S., Prasad, M., Wang, X., Zhu, Q., Zhang, J., Ball, H., Feng, J., Butler, W.T.*, et al.* (2010). Key proteolytic cleavage site and full-length form of DSPP. Journal of dental research *89*, 498-503.

Suzuki, S., Nakata, M., and Eto, K. (1977). Clinical and histologic observations of opalescent dentin associated with enamel defects. Oral surgery, oral medicine, and oral pathology *44*, 767-774.

Suzuki, S., Sreenath, T., Haruyama, N., Honeycutt, C., Terse, A., Cho, A., Kohler, T., Muller, R., Goldberg, M., and Kulkarni, A.B. (2009). Dentin sialoprotein and dentin phosphoprotein have distinct roles in dentin mineralization. Matrix biology : journal of the International Society for Matrix Biology *28*, 221-229.

Tang, X.N., Zhu, Y.Q., Marcelo, C.L., and Ritchie, H.H. (2011). Expression of mineralized tissue associated proteins: dentin sialoprotein and phosphophoryn in rodent hair follicles. Journal of dermatological science *64*, 92-98.

Tsuchiya, S., Simmer, J.P., Hu, J.C., Richardson, A.S., Yamakoshi, F., and Yamakoshi, Y. (2011). Astacin proteases cleave dentin sialophosphoprotein (Dspp) to generate dentin phosphoprotein (Dpp). Journal of bone and mineral research : the official journal of the American Society for Bone and Mineral Research *26*, 220-228.

Tsukumo, Y., Tsukahara, S., Saito, S., Tsuruo, T., and Tomida, A. (2009). A novel endoplasmic reticulum export signal: proline at the +2-position from the signal peptide cleavage site. The Journal of biological chemistry *284*, 27500-27510.

Urano, F., Wang, X., Bertolotti, A., Zhang, Y., Chung, P., Harding, H.P., and Ron, D. (2000). Coupling of stress in the ER to activation of JNK protein kinases by transmembrane protein kinase IRE1. Science (New York, NY) *287*, 664-666.

Veis, A., and Perry, A. (1967). The phosphoprotein of the dentin matrix. Biochemistry *6*, 2409-2416.

Verdelis, K., Ling, Y., Sreenath, T., Haruyama, N., MacDougall, M., van der Meulen, M.C., Lukashova, L., Spevak, L., Kulkarni, A.B., and Boskey, A.L. (2008). DSPP effects on in vivo bone mineralization. Bone *43*, 983-990.

Verdelis, K., Szabo-Rogers, H.L., Xu, Y., Chong, R., Kang, R., Cusack, B.J., Jani, P., Boskey, A.L., Qin, C., and Beniash, E. (2016). Accelerated enamel mineralization in Dspp mutant mice. Matrix biology : journal of the International Society for Matrix Biology *52-54*, 246-259.

Villarreal-Ramirez, E., Eliezer, D., Garduno-Juarez, R., Gericke, A., Perez-Aguilar, J.M., and Boskey, A. (2017). Phosphorylation regulates the secondary structure and function of dentin phosphoprotein peptides. Bone *95*, 65-75.

Villarreal-Ramirez, E., Garduno-Juarez, R., Gericke, A., and Boskey, A. (2014). The role of phosphorylation in dentin phosphoprotein peptide absorption to hydroxyapatite surfaces: a molecular dynamics study. Connective tissue research *55 Suppl 1*, 134-137.

von Marschall, Z., and Fisher, L.W. (2010). Dentin sialophosphoprotein (DSPP) is cleaved into its two natural dentin matrix products by three isoforms of bone morphogenetic protein-1 (BMP1). Matrix biology : journal of the International Society for Matrix Biology *29*, 295-303.

von Marschall, Z., Mok, S., Phillips, M.D., McKnight, D.A., and Fisher, L.W. (2012). Rough endoplasmic reticulum trafficking errors by different classes of mutant dentin sialophosphoprotein (DSPP) cause dominant negative effects in both dentinogenesis imperfecta and dentin dysplasia by entrapping normal DSPP. Journal of bone and mineral research : the official journal of the American Society for Bone and Mineral Research *27*, 1309-1321.

Walter, P., and Ron, D. (2011). The unfolded protein response: from stress pathway to homeostatic regulation. Science (New York, NY) *334*, 1081-1086.

Wan, C., Yuan, G., Luo, D., Zhang, L., Lin, H., Liu, H., Chen, L., Yang, G., Chen, S., and Chen, Z. (2016). The Dentin Sialoprotein (DSP) Domain Regulates Dental Mesenchymal Cell Differentiation through a Novel Surface Receptor. Scientific reports *6*, 29666.

Wang, H., Hou, Y., Cui, Y., Huang, Y., Shi, Y., Xia, X., Lu, H., Wang, Y., and Li, X. (2009). A novel splice site mutation in the dentin sialophosphoprotein gene in a Chinese family with dentinogenesis imperfecta type II. Mutation research *662*, 22-27.

Wang, S.K., Chan, H.C., Rajderkar, S., Milkovich, R.N., Uston, K.A., Kim, J.W., Simmer, J.P., and Hu, J.C. (2011). Enamel malformations associated with a defined dentin sialophosphoprotein mutation in two families. European journal of oral sciences *119 Suppl 1*, 158-167.

White, S.N., Paine, M.L., Ngan, A.Y., Miklus, V.G., Luo, W., Wang, H., and Snead, M.L. (2007). Ectopic expression of dentin sialoprotein during amelogenesis hardens bulk enamel. The Journal of biological chemistry *282*, 5340-5345.

Witkop, C.J. (1957). Hereditary defects in enamel and dentin. Acta genetica et statistica medica *7*, 236-239.

Witkop, C.J., Jr. (1971). Manifestations of genetic diseases in the human pulp. Oral surgery, oral medicine, and oral pathology *32*, 278-316.

Witkop, C.J., Jr. (1988). Amelogenesis imperfecta, dentinogenesis imperfecta and dentin dysplasia revisited: problems in classification. Journal of oral pathology *17*, 547-553.

Witkop, C.J., Jr., MacLean, C.J., Schmidt, P.J., and Henry, J.L. (1966). Medical and dental findings in the Brandywine isolate. The Alabama journal of medical sciences *3*, 382-403.

Xiao, S., Yu, C., Chou, X., Yuan, W., Wang, Y., Bu, L., Fu, G., Qian, M., Yang, J., Shi, Y., *et al.* (2001). Dentinogenesis imperfecta 1 with or without progressive hearing loss is associated with distinct mutations in DSPP. Nature genetics *27*, 201-204.

Yamakoshi, Y., Hu, J.C., Fukae, M., Zhang, H., and Simmer, J.P. (2005). Dentin glycoprotein: the protein in the middle of the dentin sialophosphoprotein chimera. The Journal of biological chemistry *280*, 17472-17479.

Yamakoshi, Y., Hu, J.C., Iwata, T., Kobayashi, K., Fukae, M., and Simmer, J.P. (2006). Dentin sialophosphoprotein is processed by MMP-2 and MMP-20 in vitro and in vivo. The Journal of biological chemistry *281*, 38235-38243.

Yamakoshi, Y., Kinoshita, S., Izuhara, L., Karakida, T., Fukae, M., and Oida, S. (2014). DPP and DSP are Necessary for Maintaining TGF-beta1 Activity in Dentin. Journal of dental research *93*, 671-677.

Yamakoshi, Y., Lu, Y., Hu, J.C., Kim, J.W., Iwata, T., Kobayashi, K., Nagano, T., Yamakoshi, F., Hu, Y., Fukae, M., *et al.* (2008). Porcine dentin sialophosphoprotein: length polymorphisms, glycosylation, phosphorylation, and stability. The Journal of biological chemistry *283*, 14835-14844.

Yamakoshi, Y., Nagano, T., Hu, J.C., Yamakoshi, F., and Simmer, J.P. (2011). Porcine dentin sialoprotein glycosylation and glycosaminoglycan attachments. BMC biochemistry *12*, 6.

Yamashiro, T., Zheng, L., Shitaku, Y., Saito, M., Tsubakimoto, T., Takada, K., Takano-Yamamoto, T., and Thesleff, I. (2007). Wnt10a regulates dentin sialophosphoprotein mRNA expression and possibly links odontoblast differentiation and tooth morphogenesis. Differentiation; research in biological diversity *75*, 452-462.

Yang, G., Yuan, G., MacDougall, M., and Zhi, C. (2017). BMP-2 induced Dspp transcription is mediated by Dlx3/Osx signaling pathway in odontoblasts. *7*, 10775.

Yang, J., Kawasaki, K., Lee, M., Reid, B.M., Nunez, S.M., Choi, M., Seymen, F., Koruyucu, M., Kasimoglu, Y., Estrella-Yuson, N.*, et al.* (2016). The dentin phosphoprotein repeat region and inherited defects of dentin. Molecular genetics & genomic medicine *4*, 28-38.

Ye, J., Rawson, R.B., Komuro, R., Chen, X., Dave, U.P., Prywes, R., Brown, M.S., and Goldstein, J.L. (2000). ER stress induces cleavage of membrane-bound ATF6 by the same proteases that process SREBPs. Molecular cell *6*, 1355-1364.

Yoshida, H., Matsui, T., Yamamoto, A., Okada, T., and Mori, K. (2001). XBP1 mRNA is induced by ATF6 and spliced by IRE1 in response to ER stress to produce a highly active transcription factor. Cell *107*, 881-891.

Yoshida, H., Okada, T., Haze, K., Yanagi, H., Yura, T., Negishi, M., and Mori, K. (2000). ATF6 activated by proteolysis binds in the presence of NF-Y (CBF) directly to the cis-acting element responsible for the mammalian unfolded protein response. Molecular and cellular biology *20*, 6755-6767.

Yuan, G., Chen, L., Feng, J., Yang, G., Ni, Q., Xu, X., Wan, C., Lindsey, M., Donly, K.J., MacDougall, M.*, et al.* (2017). Dentin Sialoprotein is a Novel Substrate of Matrix Metalloproteinase 9 in vitro and in vivo. Journal of molecular histology *7*, 42449.

Yuan, G., Yang, G., Song, G., Chen, Z., and Chen, S. (2012). Immunohistochemical localization of the NH(2)-terminal and COOH-terminal fragments of dentin sialoprotein in mouse teeth. Cell and tissue research *349*, 605-614.

Zerbino, D.R., Achuthan, P., Akanni, W., Amode, M R., Barrell, D., Bhai, J., Billis, K., Cummins, C., Gall, A., Girón, C.G., *et al.* (2018). Ensembl 2018. Nucleic Acids Research *46*, D754-D761.

Zhang, H., Jani, P., Liang, T., Lu, Y., and Qin, C. (2017). Inactivation of bone morphogenetic protein 1 (Bmp1) and tolloid-like 1 (Tll1) in cells expressing type I collagen leads to dental and periodontal defects in mice. *48*, 83-98.

Zhang, H., Jiang, Y., Qin, C., Liu, Y., Ho, S.P., and Feng, J.Q. (2015). Essential role of osterix for tooth root but not crown dentin formation. Journal of bone and mineral research : the official journal of the American Society for Bone and Mineral Research *30*, 742-746.

Zhang, H., Liu, P., Wang, S., Liu, C., Jani, P., Lu, Y., and Qin, C. (2016). Transgenic expression of dentin phosphoprotein inhibits skeletal development. European journal of histochemistry : EJH *60*, 2587.

Zhang, H., Xie, X., Liu, P., Liang, T., Lu, Y., and Qin, C. (2018). Transgenic expression of dentin phosphoprotein (DPP) partially rescued the dentin defects of DSPP-null mice. PloS one *13*, e0195854.

Zhang, J., Wang, J., Ma, Y., Du, W., Zhao, S., Zhang, Z., Zhang, X., Liu, Y., Xiao, H., Wang, H., *et al.* (2011). A novel splicing mutation alters DSPP transcription and leads to dentinogenesis imperfecta type II. PloS one *6*, e27982.

Zhang, X., Chen, L., Liu, J., Zhao, Z., Qu, E., Wang, X., Chang, W., Xu, C., Wang, Q.K., and Liu, M. (2007). A novel DSPP mutation is associated with type II dentinogenesis imperfecta in a Chinese family. BMC medical genetics *8*, 52.

Zhang, X., Zhao, J., Li, C., Gao, S., Qiu, C., Liu, P., Wu, G., Qiang, B., Lo, W.H., and Shen, Y. (2001). DSPP mutation in dentinogenesis imperfecta Shields type II. Nature genetics *27*, 151-152.

Zhang, Y., Song, Y., Ravindran, S., Gao, Q., Huang, C.C., Ramachandran, A., Kulkarni, A., and George, A. (2014). DSPP contains an IRES element responsible for the translation of dentin phosphophoryn. Journal of dental research *93*, 155-161.

Zhu, Q., Gibson, M.P., Liu, Q., Liu, Y., Lu, Y., Wang, X., Feng, J.Q., and Qin, C. (2012a). Proteolytic processing of dentin sialophosphoprotein (DSPP) is essential to dentinogenesis. The Journal of biological chemistry *287*, 30426-30435.

Zhu, Q., Prasad, M., Kong, H., Lu, Y., Sun, Y., Wang, X., Yamoah, A., Feng, J.Q., and Qin, C. (2012b). Partial blocking of mouse DSPP processing by substitution of Gly(451)-Asp(452) bond suggests the presence of secondary cleavage site(s). Connective tissue research *53*, 307-312.

Zhu, Q., Sun, Y., Prasad, M., Wang, X., Yamoah, A.K., Li, Y., Feng, J., and Qin, C. (2010). Glycosaminoglycan chain of dentin sialoprotein proteoglycan. Journal of dental research *89*, 808-812.
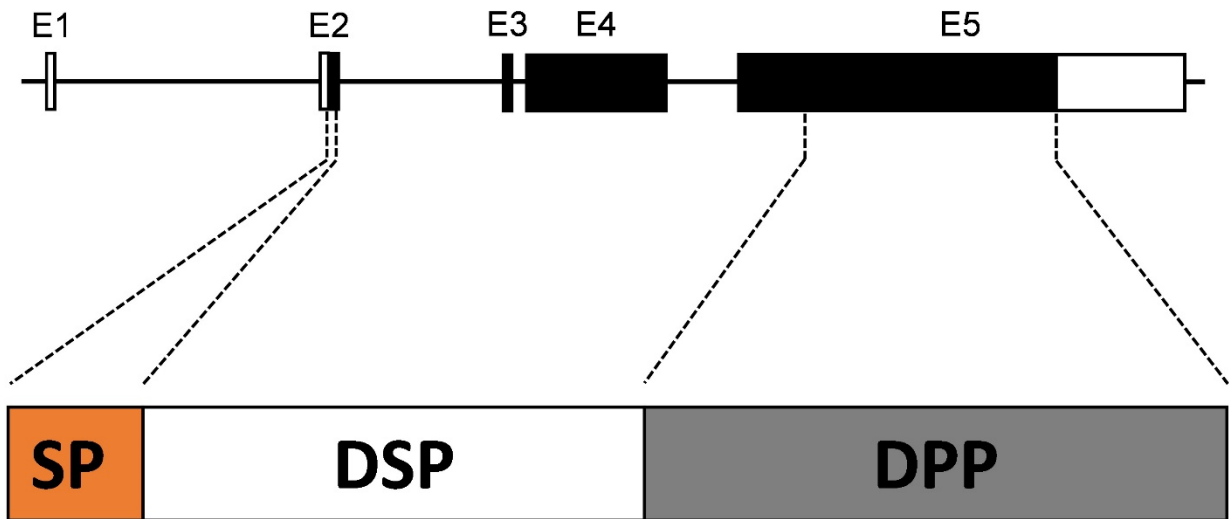
Fig. 1 Dentin Sialophosphoprotein (DSPP) Gene and Protein.
The upper panel indicates that the human *DSPP* gene consists of 5 exons (E1-E5) and 4 introns. The black areas are coding sequences, the white areas are untranslated regions. The lower panel shows that DSPP protein can be cleaved into dentin sialoprotein (DSP) and dentin phosphoprotein (DPP) after the removal of signal peptide (SP).
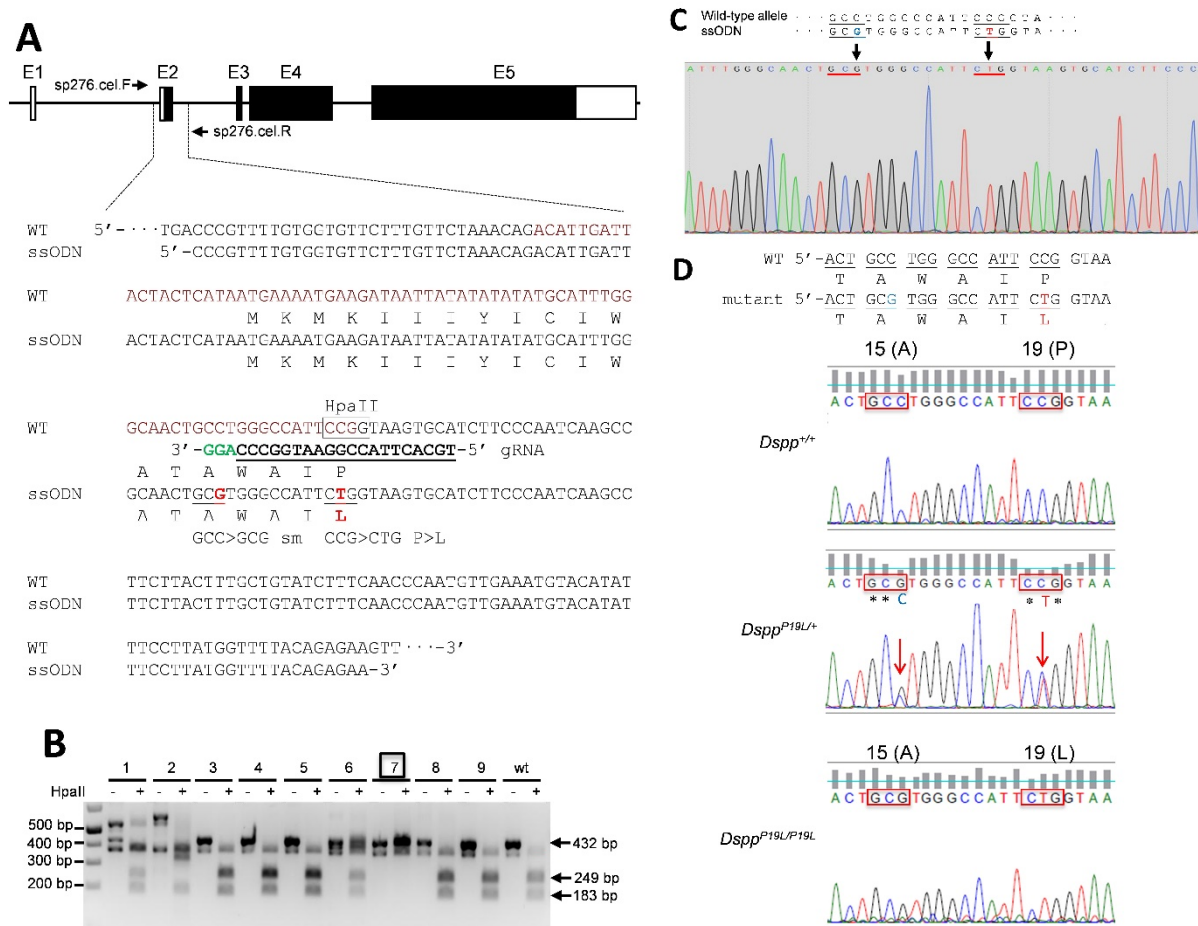
Fig. 2 Generation of *Dspp^{P19L/+}* Knock-in Mice.
A. Strategy for generating *Dspp^{P19L/+}* knock-in mice. Top panel shows a schematic representation of the mouse *Dspp* gene, which consists of 5 exons (E1-E5). Arrows indicate the locations of the PCR primers, sp276.cel.F and sp276.cel.R. Lower panel shows the sequence of the wild-type (WT) *Dspp* allele, and the corresponding positions of the sgRNA guide sequence (gRNA) and ssODN. The nucleotide sequence of exon 2 is in dark red. The sgRNA guide sequence was bolded and underlined. The PAM sequence (AGG) is in green. The deduced amino acid sequences from the WT *Dspp* allele and ssODN are shown below their corresponding nucleotide sequences. The substitution of codon 15 (GCC) by GCG resulted in a silent mutation (sm). The substitution of codon 19 (CCG) by CTG led to the substitution of proline residue by leucine residue. The restriction enzyme HpaII recognition site (CCGG) is enclosed in the box. **B.** Screening for potential *Dspp^{P19L/+}* knock-in founder mice. The PCR products amplified by the sp276.cel.F and sp276.cel.R primers from the nine potential founders and a wild-type control mouse were resolved on 1% agarose gel before (left lane) or after (right lane) HpaII digestion. Mouse #7 was a potential homozygous founder that carried the desired P19L mutation. **C.** DNA sequencing results from potential founder #7. The arrows point to the successfully substituted nucleotides in mouse #7. **D.** DNA sequencing results from generation F3. Both heterozygous *Dspp^{P19L/+}* and homozygous *Dspp^{P19L/P19L}* showed the desired mutations.

95
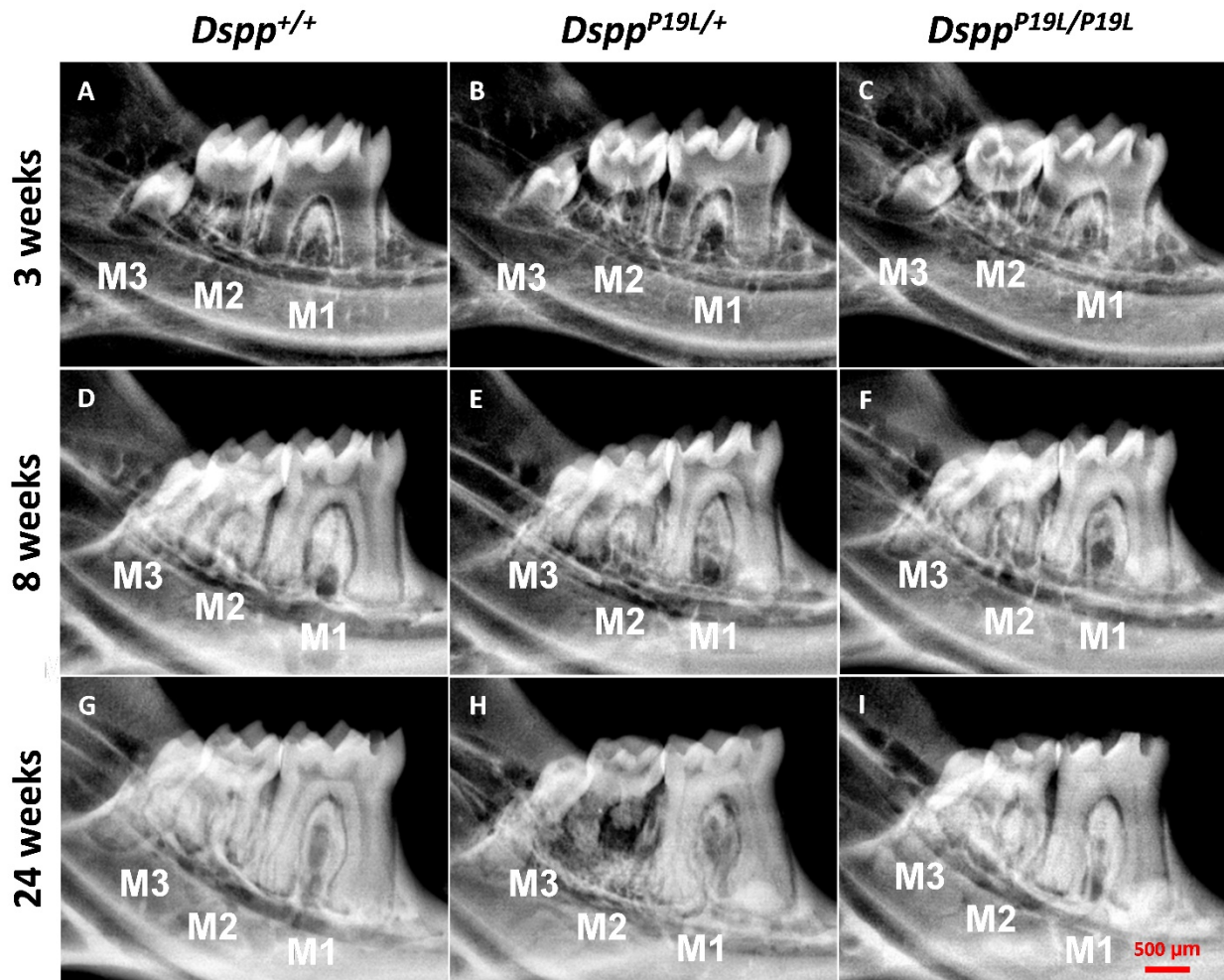
**Fig. 3 Plain X-ray Radiographic Analyses of the Mandibular Molars.**
Shown are the representative plain X-ray radiographs of the mandibular molars of 3-week-old (A-C), 8-week-old (D-F) and 24-week-old (G-I) $Dspp^{+/+}$ (A, D and G), $Dspp^{P19L/+}$ (B, E and H), and $Dspp^{P19L/+}$ (C, F and I) mice. Abbreviations: M1, first molar; M2, second molar; M3, third molar.

96
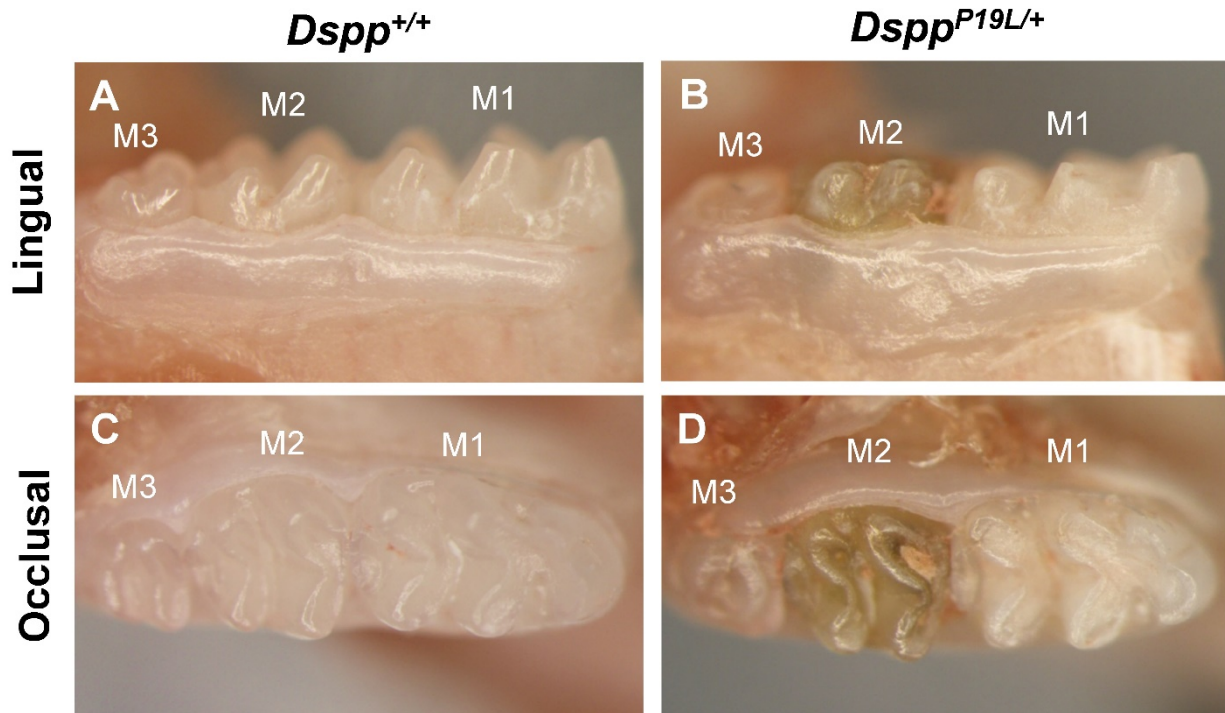
**Fig. 4 Stereo Microscopic Analyses of the Mandibular Molars.**
Shown are the representative photographs of the lingual views (A and B) and occlusal views (C and D) of the mandibular molars of 24-week-old WT (A and C) and $Dspp^{P19L/+}$ mice (B and D). Abbreviations: M1, first molar; M2, second molar; M3, third molar.
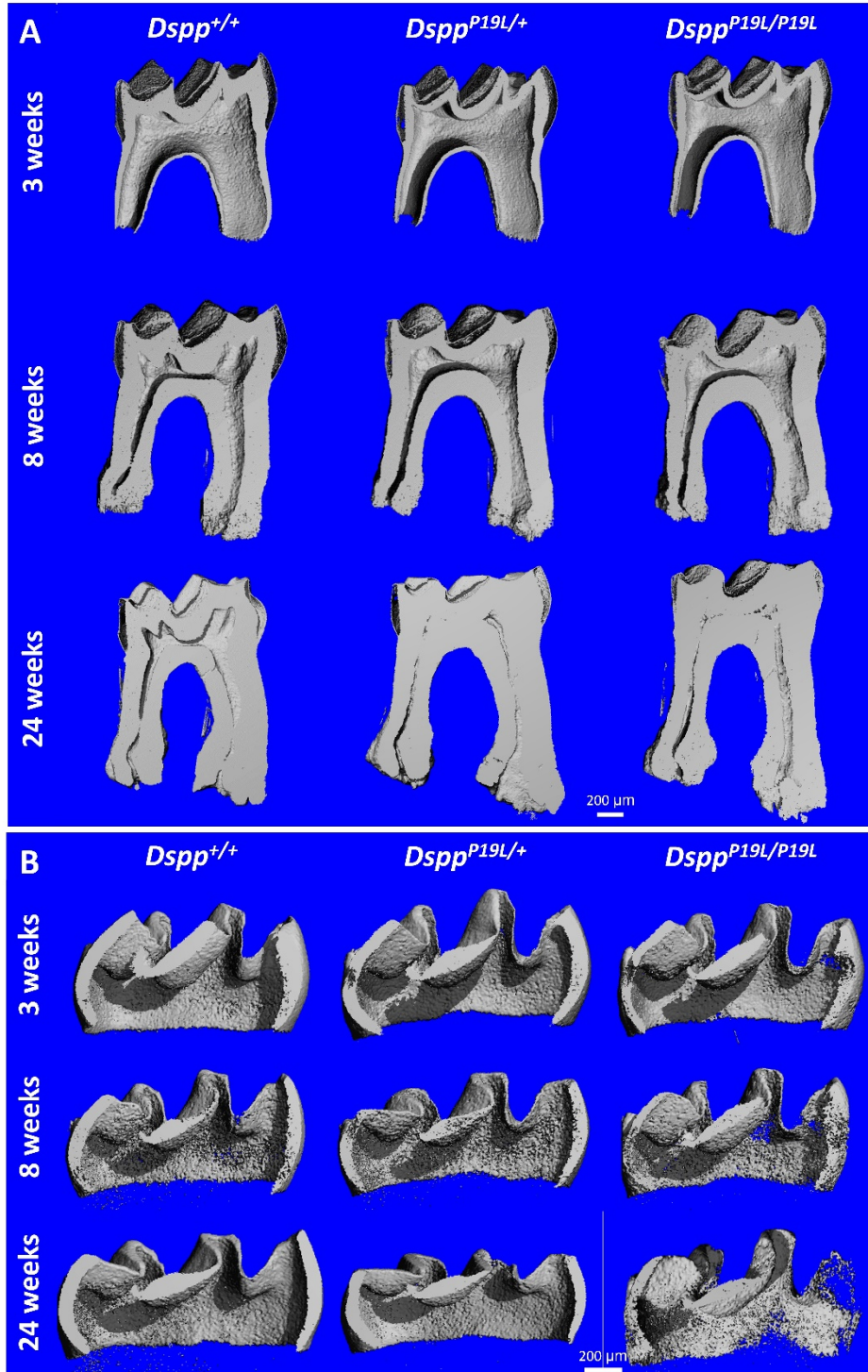
Fig. 5 μCT Analyses of the Mandibular First Molars.
Shown are the representative reconstructed μCT images (sagittal sections) of the dentin (A) and enamel (B) of the mandibular first molars of 3-, 8- and 24-week-old $Dspp^{+/+}$, $Dspp^{P19L/+}$, and $Dspp^{P19L/P19L}$ mice. The proximal walls of dentin and enamel are positioned towards the right.

98

Fig. 6 Scanning Electron Microscopy (SEM) Analyses of the Mandibular First Molars.
Shown are the representative scanning images of the mandibular first molars of 3-week-old (A-F) and 24-week-old (G-L) $Dspp^{+/+}$(A, D, G, and J), $Dspp^{P19L/+}$(B, E, H, and K), and $Dspp^{P19L/P19L}$ (C, F, I, and L) mice. The buccal sides of teeth are positioned up. Scanning images by backscattered detector in BES mode (BS) are shown in A-C, and G-I; scanning images after etching (SEM) are shown in D-F, and J-L. A'-L' are the corresponding magnified areas marked in red boxes. A"-L" are the corresponding magnified areas marked in orange boxes. D'''-F''' and J'''-L''' are the corresponding magnified areas marked in green boxes. D''''-F'''' and J''''-L'''' are the corresponding magnified areas marked in blue boxes. Abbreviations: e, enamel; d, dentin; p, pulp; DEJ, dentinoenamel junction. Gap indicates the gap between enamel and dentin.
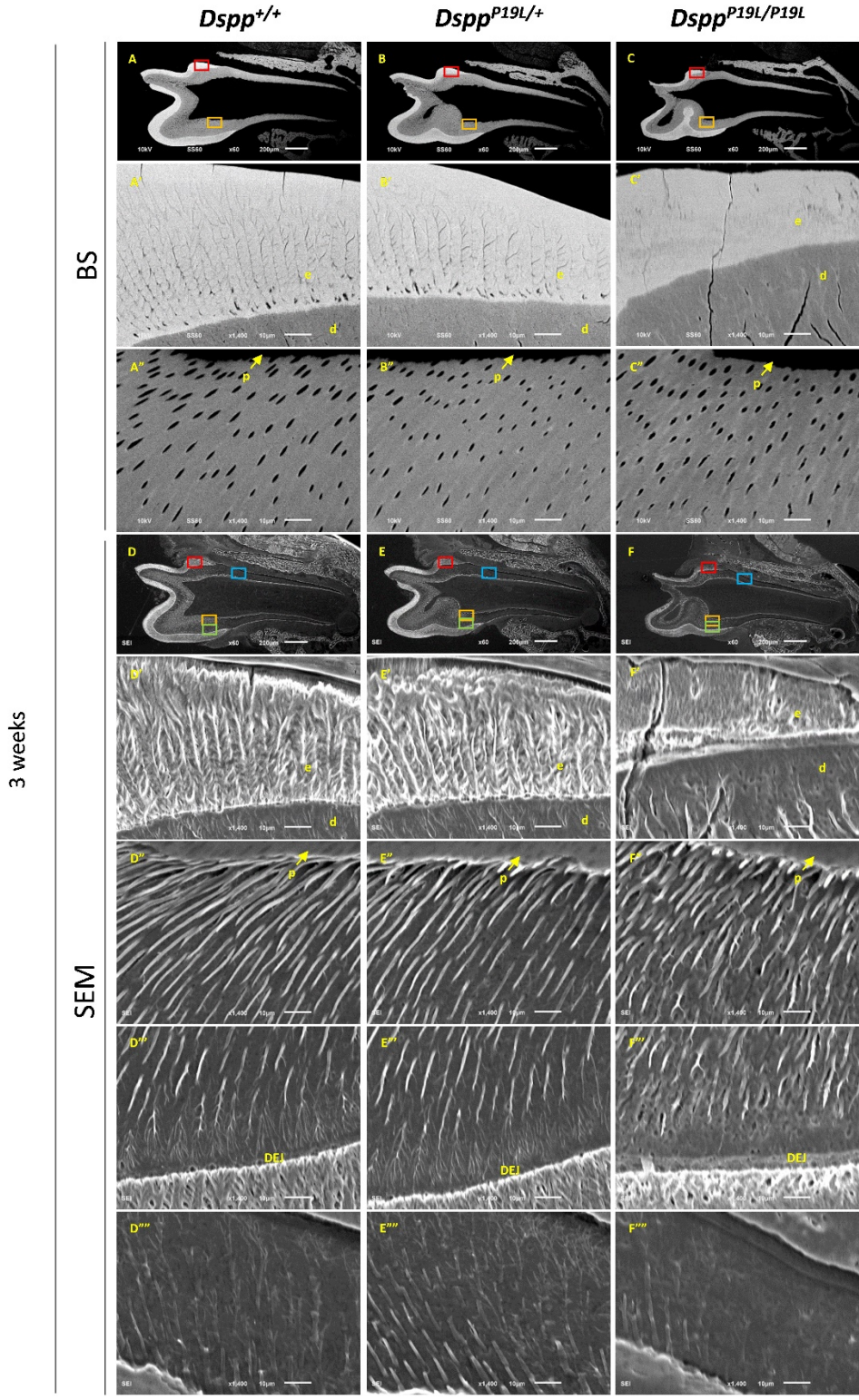
**Fig. 6 Scanning Electron Microscopy (SEM) Analyses of the Mandibular First Molars.**

Fig. 6 Continued

101
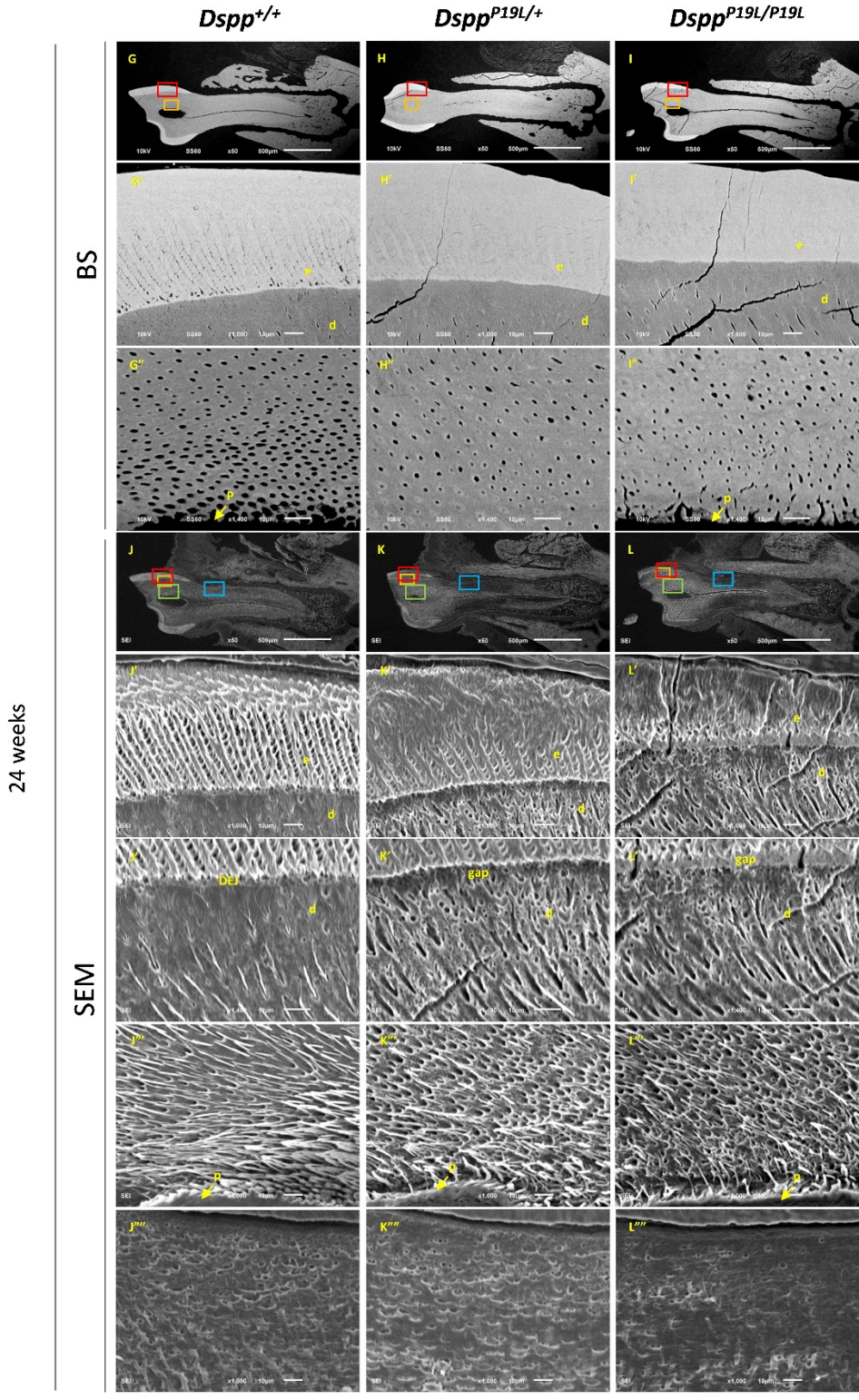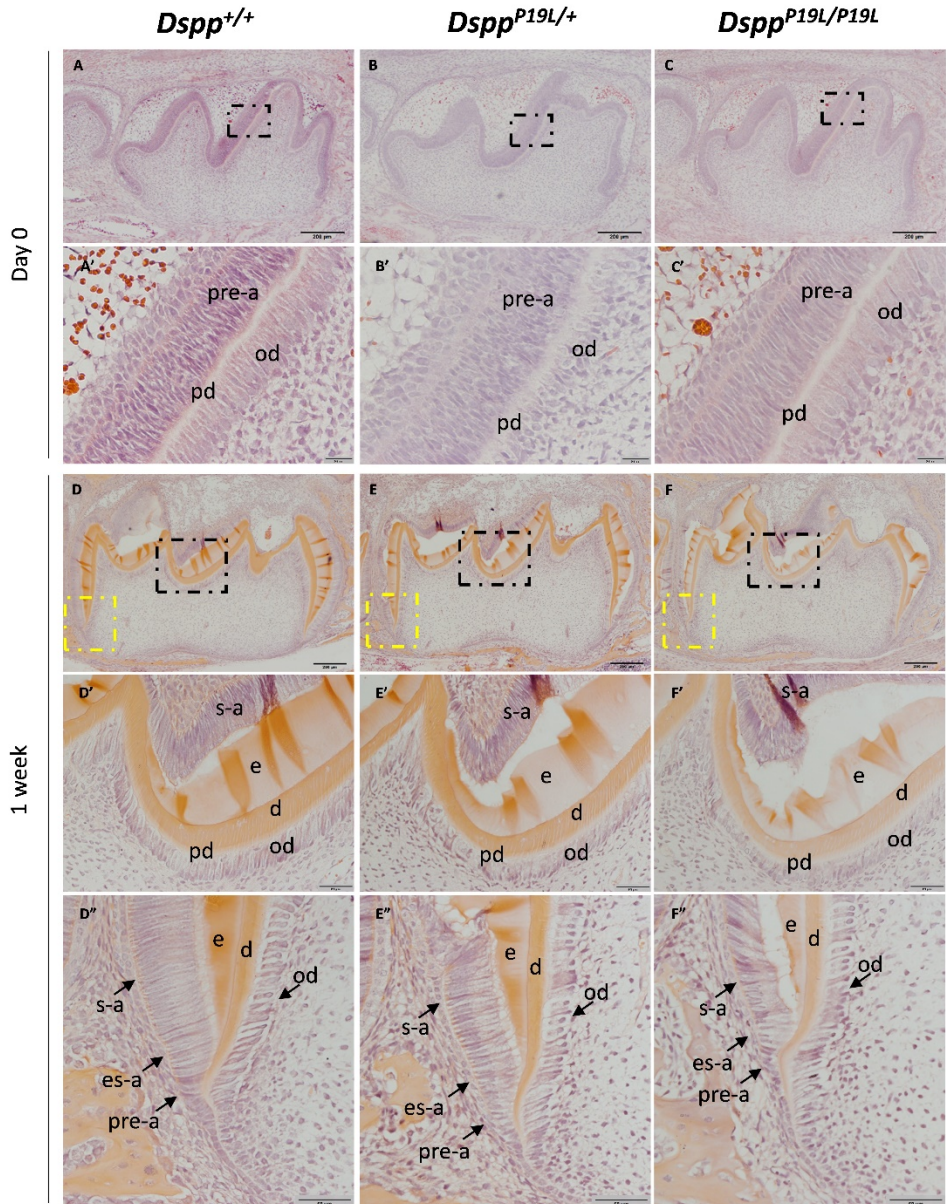
Fig. 7 Hematoxylin and Eosin (H&E) Stainings and Predentin Thickness of the Mandibular First Molars.

A-I. Shown are the representative H&E staining images of the mandibular first molars of postnatal day 0 (day 0, A-C), 1-week-old (D-F), and 3-week-old (G-I) $Dspp^{+/+}$ (A, D, and G), $Dspp^{P19L/+}$ (B, E, and H), and $Dspp^{P19L/P19L}$ (C, F, and I) mice. The proximal sides of teeth are positioned right. A'-I' are the corresponding magnified areas marked in black boxes. D"-L" are the corresponding magnified areas marked in yellow boxes. Abbreviations: d, dentin; pd, predentin; od, odontoblast; e, enamel; pre-a, presecretory ameloblast; es-a, early secretory ameloblast; s-a, secretory ameloblast. **J-L**. The predentin thickness of 1-week-old (1w) roof dentin (J), 3-week-old (3w) roof (K) and floor (L) dentin. n=4. * indicates significant difference at α=.05.
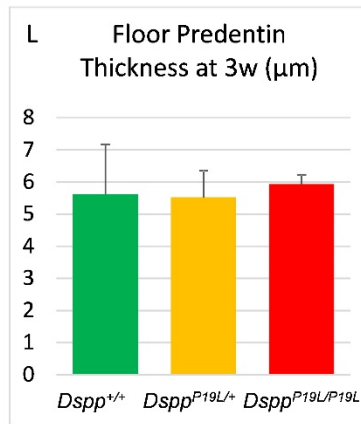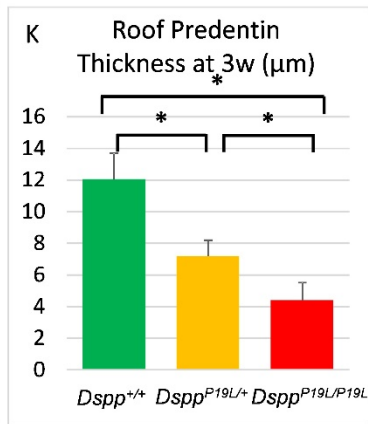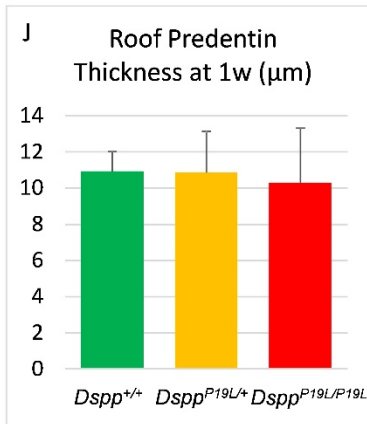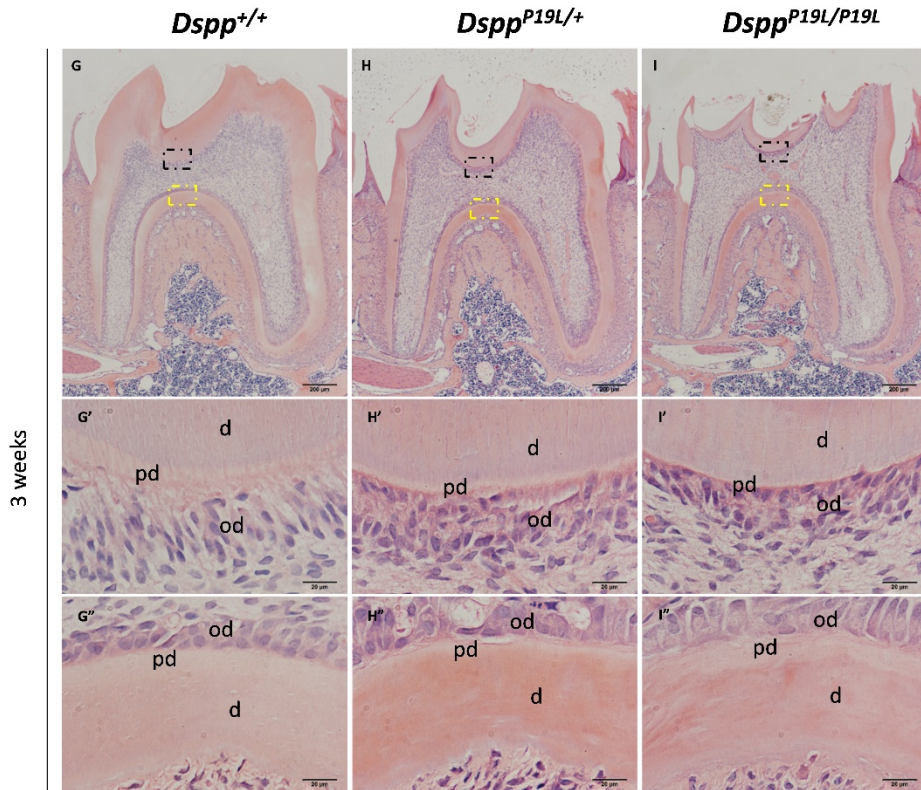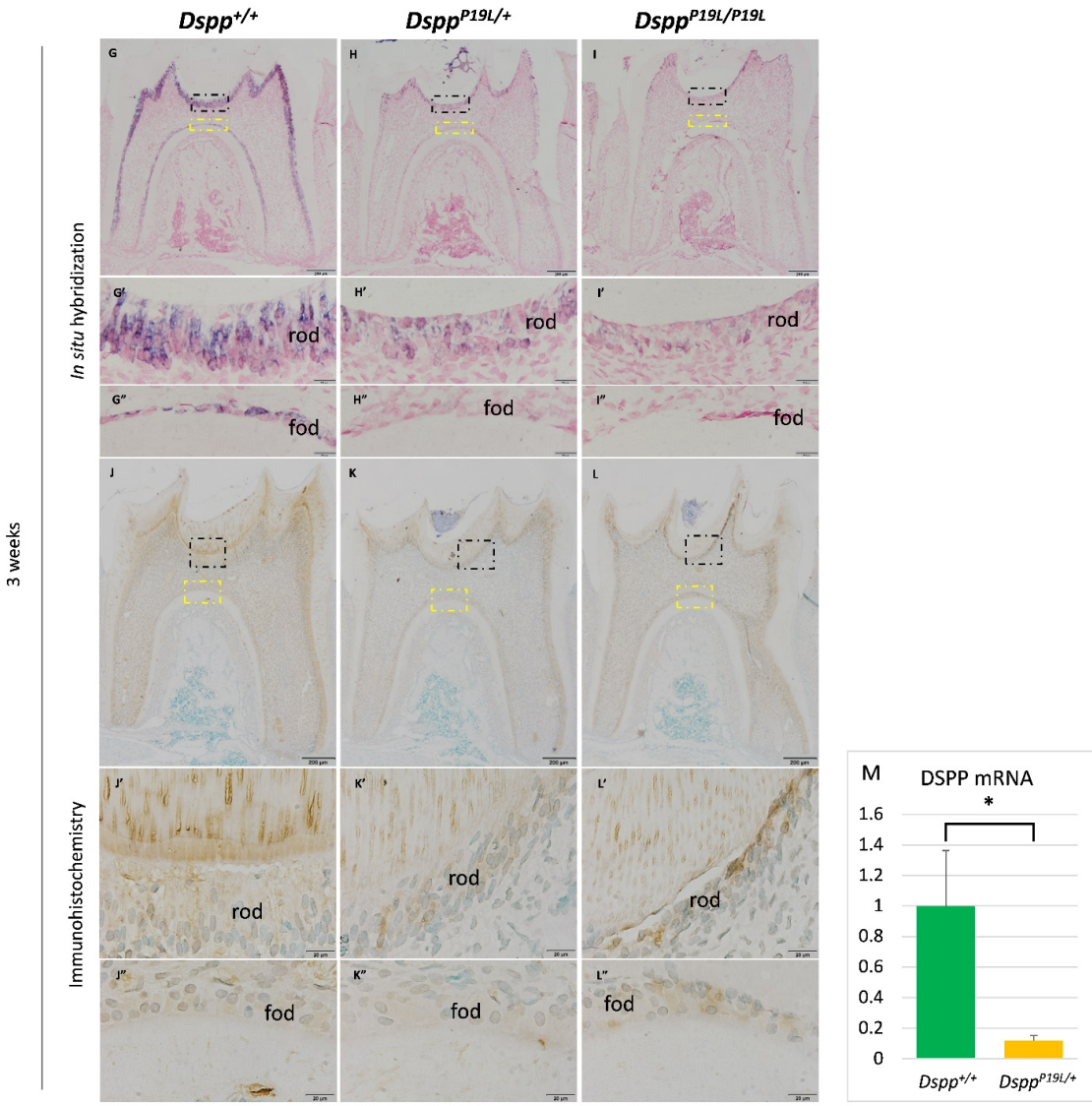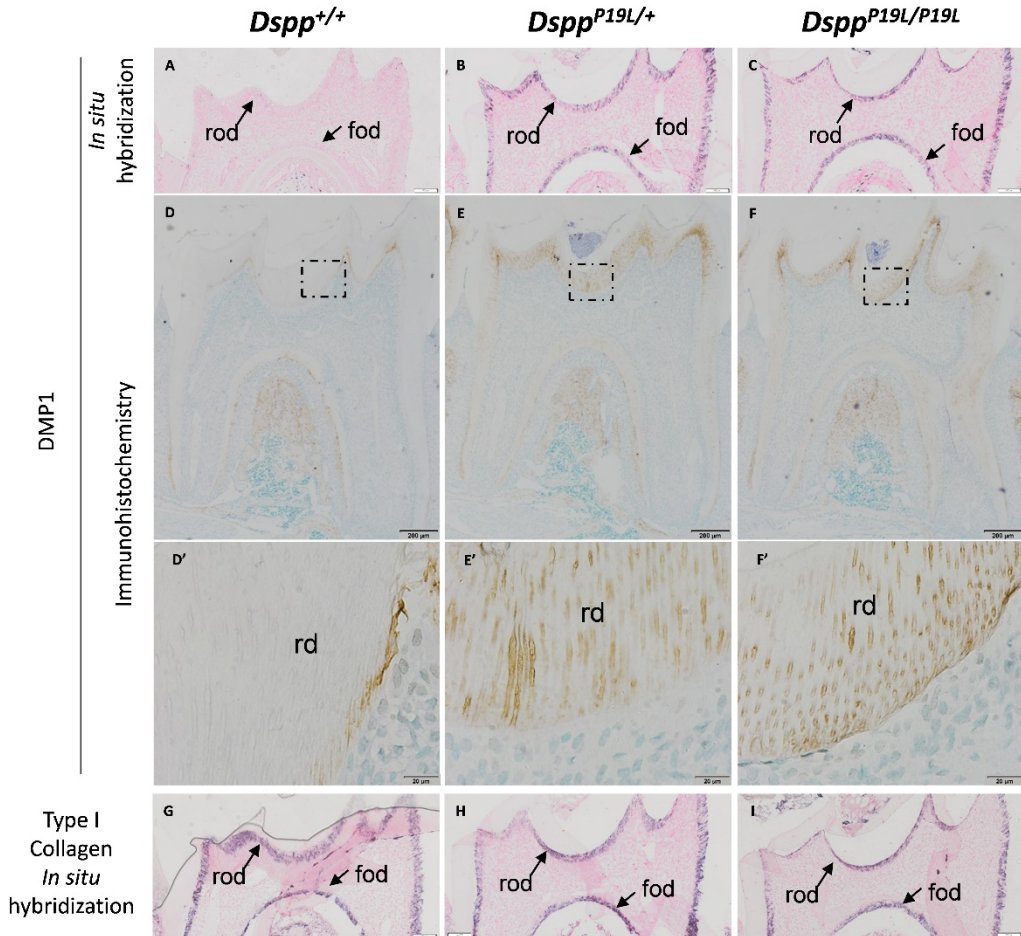
Fig. 7 Continued
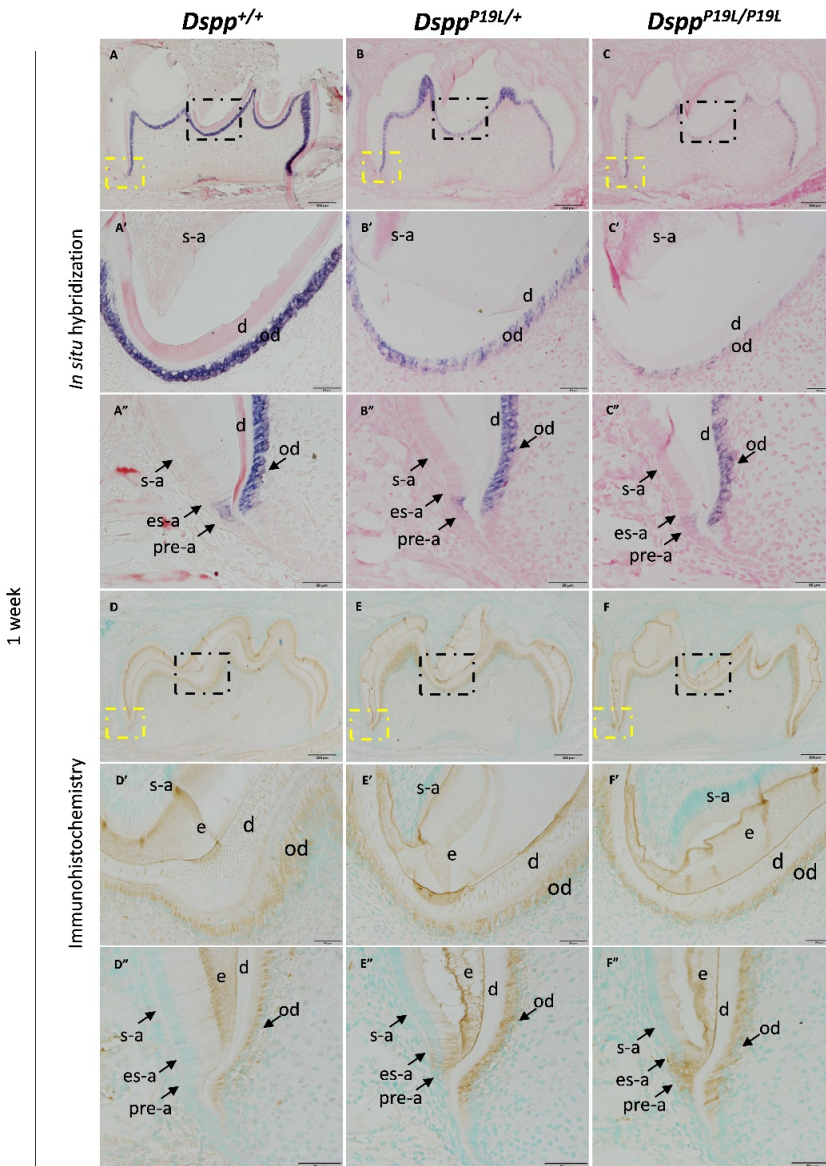
Fig. 8 DSPP Expressions in the Mandibular First Molars.
A-L. Shown are the representative DSPP *in situ* hybridization staining images (A-C, and G-I), and DSP immunohistochemistry staining images (D-F, and J-L) of the mandibular first molars of 1-week-old (A-F), and 3-week-old (G-L) $Dspp^{+/+}$(A, D, G, and J), $Dspp^{P19L/+}$(B, E, H, and K), and $Dspp^{P19L/P19L}$ (C, F, I, and L) mice. The proximal sides of teeth are positioned right. A'-L' are the corresponding magnified areas marked in black boxes. A"-L" are the corresponding magnified areas marked in yellow boxes. Abbreviations: d, dentin; pd, predentin; od, odontoblast; rod, roof-forming odontoblast; fod, floor-forming odontoblast; e, enamel; pre-a, presecretory ameloblast; es-a, early secretory ameloblast; s-a, secretory ameloblast. **M**. qPCR result of DSPP mRNA extracted from the molars of 3-week-old $Dspp^{+/+}$ and $Dspp^{P19L/+}$ mice. The DSPP mRNA level of $Dspp^{+/+}$ mice is set as 1. n=4. * indicates significant difference at α=.05.
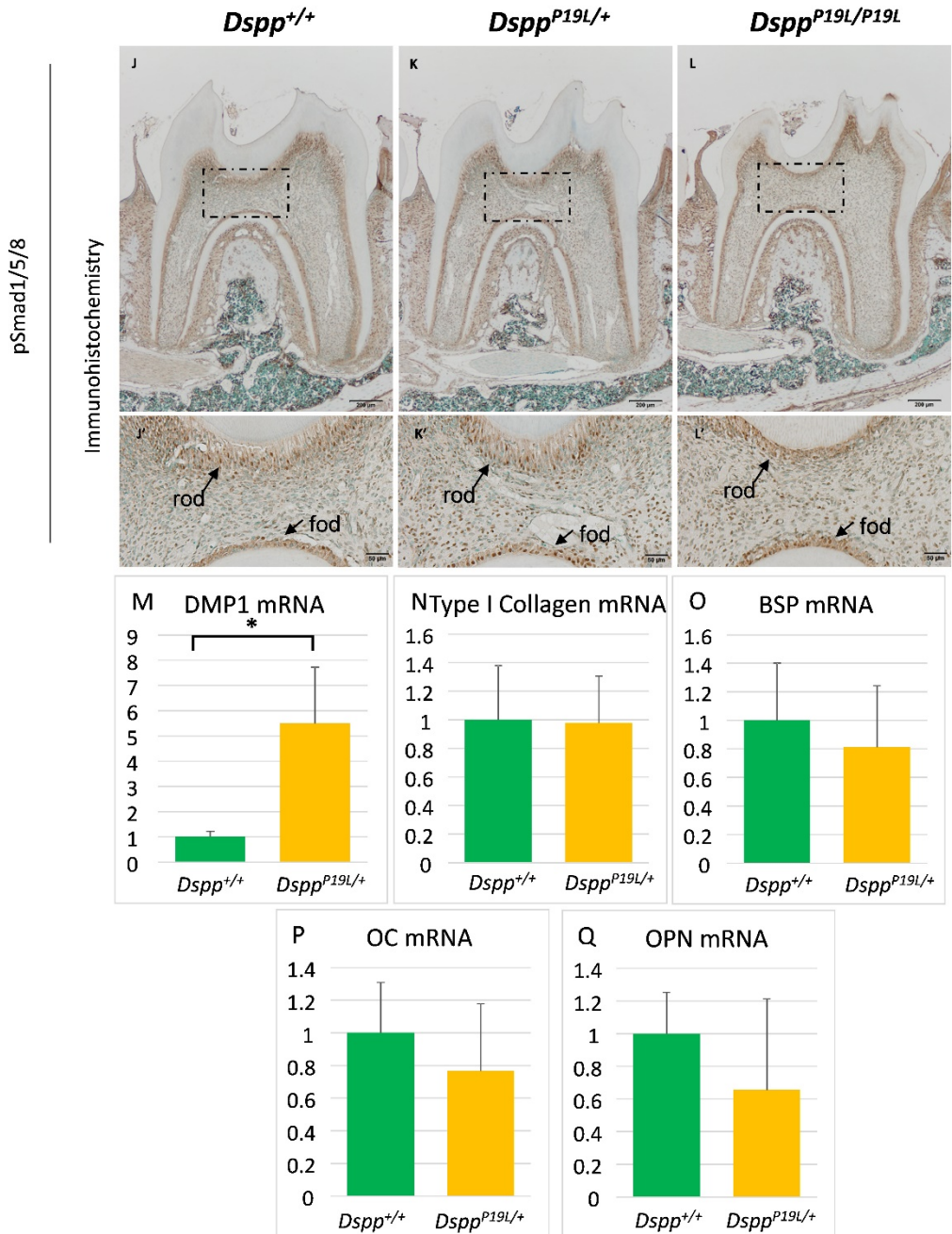
Fig. 8 Continued

Fig. 9 Expressions of Dentin Matrix Proteins and Phosphorylation of Smad1/5/8 in the Mandibular First Molars.

A-L. Shown are the representative *in situ* hybridization staining images (A-C, and G-I), and immunohistochemistry staining images (D-F, and J-L) of DMP1 (A-F), type I collage (G-I), and phosphorylated Smad1/5/8 (J-L) of the mandibular first molars of 3-week-old $Dspp^{+/+}$(A, D, G, and J), $Dspp^{P19L/+}$(B, E, H, and K), and $Dspp^{P19L/P19L}$ (C, F, I, and L) mice. The proximal sides of teeth are positioned right. D'-F', and J'-L' are the corresponding magnified areas marked in black boxes. Abbreviations: rd, roof dentin; fd, floor dentin; rod, roof-forming odontoblast; fod, floor-forming odontoblast. **M-Q**. qPCR result of mRNA of dentin matrix proteins extracted from the molars of 3-week-old $Dspp^{+/+}$ and $Dspp^{P19L/+}$ mice. These dentin matrix proteins are dentin matrix protein 1 (DMP1) (M), type I collagen (N), bone sialoprotein (BSP) (O), osteocalcin (OC) (P), osteopontin (OPN) (Q). The mRNA levels of $Dspp^{+/+}$ mice are set as 1. n=4. * indicates significant difference at α=.05.
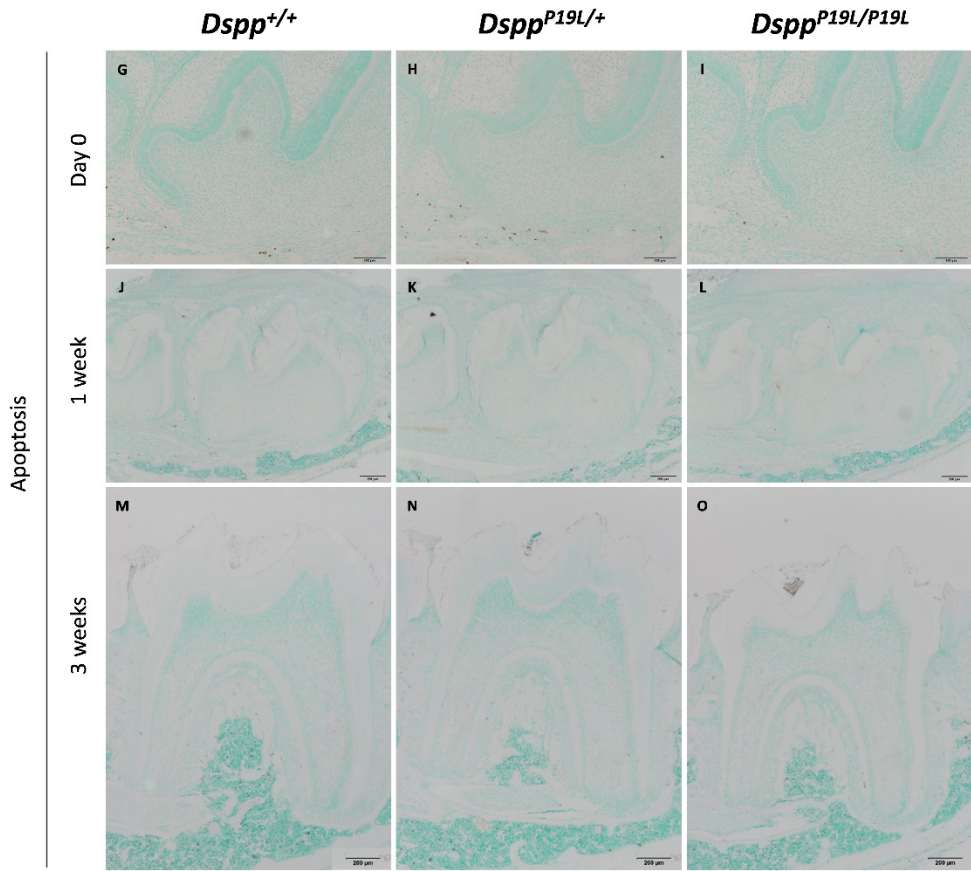
Fig. 9 Continued
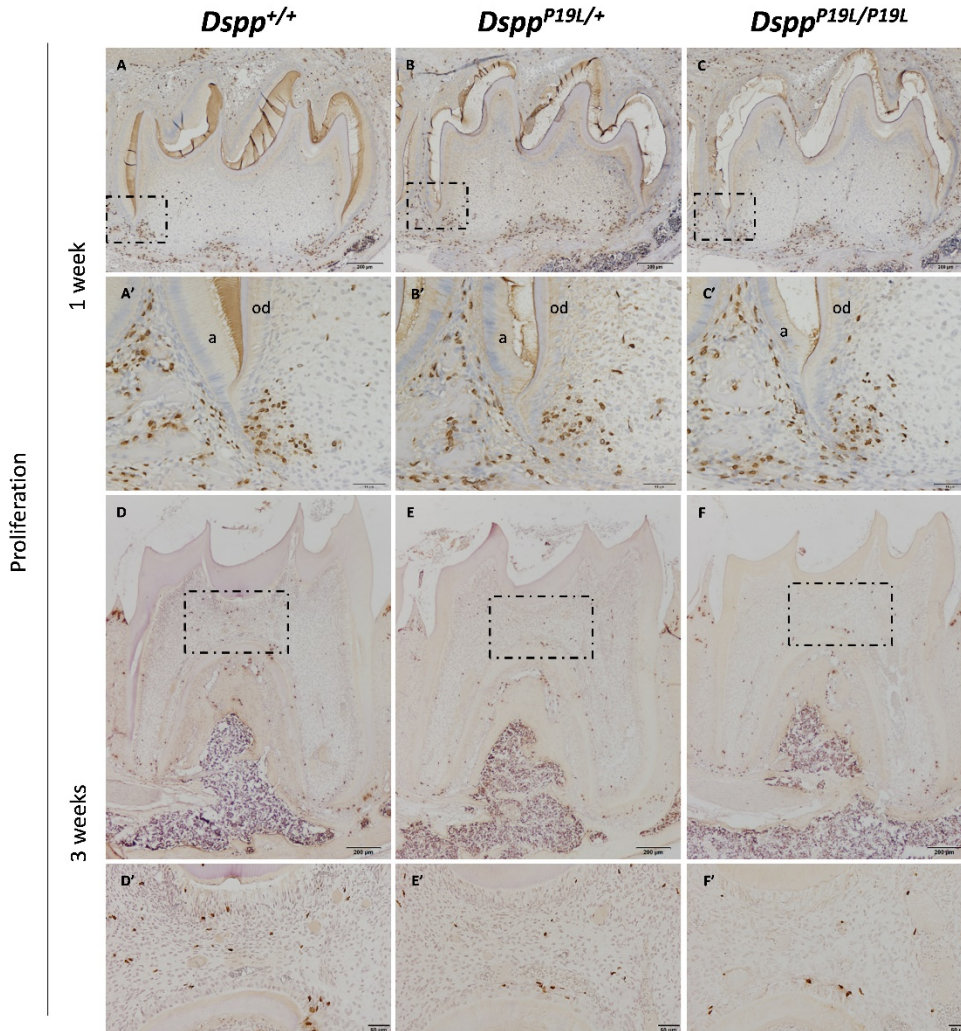
Fig. 10 Proliferation and Apoptosis in the Mandibular First Molars.
A-F. Shown are the representative BrdU staining images of the mandibular first molars of 1-week-old (A-C) and 3-week-old (D-F) $Dspp^{+/+}$(A, and D), $Dspp^{P19L/+}$(B, and E), and $Dspp^{P19L/P19L}$ (C, and F) mice. The proximal sides of teeth are positioned right. A'-F' are the corresponding magnified areas marked in black boxes. Abbreviations: od, odontoblast; a, ameloblast. **G-O**. Shown are the representative TdT staining images of the mandibular first molars of postnatal day 0 (day 0, G-I), 1-week-old (J-L) and 3-week-old (M-O) $Dspp^{+/+}$(G, J, and M), $Dspp^{P19L/+}$(H, K, and N), and $Dspp^{P19L/P19L}$ (I, L, and O) mice. The proximal sides of teeth are positioned right.

Fig. 10 Continued
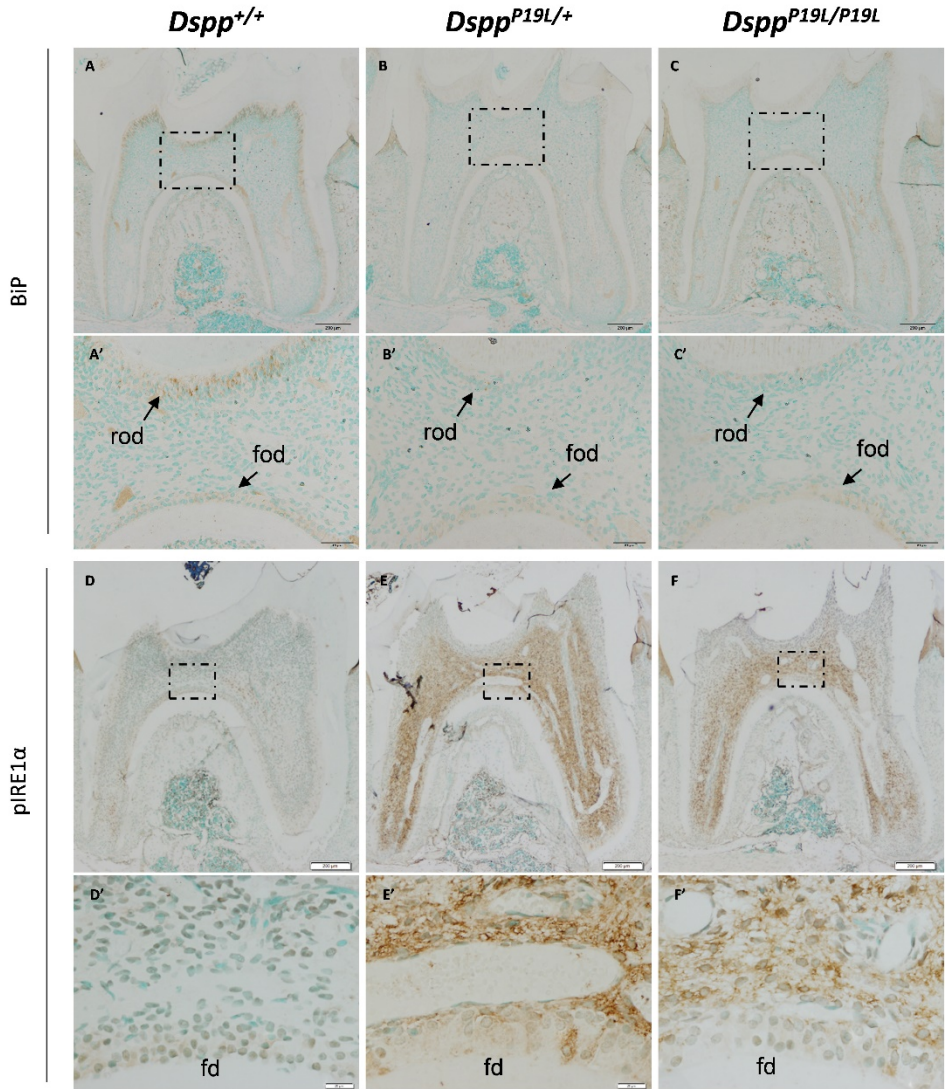
Fig. 11 Activation of Unfolded Protein Response (UPR) in the Mandibular First Molars.
A-I. Shown are the representative immunohistochemistry staining images of BiP (A-C), phosphorylated IRE1a (D-F), and XBP1 (G-I) of the mandibular first molars of 3-week-old $Dspp^{+/+}$(A, D, and G), $Dspp^{P19L/+}$(B, E, and H), and $Dspp^{P19L/P19L}$ (C, F, and I) mice. The proximal sides of teeth are positioned right. A'-I' are the corresponding magnified areas marked in black boxes. Abbreviations: fd, floor dentin; rod, roof-forming odontoblast; fod, floor-forming odontoblast. **J-S**. qPCR result of mRNA extracted from the molars of 3-week-old $Dspp^{+/+}$ and $Dspp^{P19L/+}$ mice. The mRNA levels of $Dspp^{+/+}$ mice are set as 1. n=4. * indicates significant difference at α=.05.
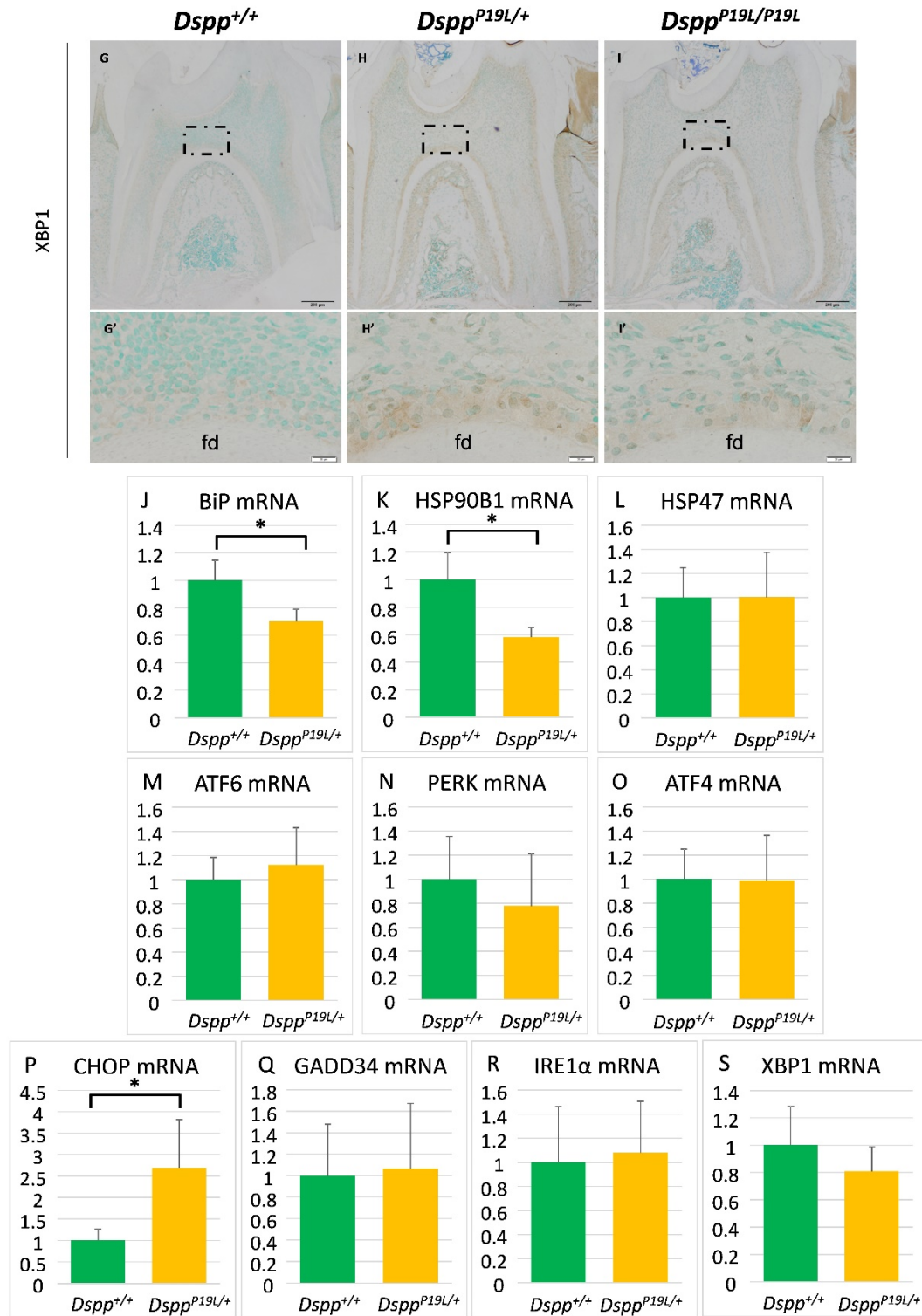
Fig. 11 Continued
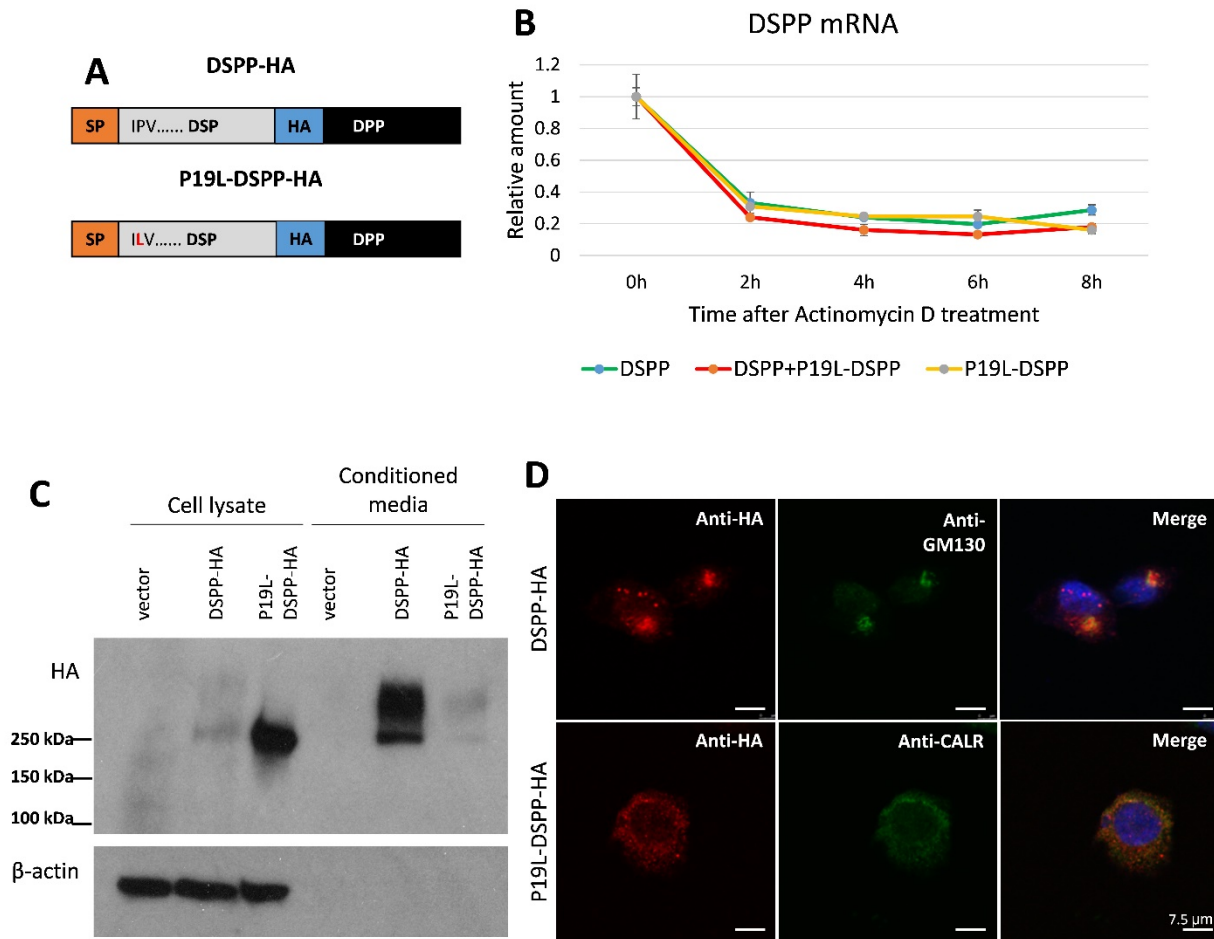
Fig. 12 P19L-DSPP Accumulated in the ER *in vitro*.
A. Shown are the recombinant normal DSPP and P19L-DSPP protein with HA tag inserted in the
N-terminal portion of DPP. **B**. Stability of normal DSPP and P19L-DSPP mRNA. DNA
constructs with normal *Dspp* or *P19L-Dspp* sequences were transfected alone or together into
293EBNA cells. Total RNA was harvested 0 hour, 2 hours, 4 hours, 6 hours, 8 hours after the
administration of Actinomycin D, an RNA synthesis inhibitor. qPCR was performed to evaluate
the relative amount of DSPP mRNA at each time point. The DSPP mRNA levels at 0 hour for
each group are set as 1. n=3. **C**. Intracellular retention of P19L-DSPP. DNA constructs with
normal *Dspp* or *P19L-Dspp* sequences were transfected into 293EBNA cells. Total cell lysate
and conditioned media were harvested 72 hours after transfection. Western blotting was
performed with α-HA.11 and α-β-actin antibodies. pcDNA3 served as negative control. β-actin
served as internal control. **D**. Accumulation of P19L-DSPP in the ER. DNA constructs with
normal *Dspp* or *P19L-Dspp* sequences were transfected into 17IIA11 cells. Immunofluorescence
was performed 48 hours after transfection. DSPP was detected by α-HA antibody. Cis Golgi
complex and ER were detected by α-GM130 and α-CALR (calreticulin) antibodies, respectively.
DAPI was performed for counterstaining.
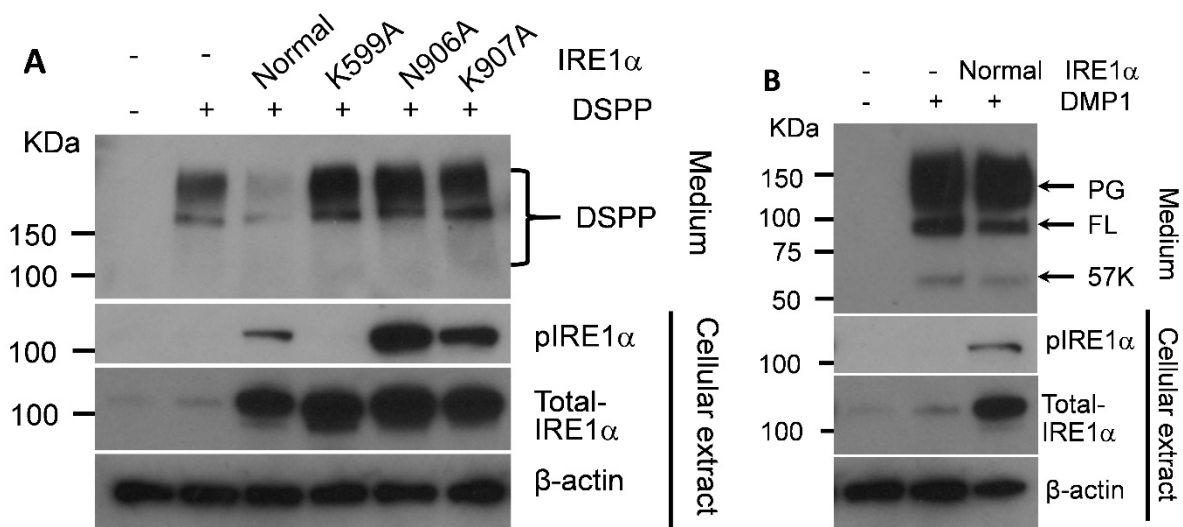
Fig. 13 IRE1α Regulated DSPP Specifically *in vitro*.
A. IRE1α inhibited DSPP expression. DNA constructs with normal DSPP-HA were transfected
with IRE1α variants into 293EBNA cells. K599A-IRE1α had an impaired ATP-binding pocket.
N906A- and K907A-IRE1α had a defective RNase domain. **B**. IRE1α did not inhibit DMP1
expression. DNA constructs with normal DMP1-HA were transfected with or without normal
IRE1α into 293EBNA cells. For both, cellular extract and conditioned media were harvested 72
hours after transfection. DSPP and DMP1 in the conditioned medium was detected by α-HA.11
antibody. The rest were detected by corresponding antibodies in the cellular extract. pcDNA3
served as negative control. β-actin served as internal control.

APPENDIX B

TABLES

Table 1 Dentinogenesis Imperfecta (DGI)/Dentin Dysplasia (DD) Classifications.

OMIM	Witkop Classification	Shields Classification	de La Dure-Molla Classification
#125400		DD type I	
#125420		DD type II	Non-syndromic DGI Mild form
	DGI	DGI type I	
#125490	Hereditary opalescent dentin	DGI type II	Non-syndromic DGI Moderate form
#125500	Brandywine isolate hereditary opalescent dentin	DGI type III	Non-syndromic DGI Severe form

Table 2 Summary of DSPP Mutations.

Location	Mutation#	cDNA	Protein	Family #	Age	Ethnicity	Diagnosis	References
Exon 2	1	c.16T>G	p.Y6D	1	7	German	DD-II	Rajpar et al.2002
	2	c.44C>T	p.A15V	2	17	American	DGI-II	Malmgren et al.2004
	3	c.49C>A	p.P17T	3		Chinese	DGI-II	Xiao et al. 2001
	4	c.49C>T	p.P17S	4	28	Chinese	DGI-II	Zhang et al. 2007
				5		Caucasian	DGI-II	Mcknight et al. 2008
				6		Brandywine	DGI-III	Hart et al. 2007
	5	c.50C>T	p.P17L	7	46	Chinese	DGI-II	Li (D) et al.2012
					44	Chinese	DGI-II	Li (D) et al.2012
				8	2.5	Korean	DGI-III	Lee et al.2013
Intron 2	6	c.52-6T>G	p.V18_Q45del (56%)	9	4	Hispanic	DD-II	Lee et al.2008
					39	Hispanic	DD-II	Lee et al.2008
					15	Hispanic	DD-II	Lee et al.2008
	7	c.52-3C>G	p.V18_Q45del(100%)	10	4	Korean	DGI-II	Kim et al. 2004
					27	Korean	DGI-II	Kim et al. 2004
	8	c.52-3C>A	p.V18_Q45del (80%)	11	10	Finnish	DGI-II	Holappa et al. 2006
					8	Finnish	DGI-II	Holappa et al. 2006
				12	15	Chinese	DGI-II	Wang et al. 2009
					45	Chinese	DGI-II	Wang et al. 2009
					65	Chinese	DGI-II	Wang et al. 2009
	9	c.52-2A>G	p.V18_Q45del	13	4	Chinese	DGI-III	Li et al. 2017
	10	c.52-1G>A	p.V18_Q45del	14	28	Chinese	DGI-II	Liu et al.2016
Exon 3	11	c.52G>T	p.V18F+p.V18_Q45del (57%)	15		Chinese	DGI-II	Xiao et al. 2001
				16	2	Korean	DGI-III	Kim et al. 2005
				17	1.8	Caucasian	DGI-II	Kim et al. 2005
					4	Caucasian	DGI-II	Kim et al. 2005
				18	5	Chinese	DGI-II	Song et al. 2006
				19		Finnish	DGI-II	Holappa et al. 2006
				20	32	Chinese	DGI-II	Li et al. 2017
					60	Chinese	DGI-II	Li et al. 2017
				21	30	Chinese	DGI-II	Li et al. 2017
					4	Chinese	DGI-II	Li et al. 2017
	12	c.53T>A	p.V18D	22	2.5	Korean	DGI-III	Lee et al. 2009
					19	Korean	DGI-II	Lee et al. 2009
					31	Korean	DGI-II	Lee et al. 2009
				23	4	Japanese	DGI-II	Kida et al. 2009
					30	Japanese	DGI-II	Kida et al. 2009
				24	6	Korean	DGI-II	Lee et al. 2011
	13	c.133C>T	p.V18_Q45del(69%)+NMD	25	6	Chinese	DGI-II	Zhang et al. 2001
				26	30	Chinese	DGI-II	Song et al. 2006
					3	Chinese	DGI-III	Song et al. 2006
Intron 3	14	c.135+1G>A	p.V18_Q45del(80%)+NMD	27		Chinese	DGI-II	Xiao et al. 2001
				28	18	Caucasian	DGI-II	Wang et al. 2011
					16	Caucasian	DGI-II	Wang et al. 2011
					17	Caucasian	DGI-II	Wang et al. 2011
				29	12	Caucasian	DGI-II	Wang et al. 2011

Table 2 Continued

Location	Mutation#	cDNA	Protein	Family #	Age	Ethnicity	Diagnosis	References
Intron 3	15	c.135+1G>T	p.V18_Q45del(81%)+NMD	30		Caucasian	DGI-II	Mcknight et al. 2008
	16	c.135+2T>C	TBD	31	12	Chinese	DGI-II	Zhang et al.2011
	17	c.135+3A>G	TBD	32	32	Mongolian	DGI-II	Bai et al. 2010
Exon 4	18	c.727G>A	p.D243N	33	37	Chinese	DGI-II	Li (L) et al. 2012
					17	Chinese	DGI-II	Li (L) et al. 2012
Exon 5	19	c.1686delT	p.D562Efs*75 2	34	4	Finnish	DD-II	Nieminen et al. 2011
	20	c.1830delC	p.S610Rfs*704	35	10	French	DD-II	Nieminen et al. 2011
	21	c.1870_1873delTCA G	p.S624Tfs*687	36		Caucasian	DD-II	Mcknight et al. 2008
	22	c.1874_1877delAC AG	p.D625Afs*68 7	37	10	Chinese	DD-II	Li et al. 2017
					46	Chinese	DD-II	Li et al. 2017
	23	c.1918_1921delTCA G	p.S640Tfs*673	38		Caucasian	DD-II	Mcknight et al. 2008
				39	10	Greek	DD-II	Nieminen et al. 2011
	24	c.1922_1925delAC AG	p.D641Afs*67 2	40	4	Finnish	DD-II	Nieminen et al. 2011
	25	c.2040delC	p.S680Rfs*633	41	5	Chinese	DD-II	Song et al. 2008
	26	c.2063delA	p.D688Vfs*62 6	42	22	Finnish	DD-II	Nieminen et al. 2011
	27	c.2272delA	p.S758Afs*554	43		Caucasian	DGI-II	Mcknight et al. 2008
	28	c.2349delT	p.S783Rfs*531	44	39	Spanish	DGI-II	Nieminen et al. 2011
	29	c.2525delG	p.S842Tfs*471	45		Caucasian	DGI-II	Mcknight et al. 2008
	30	c.2593delA	p.S865Vfs*448	46	24	Chinese	DGI-II	Song et al. 2008
	31	c.2666delG	p.S889Tfs*425	47	8	Greek	DGI-II	Nieminen et al. 2011
	32	c.2684delG	p.S895Mfs*41 8	48	10	Chinese	DGI-II	Song et al. 2008
				49	22	Chinese	DGI-II	Li et al. 2017
					44	Chinese	DGI-II	Li et al. 2017
	33	c.2688delT	p.D896Efs*41 7	50	6.5	Korean	DGI-II	Lee et al. 2011
				51	9	Korean	DGI-II	Lee et al. 2011
	34	c.3135delC	p.S1045Rfs*26 9	52	78	Caucasian	DD-II	Yang et al.2016
					49	Caucasian	DD-II	Yang et al.2016
					43	Caucasian	DD-II	Yang et al.2016
					30	Caucasian	DD-II	Yang et al.2016
					23	Caucasian	DD-II	Yang et al.2016
					2	Caucasian	DD-II	Yang et al.2016
	35	c.3438delC	p.D1146Efs*1 67	54	39	Chinese	DGI-II	Song et al. 2008
	36	c.3504_3508dup	p.D1170Afs*1 46	55	10	Spanish	DGI-II	Yang et al.2016
	37	c.3509_3521del13bp	p.D1170Afs*1 39	56	26	Chinese	DGI-II	Li et al. 2017
	38	c.3546_3550delTAG CAinsG	p.D1182Efs*1 30	57	12	Chinese	DGI-II	Song et al. 2008

Table 2 Continued

Location	Mutation#	cDNA	Protein	Family #	Age	Ethnicity	Diagnosis	References
	39	c.3560delG	p.S1187Mfs*126	58		Korean	DGI-II	Lee et al. 2011
Exon 5	40	c.3582_3591del10bp	p.D1194Efs*117	59	10	Finnish	DGI-II	Nieminen et al. 2011
	41	c.3625_3700del76bp	p.D1209Afs*80	60	13	Vietnamese	DGI-II	Nieminen et al. 2011
	42	c.3676delA	p.S1226Afs*88	61	23	Madagascar	DGI-II	Bloch-Zupan et al. 2016

Notes: According to Lee et al. 2011, in mRNA splicing mutation related to exon 3, the percentage indicated the proportion of exon 3 skipping; the rest was proposed to be wildtype mRNA splicing, or degraded by nonsense mediated decay (NMD). TBD, to be determined.

Table 3 The Proline Residue at the +2-position from the Signal Peptide Cleavage Site in DSPP Is Highly Conserved across Species.

Species	Amino acid sequence	GenBank Accession #
Human	MKIITYFCIWAVAWAIPVPQSKPLERHVEKSMNLHLLARSNVSV	NP_055023.2
Chimpanzee	MKIITYFCIWAVAWAIPVPQSKPLERHVEKSVNLHLLARSNVSV	XP_016807336.1
Monkey	MKIIAYFCIWAVAWAIPVPQSKPLERHVEKSMNLHLLARSNVSE	XP_001098430.1
Cow	MKIIVYFCIWAVAWAIPVPQIKPLERHAVDKSVNVNLLAKSKVP	XP_015319322.1
Dog	MKIIIYFCIWAAAWAIPVPQIKPLDRHAVDKSANLNLPEKVKLP	XP_003434051.1
Guinea pig	MKIIIYFCIWAAAWAIPVPQFGPSERHTLEKSENVHLLEKSKVP	XP_005003520.1
Mouse	MKMKIIIYICIWATAWAIPVPQLVPLERDIVENSVAVPLLTHPG	AAI29803.1
Rat	MKTKIIIYICIWATAWAIPVPQLVPLERDIVEKSADVPFLAHPG	NP_036922.2

Notes: The signal peptide (underlined) was predicted using SignalP 4.1 server (http://www.cbs.dtu.dk/services/SignalP/). The proline (P) residue at the +2-position from the signal peptide cleavage site is in bold.

Table 4 µCT Analysis of First Mandibular Molars.

		3 weeks	8 weeks	24 weeks
Roof Dentin Thickness (µm)	$Dspp^{+/+}$	143.61±4.39	236.30±5.86	248.57±11.38
	$Dspp^{P19L/+}$	89.09±5.77*	138.25±16.36*	167.80±10.82*
	$Dspp^{P19L/P19L}$	83.16±2.53*	104.50±10.19*	144.56±10.80*
Floor Dentin Thickness (µm)	$Dspp^{+/+}$	25.77±1.26	120.64±9.27	142.74±5.49
	$Dspp^{P19L/+}$	39.64±3.39*	192.26±3.72*	217.21±8.53*
	$Dspp^{P19L/P19L}$	43.81±3.45*	202.81±4.31*	217.85±20.47*
Pulp Volume (mm³)	$Dspp^{+/+}$	0.3354±0.0040	0.1355±0.0032	0.1310±0.0031
	$Dspp^{P19L/+}$	0.3568±0.0055*	0.1236±0.0040	0.0940±0.0086*
	$Dspp^{P19L/P19L}$	0.3805±0.0035*#	0.1309±0.0033	0.0751±0.0085*
Dentin+Cementum Volume (mm³)	$Dspp^{+/+}$	0.3886±0.0057	0.8051±0.0239	0.9981±0.0178
	$Dspp^{P19L/+}$	0.3490±0.0112*	0.7767±0.0166	0.9579±0.0320
	$Dspp^{P19L/P19L}$	0.3573±0.0057*	0.7364±0.0227	0.9253±0.0423
Dentin+Cementum Density (mg HA/ccm)	$Dspp^{+/+}$	989.35±4.94	1071.83±5.37	1108.78±4.72
	$Dspp^{P19L/+}$	951.89±8.74*	1027.24±5.78*	1071.04±3.44*
	$Dspp^{P19L/P19L}$	953.81±5.23*	1029.79±8.53*	1077.33±15.42
Enamel Volume (mm³)	$Dspp^{+/+}$	0.1617±0.0058	0.1451±0.0046	0.1496±0.0046
	$Dspp^{P19L/+}$	0.1245±0.0100*	0.0962±0.0084*	0.1049±0.0070*
	$Dspp^{P19L/P19L}$	0.1129±0.0066*	0.0884±0.0045*	0.0751±0.0108*
Enamel Density (mg HA/ccm)	DSPP^{+/+}	1779.91±14.18	1850.82±18.59	1899.49±17.37
	DSPP[P19L/+]	1723.43±17.59	1798.39±17.17	1833.88±8.56*
	DSPP[P19L/P19L]	1729.06±13.58	1793.61±17.60	1819.08±7.04*
Total Volume (mm³)	$Dspp^{+/+}$	0.9140±0.0139	1.1198±0.0219	1.2885±0.0207
	$Dspp^{P19L/+}$	0.8590±0.0233	1.0313±0.0176	1.1666±0.0439
	$Dspp^{P19L/P19L}$	0.8794±0.0056	0.9902±0.0226*	1.0862±0.0387*
Total Density (mg HA/ccm)	$Dspp^{+/+}$	787.50±8.73	1073.91±14.12	1103.62±2.12
	$Dspp^{P19L/+}$	691.67±19.70*	1009.87±14.64	1069.25±11.99
	$Dspp^{P19L/P19L}$	664.82±8.35*	996.52±11.37*	1070.01±12.56
Sample Size	$Dspp^{+/+}$	5	4	4
	$Dspp^{P19L/+}$	5	4	4
	$Dspp^{P19L/P19L}$	5	4	3

Notes: Values are mean±SEM. *: statistically different from $Dspp^{+/+}$ (α=.05). #: statistically different from $Dspp^{P19L/+}$ (α=.05).

Table 5 Primers Used for qPCR.

Target	Forward primer	Reverse primer
DSPP	5'-CAGCAAGGATAGCAGTTCTGA-3'	5'-TGTCACTGCCTTCACTGTCAC-3'
DMP1	5'-AGTGAGTCATCAGAAGAAAGTCAAGC-3'	5'-CTATACTGGCCTCTGTCGTGCC-3'
BSP	5'-GAGACGGCGATAGTTCC-3'	5'-AGTGCCGCTAACTCAA-3'
OC	5'-CTTGAAGACCGCCTACAAAC-3'	5'-GCTGCTGTGACATCCATAC-3'
OPN	5'-TGATGCCACAGATGAGGACCT-3'	5'-CAGAGGGCATGCTCAGAAGC-3'
Type I Collagen	5'-CTCACGTCCAGATTCACCA-3'	5'-AGAGAGGAGAAAGAGGCTTC-3'
BiP	5'-ATCTTTGGTTGCTTGTCGCT-3'	5'-ATGAAGGAGACTGCTGAGGC-3'
HSP90B1	5'-TCTGTTGCTTCCCGACTTTC-3'	5'-GAGGCGGAATCTTCTCCATT-3'
HSP47	5'-AAGATGCAGAAGAAGGCTGT-3'	5'-CGATAGGTCTGCCTTGTTCT-3'
ATF6	5'-GATTTGATGCCTTGGGAGTC-3'	5'-AAATCCAACTCCTCAGGAAC-3'
PERK	5'-AACCTCAAAGACTGGATGAA-3'	5'-CCAACCTTGACCACATCATC-3'
ATF4	5'-AGCCTAGGTCTCTTAGATGA-3'	5'-CTCCAACATCCAATCTGTCC-3'
CHOP	5'-GACCAGGTTCTGCTTTCAGG-3'	5'-CAGCGACAGAGCCAGAATAA-3'
GADD34	5'-TCTAAAAGCTCGGAAGGTACAC-3'	5'-CTTCGATCTCGTGCAAACTG-3'
IRE1α	5'-AAGATCCAGTCCTGCAGGTC-3'	5'-GGAAGTTTCGTCAGGCCTTC-3'
XBP1	5'-CCGTGAGTTTTCTCCCGTAA-3'	5'-AGAAAGAAAGCCCGGATGAG-3'
GAPDH	5'-CTCCTGGAAGATGGTGATGG-3'	5'-GGCAAAGTGGAGATTGTTGC-3'